UC San Diego

UC San Diego Electronic Theses and Dissertations

Title

Integration of visual information and the organization of receptive fields in V1 of the California ground squirrel

Permalink

https://escholarship.org/uc/item/4tn7q85d

Author

Yu, Hsin-Hao

Publication Date

2007

Peer reviewed|Thesis/dissertation

eScholarship.org Powered by the California Digital Library
University of California

UNIVERSITY OF CALIFORNIA, SAN DIEGO

Integration of visual information and the organization of receptive fields in V1 of the California ground squirrel

A dissertation submitted in partial satisfaction of the requirements for the degree Doctor of Philosophy

in

Cognitive Science

by

Hsin-Hao Yu

Committee in charge:

Virginia de Sa, Chair
Martin Sereno, Co-Chair
Andrea Chiba
E.J. Chichilnisky
Karen Dobkins

2007

Copyright
Hsin-Hao Yu, 2007
All rights reserved.

The dissertation of Hsin-Hao Yu is approved, and it is acceptable in quality and form for publication on microfilm:

_____

_____

_____

_____
Co-Chair

_____
Chair

University of California, San Diego

2007

DEDICATION

This dissertation is dedicated to the memory of my mother.

TABLE OF CONTENTS

Signature Page iii

Dedication iv

Table of Contents v

List of Figures viii

List of Tables x

Acknowledgements xi

Vita xii

Abstract of the Dissertation xiii

Chapter 1. Introduction 1
1.1. Introduction 1
1.2. Goals 2
1.3. Outline 3

Chapter 2. Issues 5
2.1. Where is the boundary between center and surround receptive field? 5
2.2. Suppression or facilitation? 8
2.3. The effect of stimulus contrast 9
2.4. Stimulus feature selectivity of the surround RF 11
2.5. Spatial organization of the surround RF 12
2.6. The anatomical substrates of receptive field organization 15
2.7. Functional roles of the surround mechanism 19
2.8. The ground squirrel as a model animal for visual neurophysiology 22

Chapter 3. Spatial summation properties 24
3.1. Introduction 24
3.2. Notes on terminology 25
3.3. Material and Methods 26
3.3.1. Animal preparation 26
3.3.2. Recording 28
3.3.3. Histology 28
3.3.4. Basic tuning curves 29
3.3.5. Center/surround grating experiments 30
3.3.6. Subfield profiles of receptive fields 33
3.4. Results 34

3.4.1. Spatial summation: Type I cells . . . 34
3.4.2. Spatial summation: Type II cells . . . 37
3.4.3. The effects of surround direction . . . 38
3.4.4. Spatial inhomogeneity of the surround . . . 40
3.4.5. Subfield profiles of receptive fields . . . 40
3.4.6. Dimension comparison: an example . . . 41
3.4.7. Relationships between summation properties and basic tuning properties . . . 42
3.5. Discussions . . . 45
3.5.1. Summary of findings . . . 45
3.5.2. The measurement of RF size . . . 46
3.5.3. How large is the CRF? . . . 48
3.5.4. Surround facilitation . . . 50
3.5.5. Orientation and direction selectivity of the surround . . . 51
3.5.6. Inhomogeneity of the surround RF . . . 53
3.5.7. Functional considerations . . . 54
3.5.8. Implications about cortical circuitry . . . 56
3.5.9. Basic tuning properties . . . 57
3.6. Acknowledgements . . . 58

Chapter 4. Spatialtemporal structure of the classical receptive fields . . . 69
4.1. Introduction . . . 69
4.2. The reverse correlation method . . . 70
4.3. Methods . . . 72
4.3.1. Data collection . . . 72
4.3.2. Stimulus . . . 72
4.3.3. Data analysis . . . 73
4.4. Results . . . 74
4.4.1. Spike-triggering features . . . 75
4.4.2. The dimensionality of the spike-triggering ensemble . . . 76
4.4.3. Nonlinearity . . . 78
4.5. Discussion . . . 78
4.6. Acknowledgements . . . 80

Chapter 5. Spatialtemporal structure of the non-classical receptive fields . . 89
5.1. Introduction . . . 89
5.2. Methods . . . 90
5.2.1. Data collection . . . 90
5.2.2. Stimulus . . . 90
5.2.3. Data analysis . . . 92
5.3. Results . . . 93
5.3.1. Spatialtemporal structure of the surround . . . 93
5.3.2. Dynamics of surround orientation . . . 99

5.4. Discussions 105
5.4.1. Receptive field organization 105
5.4.2. Time courses of facilitation and suppression 108
5.4.3. Cortical circuitry 109
5.5. Acknowledgements 110

Bibliography 112

LIST OF FIGURES

Figure 2.1. Various terms for describing the spatial organization of the nCRF. 14

Figure 3.1. Iconic representations of the various grating stimuli used in Chapter III. 31
Figure 3.2. Grating summation curves and grating subtraction curves of five representative Type I cells. 59
Figure 3.3. Grating summation curves under two different stimulus contrast. 60
Figure 3.4. Orientation tuning measured by annular gratings. 60
Figure 3.5. Population distributions of estimated summation field size. . . . 61
Figure 3.6. Joint distributions of d and d' for Type I cells. 62
Figure 3.7. Grating summation curves and grating summation curves for Type II cells. 63
Figure 3.8. Orientation modulation curves of Type Ifs cells. 64
Figure 3.9. Orientation modulation curves of Type If cells. 65
Figure 3.10. Orientation modulation curves of Type II cells. 65
Figure 3.11. Spatial inhomogeneity of the surround. 66
Figure 3.12. Estimating the width of the CRF by the reverse correlation method 67
Figure 3.13. Dimension comparison: an example 68

Figure 4.1. The reverse correlation method 70
Figure 4.2. STA/STC analysis of an "energy-model" complex cell. 81
Figure 4.3. Two more examples of "energy-model" complex cells. 82
Figure 4.4. STA/STC analysis of a "non-energy-model"complex cell. 83
Figure 4.5. Two more examples of "non-energy-mode" complex cell. 83
Figure 4.6. STA/STC analysis of a simple cell 84
Figure 4.7. STA/STC analysis of a complex cell whose STA is similar to simple cells. 85
Figure 4.8. Estimation of the dimensionality of the spike-triggered ensemble 86
Figure 4.9. Distribution of the dimensionality of the spike-triggered ensemble 87
Figure 4.10. Nonlinearities of a complex cell. 88
Figure 4.11. Nonlinearities of a simple cell 88

Figure 5.1. Reverse correlation stimuli used for studying the dynamic interactions between the center and the surround 91
Figure 5.2. Grating summation curves of a representative complex cell, whose reverse correlation kernels are display in Figure 5.3. 95
Figure 5.3. Reverse correlation kernels of the cell whose grating summation behavior is shown in Figure 5.2 96
Figure 5.4. Center/surround STC analysis of an additional complex cell . . 97
Figure 5.5. Center/surround STC analysis of an additional complex cell . . 98

Figure 5.6. Orientation dynamics of a representative cell 101
Figure 5.7. Orientation dynamics of an additional cell 102
Figure 5.8. Orientation dynamics of a Type II cell 103
Figure 5.9. An example of orientation dynamics where no difference in timing was found 104
Figure 5.10. Proposed RF organizations for Type I cells (a) and Type II cells (b). The black-and-white squares represent the most sensitive (supra-threshold) part of the integration field, revealed by two-dimensional reverse correlation experiments. They are slightly larger than the MRF. The regions colored in light red represent sub-thrshold areas of the integration field. They are silent by themselves but can trigger spikes if stimulated concurrently. Both supra-threhold and sub-threshold regions are orientation and spatial frequency selective. The circle in light blue represents a suppressive mechanism that is not orientation selective and has a slightly different time course from that of the integration field. Suppression being non-localized in space is speculative. 107

LIST OF TABLES

Table 3.1. The number of cells for each summation type. 44
Table 3.2. Half-orientation bandwidth of direction tuning. 44
Table 3.3. Statistics about d and d' 45

ACKNOWLEDGEMENTS

Some of the histology was performed with the assistance of Brittnay Davis, Samuel Failor, Chris McCall, and Adrian Scott.

The work would not have been possible without the generosity of Andrea Chiba's Lab. Special thanks to Matt Gielow, Irene Merzlyak, Victor Minces, and Laleh Quinn.

Parts of Chapter III and Chapter IV are being prepared for submission as "Integration of visual information in V1 of the California ground squirrel (*Spermophilus beecheyi*)" by Hsin-Hao Yu, Virginia R. de Sa, and Martin I. Sereno.

Parts of Chapter III and Chapter V are being prepared for submission as "Spatialtemporal properties of classical/non-classical interaction in the orientation domain of V1 neurons of the California ground squirrel (*Spermophilus beecheyi*)" by Hsin-Hao Yu, Virginia R. de Sa, and Martin I. Sereno.

VITA

2007	University of California, San Diego, Ph.D.
1999	National Chiao-Tung University (Hsin-Chu, Taiwan), Applied Mathematics, B.S.

PUBLICATIONS

"Intermediate-level shape processing - fMRI and modeling." (Poster) The 8th Annual Joint Symposium on Neural Computation.

"Nonlinear receptive-field mapping with synthesized naturalistic stimuli." Neurocomputing, 58–60 (2004) 909-913.

"The organization of classical and non-classical receptive fields of the California ground squirrel." Society of Neuroscience Abstracts, 2005.

ABSTRACT OF THE DISSERTATION

Integration of visual information and the organization of receptive fields in V1 of the California ground squirrel

by

Hsin-Hao Yu

Doctor of Philosophy in Cognitive Science

University of California, San Diego, 2007

Virginia de Sa, Chair

Martin Sereno, Co-Chair

The research was an effort to provide a detailed characterization of the classical receptive field (CRF) and the non-classical receptive field (nCRF) in the primary visual cortex (V1) of the California ground squirrel, using conventional grating stimuli, as well as dynamic stimuli. The California ground squirrel (Spermophilus beecheyi) is a highly visual rodent whose V1 seems to lack a systematic map of orientation tuning (van Hooser 2005) - a unusual feature which makes it an attractive animal for the study of CRF/nCRF interaction.

The spatial extent over which V1 neurons integrates visual information was estimated by four independent measures: the minimal response field ("hand-mappe" RF), the response to gratings of varying diameter, the response to annular gratings, and reverse correlation. For the majority of the recorded neurons, the size of the grating summation field was surprising large: 15deg in diameter in

average, about twice the size of the subfield map produced by reverse correlation. The facilitation was found to originate from localized regions (the co-axial"end"-positions) outside the CRF (as defined by reverse correlation kernels), and was orientation selective. Surround gratings at ortho-orientation were found to be suppressive. Many neurons responded to annular gratings in a stimulus-feature selective manner, when the CRF was excluded from stimulation. This behavior is possibly related to the detection of illusory contours. A small population of neurons (10%) was found to be suppressed, regardless of the orientation of the surround gratings.

The organization of the receptive field is most parsimoniously explained by large, elongate integration field, which is mostly sub-threshold except for a circular (or rectangular) CRF exposed above the threshold. This was based on reverse correlation experiments where the CRF and the nCRF were stimulated independently. The spatialtemporal structures of the two components were strikingly similar. The suppressive effect was explored by a dynamic stimulus where the orientation of the surround was updated at high refresh rate. A dissociation of facilitation and suppression was found in the temporal domain. Suppression was found to be orientation unspecific and had a different time course than that of facilitation.

Chapter 1

Introduction

1.1 Introduction

When a person sees the world, what does a neuron in his/her brain see? This seemingly innocent question underlies one of the the most fundamental issues in cognitive science and neuroscience: the representation and processing of sensory information in the brian. The pioneering works of Hartline and Kuffler provided the first important insight: a single neuron in the visual system typically "sees" only a small region of the visual world. The region of the visual field where a neuron responds to a small stimulus is called its *classical receptive field* (CRF).

Much effort is made to elucidate the CRF structures of neurons in the primary visual cortex (V1), the first area in the cortex to receive visual information originated from the retina. From these studies, it becomes clear that the visual world is represented in V1 as a mosaic of small fragments, each coded by various features (orientation, spatial frequency, colors...etc.). However, just like a pointist painting is not perceived as a collection of dots but as a scene, fragments in the visual mosaic must be integrated such that extended features such as contours and surfaces can be extracted for further processing. To understand how important visual functions, such as object recognition, are performed by the brain, it is

essential to understand how local information is integrated into global features.

Visual information outside the CRF can influence the behavior of CRF. The structure of the interaction is called the center/surround organization of the receptive field. This work reports an attempt to systematically investigate the center/surround organization of V1 neurons of the California ground squirrel (*Spermophilus beecheyi*), a high visual rodent.

1.2 Goals

The goals of the project were two folded: an exercise in comparative physiology, and an attempt to use the center/surround system of the squirrels as a platform for developing novel techniques for studying receptive field structures.

Comparative physiology The physiological behaviors of V1 neurons are intriguingly similar among the various mammals that have been studied. Although many quantitative differences have been reported, the *types* of physiological properties of V1 neurons (such as orientation selectivity, spatial frequency selectivity, the distinction between simple and complex cells...etc.) seem to be quite conservative across species. The striking similarity of CRF properties among various mammals led some researchers to theorize that some of the properties might represent optimal strategies for encoding and processing visual information.

The center/surround RF organization reported in the literature is less uniform with various conflicting results. However, the available data from monkeys and cats seem to suggest a general picture: the surround is primarily suppressive and the suppression is maximal when the surround stimulus is iso-orientation with preferred orientation of the center. Does this reflect an optimal solution for integrating local visual information? Comparison of physiological data from various branches of mammalian evolution and various ecological niches will be very helpful to answer this question. The first goal of the project was to produce a comprehensive description of center/surround behaviors of squirrel V1 neurons and compare

them to other mammals.

The use of ground squirrel as a model animal is motivated by anatomical findings showing some unusual features: First, orientation selectivity of squirrel V1 neurons is *not* organized into maps (ie. no orientation columns) and second, terminals of horizontal axons do not form discrete clusters as found in cats and primates. As will be discussed in Chapter II, these features are relevant anatomical substrates of center/surround receptive field. It is therefore important to investigate how these unusual anatomical features influence physiological behavior.

Chapter III and Chapter IV are devoted to comparative physiology.

Development of new experimental methods Gratings are the most widely used stimuli for visual neuroscience due to their simple spatialtemporal structure. However, they are limited by their rigid periodic structure. The reverse correlation method is a paradigm of experimental design that is capable of exploring a much larger stimulus space and revealing finer details of the receptive field. The methodology has been successfully used in the investigation of the CRF but rarely used in the domain of center/surround interaction. In this study, novel applications of the reverse correlation paradigm were developed to investigate the center/surround organization of the receptive field. The results are discussed in Chapter V.

1.3 Outline

Chapter II: *Issues*

An overview of relevant issues and a brief summary of results from previous studies.

Chapter III: *Spatial summation properties*

A systematic investigation of center/surround interaction using gratings stimuli. The report focuses on the classification of basic patterns of behavior

and the estimation of the size of the CRF.

Chapter IV: *Spatialtemporal structure of the classical receptive fields*

The reverse correlation method applied to the study of the CRF of ground squirrel V1 neurons.

Chapter V: *Spatialtemporal structure of the non-classical receptive fields*

The reverse correlation methods applied to the study of center/surround interaction in the spatialtemporal domain as well as the orientation domain.

Chapter 2

Issues

2.1 Where is the boundary between center and surround receptive field?

The receptive field is often conceptualized as being composed of spatially discrete regions (such as the CRF and the nCRF) which can be defined independently of experimental paradigms and can be mapped directly to computational mechanisms and/or anatomical circuits. Under such a model, it is crucial for the experimental scientists to develop procedures to locate the boundaries of these components. Several methods are used as the operational definitions of the CRF, and so far there seems to be no consensus on which being the "correct" one. The multitude of schemes of center/surround division undoubtably contributes to the large array of surround effects reported, some of which contradicting or unreproduced under a different stimulus design. More recently, the concept of receptive field organization is beginning to be replaced by one where the division of center and surround depends on the balance between spatially overlapping mechanisms (Levitt and Lund, 1997; Sceniak et al., 1999; Kapadia et al., 1999; Mizobe et al., 2001). This more sophisticated model nonetheless does not completely eliminate the problem of devising a meaningful way of dividing space into two (or more)

components - it only calls for a more systematic exploration of possible configurations. The measurements most commonly used to make the center/surround division are discussed below. In essence, they are based on two different views of receptive fields: the receptive field as defined by an impulse input (the region that responses to a spot of light) or as defined by integration (the region where a larger stimulus triggers larger responses).

The minimal response field (MRF)[1], defined as the region where a small stimulus (a light spot, a thin stationary bar, or a moving bar) elicits spikes on the onset or the offset of presentation, is almost the *de-facto* technique for defining the CRF. A somewhat unsatisfactory consequence of using the MRF as the center is that the region surrounding the MRF, although silent when stimulated by a small stimulus, might produce spikes when stimulated by more extensive patterns such as a big annulus of grating or texture (Knierim and Van Essen, 1992; Sillito et al., 1995), thus violating the intuition that the surround only modulates and does not "drive" the cell. To enforce the "silent surround" condition, an alternative procedure displays a big annulus of optimally-tuned grating with fixed outer diameter and varying inner diameter. The annular minimal response filed (AMRF) is defined as the smallest diameter such that the annulus elicits no more spikes than the spontaneous activity (Li and Li, 1994; Sengpiel et al., 1997; Cavanaugh et al., 2002a). Li and Li (1994) used the AMRF as the center/surround boundary. Finally, the grating summation field (GSF) is defined as the diameter of an optimally-tuned grating beyond which the neuronal response plateaus or begins to be suppressed (Sengpiel et al., 1997; Walker et al., 2000; Cavanaugh et al., 2002a,b).

More than one measures are often collected (Li and Li, 1994; Sengpiel et al., 1997; Jones et al., 2001, 2002; Cavanaugh et al., 2002a,b; Levitt and Lund, 2002). Levitt and Lund (2002) reported close agreement among the three measurements for high contrast stimuli, although the MRF is usually found to be smaller than the

[1]Also known as the minimal discharge field (MDF), excitatory receptive field (ERF) and the excitatory discharge center (XDC) in literature

GSF and the AMRF in other studies. The GSF and the AMRF were almost identical in (Sengpiel et al., 1997) but Cavanaugh et al. (2002a) reported a consistent bigger AMRF than the GSF. The variation is possibly due to stimulus contrast or the exact implementation of the stimulus. When the AMRF is found to be larger than the GSF, a gap of uniform gray is sometimes inserted between the circular center and the annular surround to make the surround estimation more conservative (Sengpiel et al., 1997; Jones et al., 2002; Cavanaugh et al., 2002a,b).

The relationship between the MRF and the GSF is of particular interest because the MRF, being the "original" definition of receptive field (Hartline, 1938, 1940; Kuffler, 1953; Hubel and Wiesel, 1962; Barlow et al., 1967), is widely used in visual physiology. The GRF is estimated to be, on the average, 1.4 to 2 times as large as the MRF (Walker et al., 2000; Jones et al., 2001; Cavanaugh et al., 2002a). Levitt and Lund (2002) reported a close match between the MRF and the GSF, but the MRF might have been overestimated. Length summation field of simple cells estimated by Kato et al. (1978) can be 30 times larger than the MRF. The variation is likely due to the stimulus contrast used in the GSF (section 2.3) and the exact experimental procedures used for measuring the MRF. Many neurophysiologists delineate the boundary of the MRF by "hand-plotting", ie., by operating the stimulus manually and listening to spikes through a loud speaker, which inevitably is subjective and tend to underestimate the MRF size. Even when hand-plotting is replaced by computer-driven, quantitative techniques, the exact implementations still vary considerably. It is argued by some researchers that the MRF underestimates the "true CRF" because it reveals only the most sensitive part of the CRF while leaving the sub-threshold region about 3 times larger undetected and should be replaced by grating summation parameters (Sengpiel et al., 1997; DeAngelis et al., 1992; Walker et al., 2000; Cavanaugh et al., 2002a). The spiking region as a tip of an iceberg of sub-threshold integration field is also supported by intracellular recording data (Ferster and Jagadeesh, 1992; Bringuier et al., 1999; Anderson et al., 2001) and optical imagining data (Grinvald et al., 1994; Das and Gilbert,

1995; Toth et al., 1996). Additionally, DeAngelis et al. (1992) and Walker et al. (2000) convincing argued that the band-pass filtering property of spatial frequency tuning of cat's V1 neurons is incompatible with the small size of the MRF, but well-matched by the GSF. On the other hand, some evidences show that the region immediately surrounding the MRF, although non-silent when stimulated by an extended stimulus, interacts with the MRF in a nonlinear way and cannot be considered a simple extension of the MRF. Knierim and Van Essen (1992); Sillito et al. (1995) reported that the non-silent region when stimulated together with the MRF suppresses the MRF response rather than facilitate it. This is also consistent with Das and Gilbert (1995) who showed that stimulating the subthreshold area immediately adjecent to the MRF (demonstrated by Bringuier et al. (1999) to be mainly depolarizing, ie. exictatory) suppressed the MRF responses.

2.2 Suppression or facilitation?

It is generally agreed that the effect of surround RF in V1 of cat and monkey is primarily suppressive. Facilitatory surround effects have been reported by a number of studies (Jones, 1970; Maffei and Fiorentini, 1976; Nelson and Frost, 1978, 1985; Gilbert and Wiesel, 1990; Li and Li, 1994; Sillito et al., 1995; Kapadia et al., 1995; Levitt and Lund, 1997; Jones et al., 2001, 2002), but other investigators found very few or no facilitation in their entire samples (Fries et al., 1977; DeAngelis et al., 1994; Knierim and Van Essen, 1992; Sengpiel et al., 1997; Walker et al., 1999, 2000; Cavanaugh et al., 2002a). Noting that many of the reports of facilitation used hand-mapped receptive field as the center and that the tuning properties of the reported facilitation tend to match those of the center, some authors argued that those facilitatory effects are due to stimulation of the grating summation area, which can be considered part of the CRF, and therefore not "true" surround effect (Sengpiel et al., 1997; Cavanaugh et al., 2002a). It is at this point not entirely clear if all facilitation can be attributed to the underestimation of the CRF. For

example, highly elaborate procedures were used in Nelson and Frost (1985) to make sure that the surround stimulus was outside the suppressive regions (end-zones and side-bands), and therefore outside the grating summation field. The discrete short bar surround stimulus used by Kapadia et al. (1995) was, in some cases, in the suppressive region as established by continuous bar. The determination of center/surround boundary in Li and Li (1994) and in Jones et al. (2001, 2002) also seems to be adequately controlled. It is unclear why the extensive facilitatory surround RF described by Li and Li (1994) is not reported by other researchers using cats. A possibility is that Li and Li (1994) used gratings whose width and length were allowed to vary independently (instead of circular grating patches) so that suppressive endzones and sidebands were not stimulated. However, similar stimuli were used by DeAngelis et al. (1994) but no facilitation was found.

Change in stimulus contrast can switch surround suppression to facilitation (c.f. Section 2.3). There doesn't seem to be a systematic difference in contrast between the studies that reported facilitation and those that did not. However, contrast threshold is possibly not absolute but varies for individual cells (Mizobe et al., 2001). It is therefore difficult to judge if stimulus contrast is sufficient for explaining the discrepancy.

Additional factors include misalignment of the stimulus to the receptive field, specific stimulus features (bars versus grating versus tetxure; stationary verse moving; discrete patch versus full field; discontinuous lines versus continuous lines ... etc.), bias in cell sampling, and the state of anesthesia.

2.3 The effect of stimulus contrast

The now slightly old-fashioned term "non-classical receptive field" reflects a mental model where the spatial organization of the receptive field is statically divided into two parts, the classical receptive field and the non-classical receptive field, with clear boundaries. This straightforward model is starting to be replaced

by a more dynamic, functional one because more and more evidences are showing that the nature of surround effects can be highly dependent on features of the stimulus. Stimulus contrast, for example, has a profound effect on the mode (suppression or facilitation) of surround modulation. The same surround stimulus showing suppression can be turned to facilitation by stimulating the center with low contrast stimuli[2] (Toth et al., 1996; Levitt and Lund, 1997; Sengpiel et al., 1997; Polat et al., 1998; Mizobe et al., 2001). The "turning point" of the contrast is not absolute, but depends on the threshold and saturation point of the contrast response of each cell, ranging from 10% to 30%. A related behavior is dependence of the GSF on stimulus contrast (Sengpiel et al., 1997; Sceniak et al., 1999; Kapadia et al., 1999; Angelucci et al., 2002b). The size of the GSF at low contrast is on average two or three times larger than at high contrast. Sceniak et al. (1999) proposed a model with overlapping facilitatory and suppressive field, each modeled as a gaussian function, to capture the relationship between summation curves and contrast. Under such a model, "center" and "surround" do not represent fixed, spatially separated mechanisms but are the result of the dynamic balance of two competing mechanisms.

The functional significance of contrast-dependent summation is unclear, but the behavior parallels that of the retinal ganglion cell, whose band-pass filtering property in spatial frequency is changed to low-pass when stimulus contrast is low. From the point of view of signal processing and information theory, this can be interpreted as a strategy to increase signal-to-noise ratio in noisy conditions (ie. low contrast) by increasing the range of spatial integration. Interestingly, Kapadia et al. (1999) demonstrated that the summation field for V1 neurons can be enlarged by embedding the stimulus in a large noisy background.

[2]However, Levitt and Lund (1997) reported higher suppression at low contrast.

2.4 Stimulus feature selectivity of the surround RF

Because orientation selectivity of the CRF is the most striking feature of V1 neurons, orientation selectivity of the surround naturally becomes the focus attention (Blakemore and Tobin, 1972; Maffei and Fiorentini, 1976; Nelson and Frost, 1978; Gilbert and Wiesel, 1990; Knierim and Van Essen, 1992; DeAngelis et al., 1994; Li and Li, 1994; Sillito et al., 1995; Sengpiel et al., 1997; Jones et al., 2002; Cavanaugh et al., 2002b). Except for a small population of cells whose surround suppression is not orientation selective (6% in Knierim and Van Essen (1992), 34% in Sengpiel et al. (1997) and 3% in Jones et al. (2002). Maffei and Fiorentini (1976) reported non-orientation-selective suppression for the majority of cells.), it is orientation selective for the majority of cells in V1 with maximal suppression occurring when the surround orientation matches (or nearly matches) the optimal orientation of the center. When the surround orientation is orthogonal to the optimal of the center, the response is either no effected or slightly facilitated. The bandwidth of surround suppression is broader than that of the orientation tuning of the center (Li and Li, 1994; Cavanaugh et al., 2002b). Although this standard pattern is reported by almost all studies, some effects are found by some investigators but not others. A notable example is iso-orientation facilitation - the center response is facilitated when the surround orientation matches the optimal orientation of the center and suppressed at other orientations (Nelson and Frost, 1985; Gilbert and Wiesel, 1990; Li and Li, 1994; Kapadia et al., 1995). Conversely, (Sillito et al., 1995; Jones et al., 2002) described cross-orientation facilitation, where the maximal effect occurs at the orientation orthogonal to the optimum of the center.

A surprising finding is that cells whose CRF are not orientation selective have been reported to have orientation selective surround. The responses of such

cells are maximally suppressed when the surround orientation matches the orientation of the center grating, regardless of the absolute orientation of the center stimulus (Knierim and Van Essen, 1992; Jones et al., 2002). This type of "orientation contrast" effect was also found in orientation selective cells (Sillito et al., 1995; Cavanaugh et al., 2002b) although some investigators failed to observe it (Sengpiel et al., 1997; Walker et al., 1999).

Direction selectivity of the surround is reported by several studies (Nelson and Frost, 1978, 1985; DeAngelis et al., 1994; Li and Li, 1994; Sengpiel et al., 1997; Walker et al., 1999; Jones et al., 2001; Cavanaugh et al., 2002b). The most detailed investigation is Jones et al. (2001) who showed that 22% of cells in monkey V1 exhibited no selectivity to surround direction. But for the rest, reversing the surround direction can reduce the degree of suppression (37%) or even turn suppression into facilitation (41%). Direction selective surround effect was found on cells whose CRF were not direction selective by itself.

Surround modulation is also shown to be selective for spatial frequency (Maffei and Fiorentini, 1976; Li and Li, 1994; DeAngelis et al., 1994) and speed (Li and Li, 1994). DeAngelis et al. (1994) reported that suppression is very weakly effected by the phase for the surround grating, even for simple cells. However, the facilitatory surround effect described by Nelson and Frost (1985) was phase sensitive. Finally, dichoptic experiments demonstrated that stimulating the surround in the dominant eye and the non-dominant eye produced similar effects (DeAngelis et al., 1994).

2.5 Spatial organization of the surround RF

Stimulus which probes the surround RF with an annulus grating circumscribing the center RF assumes the surround RF to be homogeneous. However, discrete regions of the surround might modulate the center response through different mechanisms. Cells which prefer gratings or bars of certain length (Hubel and

Wiesel, 1965, 1968; Dreher, 1972; Gilbert, 1977; Kato et al., 1978; Orban et al., 1979b,c; Nelson and Frost, 1985; Knierim and Van Essen, 1992; DeAngelis et al., 1994; Li and Li, 1994) or width (Bishop et al., 1973; Albus and Fries, 1980; Born and Tootell, 1991; Nelson and Frost, 1985; Knierim and Van Essen, 1992; DeAngelis et al., 1994; Li and Li, 1994) lead some researchers to conceptualize the MRF[3] to be surrounded by suppressive "end-zones" and "side-bands" (Figure 2.1). These regions are silent when stimulated alone but suppress the center response when concurrently activated with the MRF. Although the end-zones and the side-bands are the parts of the surround receptive field, they do not account for all the effects from outside the MRF. Nelson and Frost (1978, 1985) demonstrated facilitatory and suppressive effects when the surround stimuli were carefully placed to exclude them. Furthermore, the correlation between the strength of suppression from end-zones and suppression by a full surround stimulus is very weak (Knierim and Van Essen, 1992; Jones et al., 2001), indicating that the end-zone accounts for only part of surround suppression. Li and Li (1994) showed that the orientation tuning curve of the surround RF cannot be predicted linearly from the tunings of the side-bands and the end-zones.

Are end-zones and side-bands part of the same suppressive mechanism, or are they independent mechanisms? The data are contradictory. It is generally agreed that the end-zones are orientation selective with a tuning curve similar to that of the MRF (Hubel and Wiesel, 1965; Orban et al., 1979b) but there is disagreement about the orientation selectivity of the side-bands. Bishop et al. (1973); Nelson and Frost (1978); Orban et al. (1979b); Albus and Fries (1980) reported that the side-bands are not orientation selective, but Fries et al. (1977); DeAngelis et al. (1994) reported that they are. DeAngelis et al. (1994) found that, except for a population of cells in layer 6 of cat's V1, end-zones and side-bands tend to co-occur and their strengths are correlated, implicating that they are actually parts of a bigger surround structure. However, Born and Tootell (1991); Li and Li

[3]For a simple cell, the MRF includes both the ON-fields and the OFF-fields.

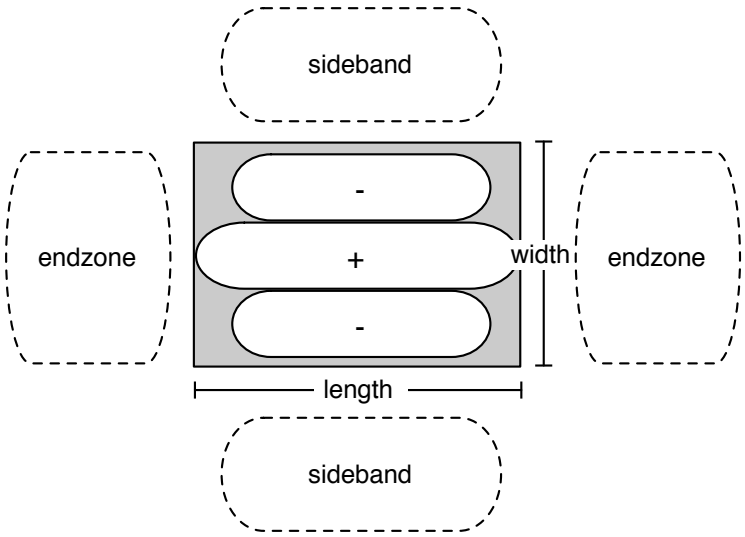

Figure 2.1: The spatial organization of the CRF and its surrounding suppressive regions. The shaded rectangle represents the CRF (also called the excitatory discharge center), which includes both the ON-fields and OFF-fields for a simple cell.

(1994); Levitt and Lund (2002) found them to be uncorrelated.

The concept of end-zones and side-bands as fixed components of the receptive field has fallen out of favor for some time now. First of all, the ends and the sides are not necessarily the loci of surround effects. Suppression can arise at any location outside the CRF and those locations are usually not symmetrically organized (Walker et al., 1999; Jones et al., 2001, 2002). Secondly, the effect of stimulus contrast on the stimulus summation also renders fixed schema such as Figure 2.1 unlikely. Mizobe et al. (2001) proposed that effects of the end-zones are the result of the dynamical balance of suppression and facilitation, which can be influenced by the activation level of the CRF.

2.6 The anatomical substrates of receptive field organization

The anatomical circuit underlying center/surround interaction is a subject of intense investigation and debate. This section only provides a brief outline of major arguments. For detailed reviews, see Allman et al. (1985); Gilbert (1992); Fitzpatrick (2000); Angelucci and Bullier (2003); Tucker and Fitzpatrick (2004).

Cortical horizontal connections Theories of anatomical substrates for surround effects focus heavily on a system of intrinsic, long-range horizontal connections running across the vertical columns. Intrinsic horizontal connections are mainly axon collaterals originated from pyramidal cells found most prominently in cortical layer 2/3, interconnecting discrete clusters of cells a few millimeters away[4]. They were first clearly described in treeshrews (Rockland et al., 1982; Rockland and Lund, 1982) but also found in cats (Gilbert and Wiesel, 1983; Matsubara et al., 1985), primates (Rockland and Lund, 1983), ferrets (Durack and Katz, 1995; Weliky et al., 1995; Ruthazer and Stryker, 1996) and squirrels. Horizontal connections seem to be the perfect candidate for the anatomical substrate underlying surround receptive fields for three major reasons: 1.) Long horizontal axons have the potential of integrating visual information from an extent several times larger than the MRF[5]. For two neurons to have non-overlapping receptive fields, the distance of separation required on the cortical surface is about 1.5-2.0mm for primates (Hubel and Wiesel, 1974) and 1.0 for cats (Das and Gilbert, 1995). The axon length of the horizontal connections is clearly long enough to reach visual space outside the MRF. 2.) The synaptic physiology of horizontal connections parallels some aspects

[4]For primates, the diameter of the terminal distribution is about 6mm, ie. 3mm on each side of the cell body (Angelucci et al., 2002b). For cats, the diameter is about 2mm-4mm (Gilbert and Wiesel, 1983).

[5]For primates, 6mm of coverage length corresponds to 4° of parafoveal visual space, or roughly 6x to 8x size of an average MRF length (Angelucci et al., 2002b). For cats, 4mm of coverage length amounts to 4° to 6° of parafoveal visual space, or roughly 2x to 4x the length of an average MRF length (Gilbert and Wiesel, 1983).

of the surround effects. EPSP's generated by stimulation of horizontal axons *in vitro* are not strong enough to trigger spikes unless the membrane potential of the target cell is depolarized – they therefore modulate but does not drive the target cells (Hirsch and Gilbert, 1991; Weliky et al., 1995). Intracellular recording and optical imaging show that visually stimulating an area surrounding the MRF, three times its size, produces no spikes but subthreshold responses (the tip-of-iceberg effect). Based on estimated propagation velocity, Bringuier et al. (1999) concluded that the subthreshold area is mediated by monosynaptic horizontal connections. Furthermore, like surround effects, horizontal axons are shown to be capable of producing both monosynaptic EPSP's and disynaptic IPSP's when stimulated *in vitro* (Hirsch and Gilbert, 1991; Weliky et al., 1995), consistent with the anatomical finding that 80% of their terminals are on pyramidal cells and spiny stellate cells (excitatory) and the rest on smooth stellate cells (inhibitory) (Kisvàrday et al., 1986; McGuire et al., 1991). Weak electric stimulation of horizontal fibers usually produce only EPSP's. Larger voltage is required to produced IPSP/IPSI compounds (Hirsch and Gilbert, 1991). This synaptic physiology parallels the contrast modulated surround effects. 3.) Horizontal connections make selective contacts among functional columns such as orientation columns (Gilbert and Wiesel, 1989; Malach et al., 1993; Weliky et al., 1995; Bosking et al., 1997; Kisvàrday et al., 1997), ocular dominance columns (Matsubara et al., 1985, 1987; Malach et al., 1993; Yoshioka et al., 1996), and blobs/interblobs (Livingstone and Hubel, 1984; Ts'o and Gilbert, 1988; Yoshioka et al., 1996; Yabuta and Callaway, 1998). Similarly, the surround effects are feature selective.

The arguments presented above, however, does not imply that horizontal connections contribute solely to the surround RF (Fitzpatrick, 2000; Chisum et al., 2003; Tucker and Fitzpatrick, 2004). The terminal density of horizontal connections are greatest near the cell body and falls with distance. The majority of the horizontal axons are short range ($< 500\mu m$) and likely contribute to the MRF. Unlike long-range horizontal connections, short-range horizontal connections are less

specific in feature selectivity, making them a potential substrate for non-specific modulation such as contrast gain control (Heeger, 1992).

A second network of long-range horizontal connections originated from GABAergic large basket cells, whose axons can travel more than 1mm and make connections to neurons with a wide range of orientation preferences (Kisvàrday, 1992; Kisvàrday et al., 1994).

Cortical feedback connections V1 neurons receive extensive feedback from extrastriate visual areas (such as V2, V3, and MT). Most of these projections are reciprocal but feedback connections can originate even from areas receiving no or very weak striate input, such as V4, TEO, and TE. Feedback connections originate from pyramidal cells and terminate mainly in layer 1, also in 2 and 5, but avoids layer 4 (Rockland and Virga, 1989). The effect of V2 feedbacks on V1 is believed to be mainly excitatory, because inactivating V2 results in a decrease in visual responsiveness in V1 (Sandell and Schiller (1982) and Mignard and Malpeli (1991), but Alonso et al. (1993)), although they are known to make connections on a small percentage of inhibitory neurons (Rockland, 1997; Anderson and Martin, 2006).

Feedback connections from extrastriate visual areas were originally believed to be too slow and too diffused to be involved in the construction of receptive fields and more likely to function mainly as substrates for "higher" visual functions such as figure-ground segmentation (Zipser et al., 1996; Lamme and Roelfsema, 2000) and attention. The picture is quickly changing. First of all, feedback is fast. Girard et al. (2001) estimated the conductance velocity of V2 to V1 feedback in primate cortex to be about 2-6 m/s, comparable to the velocity of feedforward connections (see also Nowak and Bullier (1997)). In comparison, the conductance velocity of horizontal connections is in the order of 0.1 - 0.2 m/s (Hirsch and Gilbert, 1991; Grinvald et al., 1994; Bringuier et al., 1999), making polysynaptic propagation of information via horizontal connection possibly too slow for surround receptive fields. Secondly, contrary to the results by Stettler et al. (2002), recent studies

using more sensitive tracers demonstrated selective projections with respect to CO compartments and orientation columns (reviewed in Angelucci and Bullier (2003)). Finally, the visual space covered by horizontal connections was found to match the integration area of low-contrast gratings, which is smaller than the whole surround RF. The surround RF therefore seems to be larger than the coverage range of monosynaptic horizontal connections, and is matched better by the divergence of feedbacks from V2, V3, or MT (Angelucci et al., 2002b).

Intralaminar connections Neurons in layer 4c of primate V1 exhibit surround suppression, and yet they receive no extensive horizontal connections, nor feedback connections from extrastriate areas. The surround effect is likely to be mediated by LGN inputs, or from the projections they receive from layer 6 (Levitt and Lund, 2002). The circuit of surround receptive field involving cortical layer 6 has been studied in some detail in the cat. A population of neurons in cat's V1 has long long (up to 8°) receptive fields (Gilbert, 1977). They are possibly constructed from the intrinsic horizontal connections in layer 5 (Bolz and Gilbert, 1990), and potentially can serve as a source of long range visual information. Inactivation of layer 6 was demonstrated to influence the length summation properties of cells in upper cortical layers (Sillito and Versiani, 1977; Bolz and Gilbert, 1986; Bolz et al., 1989b; Grieve and Sillito, 1991), although the exact mechanisms remain unclear.

Giving the highly specialized distribution of cell types and projections in the six cortical layers, it is natural to predict systematic, differential patterns of surround effect in different layers. Existing data, puzzlingly, show a more uniform distribution than expected. Early investigators reported a higher concentration of end-stopped cells in upper layers in cat's V1 (Gilbert, 1977; Kato et al., 1978), but DeAngelis et al. (1994) found no significant laminar difference in terms of the strength of suppression or the optimal length, except for layer 6 with its very long receptive fields. Walker et al. (2000) and Mizobe et al. (2001) also reported uniform laminar distribution of surround suppression in cats. For primates, Born and Tootell (1991) claimed that side suppression was primarily found in layer

2/3, but other researchers found only weak evidence for this laminar difference (Sceniak et al., 1999; Levitt and Lund, 2002). Large and small summation fields can be found in all cortical layers. Likewise, suppression can be strong or weak in all layers.

Subcortical sources Surround effects are believed to be mainly mediated by cortical circuits because they are orientation selective and can be elicited from both eyes. However, neurons in subcortical areas such as the LGN and the superior colliculus already exhibit surround effects and therefore can be the origin of some of the surround effects found in cortical neurons[6] (Allman et al., 1985). Neurons in the LGN, for example, are not orientation selective by themselves but can be modulated in a way similar to the orientation contrast effects described by (Knierim and Van Essen, 1992; Sillito et al., 1995; Jones et al., 2002; Cavanaugh et al., 2002b). LGN neurons receives massive feedback projections from layer 6 of V1 (Lund et al., 1975), which could be the source of the orientation signal (Murphy and Sillito, 1987; Marrocco et al., 1982; Sillito et al., 1993; Sillito and Jones, 2004). Another possible subcortical source of surround effect is from the claustrum, which is retinotopically organized and contains cells optimally driven by oriented long bars. Sherk and LeVay (1983) showed that inactivation of the claustrum reduced the number of end-stopped neurons in V1. Finally, the pulvinar is also a possible source of surround effects.

2.7 Functional roles of the surround mechanism

Surround mechanisms as substrates of visual feature selectivity The orientation selectivity of V1 neurons is generated, according to one of many theories, by a broad orientation bias created by the spatial arrangement of geniculocortical connections, and sharpened by suppressive cortical mechanisms (Ferster and Koch, 1987; Ferster and Miller, 2000). To test if surround receptive field

[6] As a matter of fact, surround effects can be seen as early as the retina.

participates in shaping the orientation tuning curve, bars of varying length or gratings of varying size are used to measure orientation selectivity. Larger stimuli were demonstrated to produce sharper orientation tuning by Orban et al. (1979b) and Li and Li (1994), although the issue is not completely settled. DeAngelis et al. (1994) argued that surround modulation is divisive (c.f. Cavanaugh et al. (2002a)) and does not effect the bandwidth of tuning.

Besides sharpening orientation tuning, localized suppression from the surround (such as end-zone suppression) is proposed to underly the detection of curvature (Dobbins et al., 1987). Furthermore, it is suggested that slight differences in length tuning interocularly can be utilized to analyze three-dimensional surface structures. This hypothesis was tested by DeAngelis et al. (1994), who found no evidence for differential length tuning for the two eyes.

Surround mechanisms as substrates for visual scene analysis The concept of receptive field implies locality. The intensive attention on the CRF leads to a wavelet theory of vision, where the visual world is broken into a mosaic of tiny pieces of local features. But the function of the visual system is to transform the mosaic to efficient representations such that important cognitive functions, such as recognition, can be performed. The next step in information processing is to piece local features into perceptually relevant categories such as contours and surfaces. The surround receptive fields, integrating information from regions far away, seem to be capable of providing the necessary medium for local-global integration and filling the gap between "early vision" and "higher-order vision". The following paragraphs discuss how context modulates the perception of a visual target, and how the surround RF might be involved. See Albright and Stoner (2002); Lamme (2004) for detailed reviews.

1.) Pop-out: The saliency of a visual target depends on the background it appears in. When a subject is asked to detect the presence or identity of a target embedded in complex background, the target "pops out", ie. becomes highly salient, when the elementary features (orientation, color, motion ... etc.) of the

background are systematically different from those of the target. To test if V1 neurons experience pop-out, experiments were conducted on alert or anesthetized animals using stimuli similar to those used in psychophysics – the "target", usually a short line segment (static or moving), presented in the CRF, is embedded in a textured background presented outside the CRF. The stimuli are similar to the center/surround stimuli, except that instead of gratings, the backgrounds are random dot textures, discrete segments of short lines, or natural images. The response to the target is usually suppressed by a background sharing similar features as the target, creating a homogeneous pattern (Hammond and MacKay, 1981; Orban et al., 1987; Gulyás et al., 1987). When the background differs from the target systematically, a center/surround contrast of stimulus feature is created and many neurons in V1 are reported to response by firing more spikes than the homogeneous condition (Knierim and Van Essen, 1992; Kastner et al., 1997; Nothdurft et al., 1999). Suppressive surround effects signal feature discontinuity and is, therefore, possibly part of the neural substrates of pop-out.

2.) Contour completion/integration: Contours in the natural world can be interrupted by occlusion and shadows, but perceptually the intrusions are often filtered and the fragmented contours perceived as continuous. Psychophysical experiments show that human subjects perceptually group axially aligned line segments among complex background (Field et al., 1993), and that the detection threshold of a discrete target is significantly decreased when flanked by two collinear stimuli (Polat and Sagi, 1993, 1994). Facilitatory surround effects of V1 are well-suited to be the underlying mechanism under contour completion and physiological recordings demonstrated that collinear line segments outside the CRF facilitate the response of the CRF (Kapadia et al., 1995; Polat et al., 1998; Kapadia et al., 2000; Mizobe et al., 2001).

Some questions remain unsolved. For example, surround facilitation is observed when contrast is low, but contour integration also happens in high contrast. Also, the results by (Kapadia et al., 2000; Mizobe et al., 2001) showed localized

facilitatory effects from the end-zones of the CRF, which was not found by other studies probing discrete zones around the CRF (c.f. section 2.5). A possible explanation lies in the exact stimulus used: most studies of surround effects use drifting gratings, while studies of contour integration use stationary discrete stimulus such as line segments and gabor patches.

3.) Figure/ground segmentation: The detection of feature discontinuity is essential to the detection of figure/ground boundary, but just like the situation of pop-out, it is not by itself sufficient for figure/ground segmentation. A V1 receptive field inside a large homogeneous figure detects no discontinuity, because the boundary is outside its receptive field. But does it "know" that it is inside the figure? Recordings in V1 show that receptive fields inside and outside the figure can be distinguished by their spiking patterns (Lamme, 1995; Zipser et al., 1996) but figure/ground information is late in latency ($>$ 100mm) and seems to be mediated by a mechanism different from the quick center/surround effects discussed so far.

Relation to visual illusion The detection of visual feature depends on the context it is in. Psychophysical experiments show that judgement of the orientation of a line can be influenced by the orientation nearby, creating the so-called "tilt illusion". Similarity, (Gilbert and Wiesel, 1990; Kapadia et al., 2000) demonstrated that the orientation tuning of the CRF could be changed by oriented lines outside the CRF.

2.8 The ground squirrel as a model animal for visual neurophysiology

The California ground squirrel (*Spermophilus beecheyi*) is a diurnal animal that has a much more highly developed visual system than the nocturnal rodents more commonly used (rats and mice). They have high visual acuity (cut-off at 4.0 cpd, slightly lower than the cat, but higher than the tree shrew and rats. See

Jacobs et al. (1980)), a greater emphasis on the center of gaze, and dichromatic color vision. The squirrel eye is large and has excellent optics, and their cortical and subcortical visual areas are much better differentiated and much larger than in rats or mice; e.g., V1 is 3 times larger and extrastriate cortex 10 times larger than in a rat of comparable body size.

Furthermore, molecular evidences show that rodents are closer to primates in their evolutionary history than than carnivores, which includes cat, the most commonly used non-primate for visual neuroscience. Primates and rodents both belong to the superorder *Euarchontoglires*, which diverged from *Laurasiatheria* (the superorder of Carnivora) about 85 to 90 million years ago during the Cretaceous. Within *Euarchontoglires*, the evolutionary paths of rodents and primates probably split about 82 to 87 million years ago (Murphy et al., 2001).

The squirrel is an excellent alternative model animal for visual research. Our knowledge about its visual system is quite extensive, including visual behavior, photoreceptor physiology, retinal circuitry, anatomy and physiology of subcortical visual areas, architecture of the visual cortex, and physiology of extrastriate areas. Compared to cats, their superior color vision, trainability, availablity, and their smaller size make them attractive to vision researchers. Physiological recordings from the squirrel LGN, V1, as well as extrastriate areas showed that the rodent visual system can provide physiological information as rich as that of monkeys and cats.

Chapter 3

Spatial summation properties

3.1 Introduction

Before studying the dynamic behavior of center/surround interaction with rapid stimuli, slow, drifting gratings were used to examine the spatial extent to which V1 neurons integrate grating stimuli. The experiments were designed to study the *steady-state behavior* of neurons, which means the analyses were based on the total number of spikes elicited by repeated presentations of drifting gratings, and ignored all transient firing patterns within the temporal period of the gratings. This is opposed to *dynamic behavior*, where the precise timing of spikes and their relation to the stimulus is taken into consideration. Due to the simple spatial-temporal structure of gratings, grating experiments have higher statistical power over dynamic experiments, making them a good starting point for investigating center/surround behavior.

Circular grating patches of varying diameters were used to examine the spatial summation properties of V1 receptive fields of the California ground squirrel. As reviewed in detail in Chapter I, similar experiments conducted with primates and carnivores showed that the firing rate of a typical V1 neuron increases with larger grating size to a moderate extent (about 5° in diameter for cats) and then

started to be reduced. The point of reduction can be conveniently used as a boundary for dividing the RF into two concentric components - a center and a surround. Suppressive effect of the surround was shown to be maximal when the surround orientation was the same as the preferred orientation of the neuron, and minimal when it was orthogonal to the preferred orientation.

Surprisingly, center/surround behavior of neurons in squirrel V1 was found to be significantly different from such patterns. Among all the cells studied, only a small population (10.6%), called Type II cells in this report, responded with reduced firing rates when the diameter of a circular patch of drifting grating grew beyond a certain size (diameter=6° in average). The rest, called Type I cells, responded to bigger gratings with higher or the same firing rates. The majority of Type I cells (74.8%) exhibited suppressive effect when the center/surround boundary was appropriately set and when the drifting direction of the surround diverged from the preferred direction of the center. Those cells are termed Type I_{fs} cells. Type I cells that did not show any suppression are termed Type I_f cells.

Special care was taken in the estimation of the RF size. Four independent measures were made: (i) The minimal response field, (ii) the grating summating field, (iii) the annular minimal response field, and (iv) the reverse correlation kernel. The relationship of these measures was compared in detail.

3.2 Notes on terminology

The meaning of the term **receptive field** (RF) can be ambiguous. It could be used in its most general sense, the region of the visual field where neural responses can be influenced by any stimuli in any way. This this sense, the word receptive field includes the "non-classical" receptive field as well. However, some authors use the term to refer to a particular definition of the "classical receptive field". In the following text, RF is always used in its most general sense. An equivalent term, **integration field** (IF), is also used as a synonym of RF.

The terms **classical receptive field** (CRF) and **non-classical receptive field** (nCRF) are used only in one specific context: in Section 3.5.3 and Section 3.5.5 where one particular operational definition of the classical receptive field (one measured by the reverse correlation technique) is argued to be the most appropriate. In contexts where the author wishes to remain agonistic about the "correct" division of CRF/nCRF, the terms **center RF** and **surround RF** are used. Center (or surround) RF is used to refer to the part of the RF that is being stimulated by the center (or surround) part of a concentric, bi-partitioned stimulus. The term **center (or surround) response** is used to refer to the response of the neuron when only the center (or the surround) stimulus was presented.

Excitation and inhibition are sometimes used in the literature to refer to the modulatory effects of the surround RF. Those terms should be reserved for describing changes of membrane potentials and are never used in the text. More appropriate terms, **facilitation** and **suppression**, are used instead.

3.3 Material and Methods

3.3.1 Animal preparation

The methods of preparation and single-cell recording were essentially the same as described in (Paolini and Sereno, 1998). Acute experiments were performed on wild-caught, adult California ground squirrels (Spermophilus beecheyi) weighting from 400 to 800 grams. The animals were anesthetized with urethane (0.5 g/kg i.p.). During the surgery, lidocaine (Xylocaine 2.5%) was used as a topical anesthetic. Ringer's solution was injected subcutaneously to prevent dehydration. The animal was placed in a stereotaxic instrument and an aluminum post was attached to the frontal part of the skull with screws and dental cement to keep the head of the animal fixed without pressure points during the electrode penetrations and without obscuring the visual field. After a small (2 to 3 millimeter

in diameter) craniotomy on the right hemisphere was made, the craniotomy was covered with a layer of agar (2-3mm thick) to reduce pulsation, as well as some viscous sterile silicone oil on the top to prevent drying.

The animal was not paralyzed. To ensure the immobility of the eye, the pupil of the left eye was first dilated with Cyclogyl (1%), then a thin ring was cemented to the margin of the cornea with a small drop (10 uL) of cyanoacrylate tissue cement. A thin film of silicone oil was placed over the cornea to prevent drying during the course of the experiment. Corrective contact lenses were not necessary to satisfactorily bring the visual display into focus on the retina, because the squirrel eye is practically emmetropic (McCourt and Jacobs, 1984a), ie. with a refractive state close to zero. Retinal focus was accessed with an ophthalmoscope. The squirrels have an extremely elongated nerve head with blood vessels coming from it visible under the ophthalmoscope. This "blind-streak" was mapped onto a translucent hemisphere by back-projecting their image with an ophthalmoscope and was used to ensure that the eye did not move during the recording sessions. The blind-steak is located in the lower hemisphere, about 10° below the horizontal meridian (Long and Fisher, 1983). It was conveniently used as a reference point for establishing the eccentricity of the receptive fields.

Experiments normally lasted 15-20 hours. The temperature of the animal was regulated throughout the session by a water-filled heating pad and a small electric heater. Most animals were supplied with humidified oxygen at the flow-rate of 1.0 mL/m during the experiment. The depth of anesthesia was regularly monitored by checking the breathing rate and heart beat rate.

At the end of the experiment the animal was sacrificed with a guillotine while it was still deeply anesthetized. The brain was immediately removed and fixed (see Histology below). All procedures were approved by the UCSD Institutional Animal Care and Use Committee and followed USDA regulations, as well as the Animal Welfare Act. Wild animal trapping conformed with California Fish and Game regulations.

3.3.2 Recording

Tungsten electrodes (250 μm diameter, 10 MΩ impedance, FHC Inc.) were used to record extracellular electrophysiological activity. The electrode was introduced vertically into the cortex using a stepping motor micromanipulator. The anesthetized animal monocularly viewed a SGI CRT monitor (mean luminance 10.9 cd/m^2, maximal luminance 28.4 cd/m^2, calibrated by a LMT L1003 photometer), placed 30-45cm away from the animal, for programmed stimulus sequences, generated by a SGI O_2 workstation running at 100Hz refresh rate. Signals were amplified and bandpass filtered (500 to 5000 Hz) by a BAK MDA-3 differential amplifier (BAK Electronics, Inc., Germantown, MD., USA.). Spikes were digitized at 44kHz and sorted with a multi-threshold discriminator using a second SGI O_2. Spike waveforms were stored for off-line spike sorting.

3.3.3 Histology

At the end of each experiment, the penetration site was marked either by lesioning the cortex with a small current or by a small amount of ink. Immediately after the brain was removed, the cortex was separated from the mesencephalon, brainstem and cerebellum, and the white matter removed with dry Q-tips (Olavarria and Van Sluyters, 1985; Tootell and Silverman, 1985). A Small cut was made in the posterior cingulate cortex and the rostral pole to facilitate the unfolding and to reduce distortion. The cortex was flattened between glass slides and fixed in 3.7% formalin with 20% sucrose added a few days later. It was then attached to the stage of a freezing microtome at -15°C, cooled further and sectioned at 50μm, and then stained for myelin the following day (Gallyas, 1979). The electrode penetration sites were recovered and confirmed to be within visual area V1, which was identified by the stereotypical myelination pattern of the flattened cortex (see Figure 1 in Paolini and Sereno (1998)).

3.3.4 Basic tuning curves

The location, dimensions, and orientation selectivity of the minimal response field (MRF) was first roughly "hand-mapped" by a manually operated, high contrast (80%), bright moving bar (width 0.5° to 1.5°; length usually 10°, shorter when appropriate) against a gray background.

Afterwards, the orientation tuning curve[1] and the spatial frequency tuning curve (in that order) of the cell were measured by large (22°-by-22°), hight contrast, square-wave, drifting gratings. The temporal frequency of the grating was not tuned for individual cell to reduce recording time. It was fixed to 3.3Hz, which was able to trigger robust spiking for most of the cells encountered and was reasonably close to the median optimal spatial frequency (5.3Hz) reported by Heimel et al. (2005).

The following parameters were extracted from the tuning curves: (a) Simple vs. complex: all cells were classified as either simple or complex, according to the amplitude of the d.c. component ($F0$) and the first harmonics ($F1$) of their peristimulus time histograms (PSTH). Cells with $F1$ greater than $F0$ were classified as simple. Otherwise, complex (eg. De Valois et al. (1982b)). This simplistic scheme of classification is sufficient for the purpose of this chapter, but will be revisited in the next chapter. (b) Half-amplitude bandwidth of orientation tuning: the half-amplitude bandwidth is defined as the sum of the degrees change in orientation to each side of the optimal direction such that the response drops to half of the optimal response (eg. De Valois et al. (1982a)). Gaps between sampled directions (30° apart) were interpolated linearly. For four cells in the data set, the firing rates of non-optimal direction did not drop to half of the peak and their bandwidths were set to 360°. (c) Direction index (DI): $DI = (R^+ - R^-)/R^+$, where R^+ represents the firing rate at the preferred direction, and R^- represents the firing

[1]Since drifting gratings were used, it is more accurate to call the tuning curve direction tuning curve. However, since "direction tuning" is often used to refer to the cell's preference of one direction over the opposite direction, orientation tuning will be used to avoid confusion.

rate at the anti-preferred direction (180° away from the preferred direction). A cell is called direction selective if DI is greater than 0.5.

After obtaining the basic tuning curves of a cell, the border of the MRF (ie. "hand-mapped" receptive field) was delineated by a manually operated, high-contrast, bright bar against a dark background. The experimenter marked-off the MRF by listening to the spikes generated by the cell via a loud speaker.

3.3.5 Center/surround grating experiments

Several arrangements of grating patches were used to examine the behavior of center/surround interactions. They are iconically illustrated in Figure 3.1. In all grating experiments, stimulus presentation for each condition lasted for 2 seconds with 5 to 10 repeats.

(a) Square-wave, drifting gratings of randomized diameters were used to find the spatial extent of stimulus summation. The orientation, spatial frequency, and temporal frequency of the gratings were set to the optimal parameters of the cell. Grating diameters typically ranged from 2° to 24° in 10 divisions. Larger range of diameter (up to 36°) was used for a few cells. Stimulus contrast was 50%. For about half of the recorded cells, gratings of 90% contrast were also used to examine the effect of stimulus contrast on grating summation.

The firing rates as functions of grating diameter will be referred to as the *grating summation curve*. For the majority of cells, the tuning curves could be accurately approximated by the integral of a gaussian function with three free parameters (d, k, r_0) (DeAngelis et al., 1994; Sceniak et al., 1999),

$$r(x) = k \int_{-x/2}^{x/2} e^{(\frac{-2s}{d})^2} ds + r_0 \tag{3.1}$$

where x is the diameter of the grating. The optimal spread of the gaussian is denoted by d. For some cells, an additional gaussian integral was needed to account

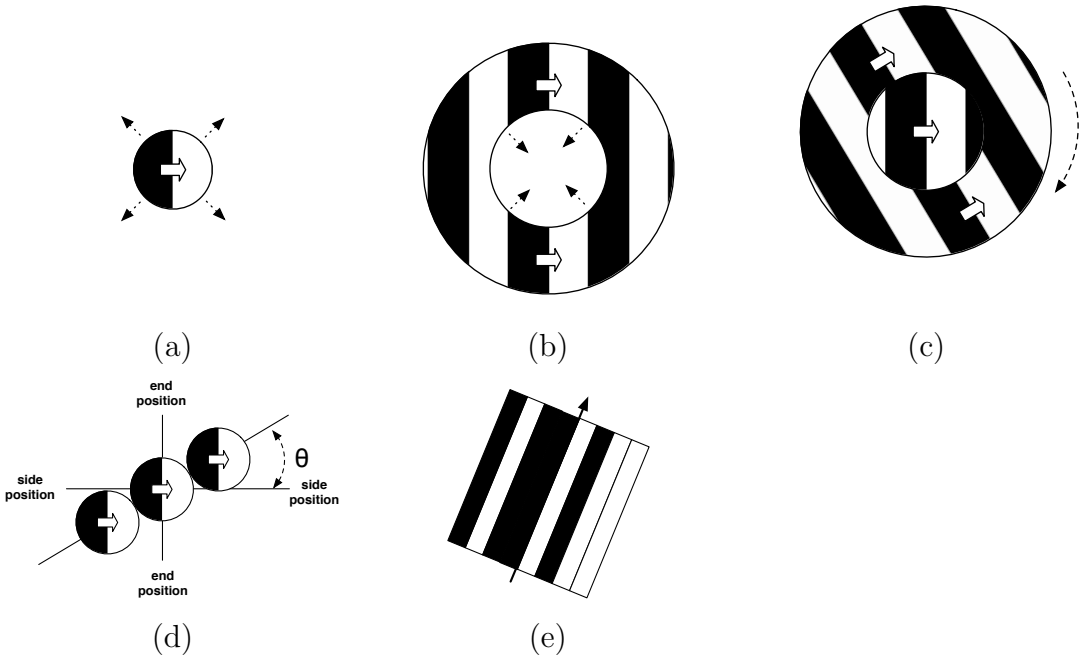

Figure 3.1: (a-d) Iconic representations of the grating stimuli used to probe the center/surround RF. (a) Optimally tuned, sqaure-wave, drifting gratings with varying diameter. (b) Annular gratings with fixed outer diameter and varying inner diameter. (c) Concentrically bipartitioned gratings with fixed drifting direction for the center grating and varying direction for the surround grating. (d) Discrete grating patches where the location of the center patch was fixed and the locations of the two surround gratings (always at the opposite side of the center) varied around the perimeter of the center. (d) The reverse correlation stimulus used to reveal the subfield profile of the RF. The arrow represents the preferred direction of the RF.

for suppression after x reached a certain size,

$$r(x) = k_e \int_{-x/2}^{x/2} e^{(\frac{-2s}{d_e})^2} ds - k_i \int_{-x/2}^{x/2} e^{(\frac{-2s}{d_i})^2} ds + r_0 \tag{3.2}$$

The nonlinear optimization was performed by the NonlinearRegression[] function in *Mathematica*. The goodness of fit was quantified by the percentage of data variance explained by the model.

(b) In addition to grating diameter tuning, a complementary stimulus was used to examine the spatial summation behavior of neurons when the center was

excluded from stimulation - an annulus grating of large outer diameter and randomized inner diameter. The outer diameter was fixed to be as large as the CRT allowed, usually 30° to 40°. Stimulus contrast was always 50%. Firing rates as functions of the inner diameter of the annulus is termed *grating subtraction curves*. The symbol d' is used to denote the point at which an annulus with larger inner diameter triggered less than 10% of the maximal firing rate.

(c) Orientation selectivity of the surround RF was measured using a concentric, bipartite stimulus where the the drifting direction of the center grating was fixed to the preferred direction of the cell, and the direction of the surround grating was randomized, sampled evenly 30° apart. The spatial frequency and temporal frequency of both the center and the surround gratings were set to the optimal parameters. When the direction of the surround grating matches that of the center grating, their spatial phases were always in sync. The boundary between the center grating and the surround grating also varied in a few independent runs (typically started with center diameter=10° and then diameter was decreased or increased). Firing rates in response to the center stimulus alone without the surround stimulus were also measured. Firing rates as functions of the direction of the surround grating are called *grating modulation curves*. The half-amplitude bandwidth of the grating modulation curve was calculated for each cell.

(d) To test if surround effects originated from spatially localized regions, such as end-zones or side-bands, stimuli consisting of three discrete gratings were used. As indicated by the diagram, the location of the surround gratings was represented by θ, which ranged from 0° to 180° (un-inclusive) with $\theta = 0°$ representing the "side" position and $\theta = 90°$ representing the "end-position". The diameter of the of the center patch was fixed and *theta* was randomly sampled. The spatial phase relationship of the three patches was programmed as if a large, optimally tuned, drifting grating was viewed through three apertures.

(e) Three-patch stimulus similar to (d) was used to test if discrete surround regions such as end-zones and side-bands had different modulatory effect

with respect to drifting direction. The direction of the two surround patches was randomly varied in tandem, while the direction of the center patch, as well as the spatial relationship of the three patches, were fixed. The phase relationship of the two surround patches was programmed as if a large drifting grating was viewed through two apertures. Only the side-configuration is illustrated in the diagram although the end-configuration was also used.

3.3.6 Subfield profiles of receptive fields

The reverse correlation method was used to reveal subfield profiles of the RFs so that their dimensions could be compared to the summation/subtraction curves. The stimuli, illustrated by Figure 3.1e, were square patches, evenly divided into 6 to 10 rectangular bars oriented to parallel the preferred direction of the RF (as measured by the drifting gratings). The color of each bar was randomly and independently painted dark or bright (at 50% contrast), updated at 50Hz. The size of the square ranged from 10°-by-10° to 20°-by-20°. The method of analysis is described in detail in the next chapter. In brief, the spike-triggered average and the spike-triggered covariance were calculated. The size of the receptive field was estimated to be the largest among all the kernels.

The significance of the magnitude of kernels was established by estimating baselines - the averaged maximal and minimal magnitude of kernels calculated from -500 ms to -400 ms before spikes. Kernels were considered significant if the magnitude was outside the range of the baselines.

For a small number of cells (N=8), two-dimensional reverse correlation stimulus was used.

3.4 Results

The results are based on 175 cells. Among them, 64 cells (36.6%) were classified as simple, and the rest (N=111, 63.4%) complex. The median half-amplitude bandwidth of orientation tuning was 61.3° (mean=81.7°, standard deviation=64.0°). 60 cells (34.3%) were direction selective. The behavior of center/surround interaction is classified into three types, I_{fs}, I_f, and Type II.

3.4.1 Spatial summation: Type I cells

Grating summation curves

The extent of spatial summation of a neuron was estimated by a circular grating patch with varying diameter (Figure 3.1a), and the firing rate of a neuron as a function of gratin diameter is called its *grating summation curve*. The responses of only a small number of cells (N=20, 11.4%) became suppressed as the diameter exceeded a certain degree. Those cells are called *Type II* cells and are analyzed in the next section. The subject of this section is *Type I cells*, the majority (N=155, 88.6%) whose firing rates increased or remained constant with larger grating diameter. Figure 3.2a depicts the grating summation curve of a representative Type I neuron. The tuning curve was accurately approximated by the integral of a gaussian function (Equation 3.1). The spread of the gaussian, denoted by d, was used as the estimate of the size of the integration field. The tuning curves of most of the cells reached a plateau as the grating diameter grew to a certain point (Figure 3.2c and 3.2d), but some cells showed almost no saturation for the whole range of diameter tested (Figure 3.2e and 3.2f). The estimated d for these tuning curves were bigger than the highest diameter tested and the fitted curves were effectively linear. To make the RF size estimation more conservative, d of these cells were clipped to the largest grating diameter tested.

Statistics involving the d parameter were all calculated from grating sum-

mation experiments using 50% stimulus contrast. However, for about one third of the recorded cells, gratings of higher contrast (90%) were also used to examine how stimulus contrast influenced grating summation. The effect of stimulus contrast on grating summation for two representative cells is depicted in Figure 3.3. The 90%-contrast curves and the 50%-contrast curves almost paralleled each other and the 50%-contrast curves never exceeded the 90%-contrast curves. This demonstrated that the 50%-contrast curves plateaued not simply because maximal firing rates were reached, but were under the influence of a mechanism similar to contrast gain normalization (Heeger, 1992), which prevents a neuron from confounding a small, high-contrast stimulus with a large, low-contrast stimulus.

The grating subtraction curves

A complementary stimulus was also used to study the behavior of spatial stimulus summation when the center of the RF was not stimulated. The stimulus, illustrated by Figure 3.1b), consisted of an annular patch of grating with a large, but fixed, outer diameter and a varying inner diameter. The firing rates as functions of the inner diameter are called the *grating subtraction curves* and are depicted by dashed lines in Figure 3.2. The point at which the tuning curve dropped below 10% of the maximum is denoted by d' and is indicated by a filled arrow in the figure.

A curious feature of the grating subtraction curves of some cells (such as (b) and (e) in Figure 3.2) was that they declined gradually (instead of abruptly like (d) and (f) in Figure 3.2) and that they had long tails. Those cells responded with above-spontaneous-rate even when the center of the RF was excluded from grating stimulation. According to the "center drives, surround modulates" model of RF organization, it is possible that when the center of the RF was not stimulated, the surround RF had nothing to modulate and therefore only served to raise firing rate and was not selective to stimulus features. This hypothesis was tested by measuring

the orientation tuning curve with an annulus stimulus. Figure 3.4a compares the orientation tuning curves as measured by a large grating (solid line) and by an annular patch of grating (dashed line). The annular grating, with a "hole" as large as 12° in diameter, produced a orientation tuning curve very similar to those produced by the full grating, therefore demonstrating that the non-silent surround RFs were selective to grating direction even when the center was not stimulated.

This pattern, however, was not found in all Type I cells. Type I_f cells, a subtype of Type I cells which will be described in Section 3.4.3, did not show clear orientation selectivity when stimulated by annular gratings. An example is shown in Figure 3.4b.

Population statistics about grating summation and subtraction

The distribution of d and d' are displayed as histograms in Figure 3.5a and 3.5b, respectively. Both were broadly distributed. d ranged from 2.9° to 38.4° with mean 15.2° and median 13.6°. d' ranged from 3.6° to 32.0° with mean=13.5° and median=13.0°. Figure 3.5c depicts the histograms of $d - d'$. The mean was 1.9. The percentage of cell with $d > d'$ was 57.2%. For 40% of the cell, the difference between d and d' was smaller than 2°. As a whole, d and d' were barely significantly different (Paired Wilcoxon test. p=0.06, V=616.5).

The joint distribution of d and d' is shown in Figure 3.6a, with red dots representing complex cells and blue dots representing simple cells. Unsurprisingly, d and d' were postively correlated (correlation=0.26, p=0.001). Figure 3.6c displays the same information in a slightly different format: d (x-axis) against $d - d'$ (y-axis). Note that except for three cells, d' for all cells with $d >= 17.0$ was smaller than d. Incidentally, $d = 17.0$ (represented by a dashed vertical line in the figure) corresponds to the valley separating two peaks in Figure 3.5a. There are 58 (37.2%) such cells among Type I cells.

In contrast to the extensive grating summation fields as estimated by d

and d', the MRF was much smaller. On average, d and d' were 3.6x and 3.0x the size of MRF. The distribution of MRF diameter, whose histogram is depicted in Figure 3.5d, ranged from 2° to 10° with mean=4.7° and median=5.0°. Mean MRF was not statistically influenced by simple/complex classification nor direction selectivity. MRF diameter correlated stronger with d' (correlation=0.58, p=0.0005) than with d (correlation=0.35, p=5.662e-10).

3.4.2 Spatial summation: Type II cells

The responses of a small number of cells (N=20, 11.4%) began to be suppressed as the grating diameter exceeded a certain degree. They are termed Type II cells. Among the Type II cells, six were simple (31.6%) and six were directionally selective (not the same six). For most cases (such as those shown in Figure 3.7a, b, and c), the tuning curves can be approximated as the balance (ie. difference) of two spatially overlapping mechanisms, one facilitatory and one suppressive, each modeled as a gaussian envelop (DeAngelis et al., 1994; Sceniak et al., 1999). The spatial extents of the two mechanisms are represented by the spreads of the two gaussian functions and are denoted by d_e and d_i, respectively. The tuning curves of three cells among the seventeen had rises and drops too steep to be approximated well by gaussian envelops. The cell depicted by Figure 3.7d was such an example, where the the model significantly underestimated the peak firing rate and accounted for 73% of the variance.

The suppressive fields of some cells were extensive. The suppression of the cells depicted in Figure 3.7a and b, for example, continued to grow for almost the entire range of grating diameter tested[2]. The suppression field of 3.7c, however, was smaller, having reached saturation before 10.0°. The annular gratings typically elicited spike rates only slightly higher than spontaneous rates, presumably due to the extensive suppression field. d' for Figure 3.7a and d could be not reli-

[2]The estimated d_i for 3.7a was 40.2°, well outside the range of grating diameter tested.

ably established because the responses were close to the spontaneously rates. The annular grating experiment was unfortunately not tested on Figure 3.7c.

The distribution of d_e ranged from 1.2° to 13.2° with mean=6.2°. They were, on average, half the size of the estimated d of Type I cells. The strength of suppression ranged from 20% to 89% with mean=63.8% and median=67.5%.

3.4.3 The effects of surround direction

Except for the small number of Type II cells, grating summation experiments failed to produce suppression. However, surround effects are known to be dependent on orientation of the surround and it is possible that suppressive effects can be demonstrated by manipulating the drifting direction of the surround stimulus. Concentric, bi-partitioned stimuli, as iconically illustrated by Figure 3.1c, were used to examine this possibility. The drifting direction of the center grating was set to the preferred direction, and the direction of the surround grating was allowed to vary randomly in 30° or 45° interval. For each cell, several settings of the center/surround boundary was sampled, while the diameter of the whole stimulus was fixed to a large value (usually 30°).

Type $\mathbf{I_{fs}}$ cells

Among Type I cells (N=155), 121 of them (69.2%) were suppressed when the direction of the surround grating deviated from the preferred direction. These cells are termed Type I_{fs} cells[3]. Four representative Type I_{fs} cells are illustrated in Figure 3.8. Among the 44 direction selective Type I_{fs} cells, the responses 21 cells (47.7%) was suppressed when the direction of the surround was the opposite of the center direction (Figure 3.8c). For the rest, the responses were not modulated or slightly facilitated (Figure 3.8d) when the surround direction is at the anti-preferred direction. Among the direction non-selective cells, 17 (14.7%) showed

[3]fs stands for facilitation/suppression

direction selectivity in the modulation curves. The direction modulation curves for Type I_{fs} cells had slightly larger half-amplitude bandwidth (1.8x on average) than the orientation tuning curves.

Type I_f cells

Thirty-four cells among the Type I cells (19.4%) did not show suppressive modulation of the center response at all surround directions tested and all center/surround boundary tested. They are termed the Type I_f cells – four of them are illustrated in Figure 3.9. The modulation curves were broadly tuned, even for cells with sharp direction tuning curves, and the facilitation had a slight bias towards the same direction as the center. In some cases, peak facilitation did not occur when the surround direction matched the center direction. Direction selective cells were facilitated by surround even at the anti-preferred direction. The half-amplitude bandwidth of modulation curves of Type I_f cells was, in average, 4.7x the bandwidth of the orientation tuning curves.

Like Type I_{fs} cells, the grating subtraction curves of many Type I_f cells declined gradually and had long tails. Unlike Type I_{fs} cells, however, Type I_f cells, unsurprisingly, showed no clear orientation selectivity when they were stimulated by annular gratings which excluded the center of the receptive field. An example was shown in Figure 3.4b.

Type II cells

The direction modulation curves of four representative Type II cells are shown in Figure 3.10. As can be clearly seen, the center responses were suppressed by the surround grating of all directions.

3.4.4 Spatial inhomogeneity of the surround

As reviewed in detail in Chapter I, some studies in primates and carnivores showed that the surround RF was not homogeneous and that surround effects originated from discrete regions, such as the "sides" or the "ends" outside the center. To look for non-homogeneous structure of the surround, twenty cells were tested with grating stimuli where the surround consisted of two discs which were axially aligned with the center disc (Figure 3.1d). The position of the two grating discs in the surround is characterized by the parameter θ. Since the two discs in the surround were always in symmetrical positions, θ ranged from 0° to 180°, not to 360°. When $\theta = 0°$, the surround discs were in the side position, and when $\theta = 90°$, the end position.

Modulation curves of one representative Type I_{fs} cell (top row), one Type I_f cell (middle row) and one Type II cell (bottom row) are illustrated in Figure 3.11. It is clear from the figure that for Type I cells, facilitatory surround effect primarily originated from the side position. Type II cells, however, appeared to have homogeneous surround RF. The surround stimulus suppressed the center response at all positions.

3.4.5 Subfield profiles of receptive fields

To receptive fields of V1 neurons are composed by elongated subfields, which account for their orientation and spatial frequency selectivity. The arrangement of the subfields can be approximated by Gabor wavelets (Jones and Palmer, 1987c), which from the foundation of many computational models of V1 neurons. The reverse correlation technique was used to provide a map (called *kernels*) of the subfields.

The reverse correlation method and the techniques for calculating kernels is described in detail in Chapter IV. To produce two-dimensional maps of the RF, two-dimensional white-noise stimuli (that is, grids of squares which are randomly

and independently turned bright or dark) were needed. Such stimuli required very long recording time for the kernels to converge and they failed to drive many V1 neurons. For these reasons, two-dimensional reverse correlation was used on only a small number of cells (N=8). To reduce recording time, the standard two-dimensional white-noise stimulus was simplified by dimension reduction: Taking advantage of the orientation selectivity of V1 neurons, RFs were assumed to be homogeneous alone the axis paralleled to the optimal orientation of individual cells. The stimulus was divided into 6 to 10 paralleled bars, as illustrated by Figure 3.1e. The color of each bar was randomly and independently turned bright or dark at 50% contrast, updated at 50Hz rate. Such stimulus produced only the profile, or cross-section, of the RF along the width dimension.

Spike-triggered average (STA) and spike-triggered covariance (STC) techniques were used to estimate the width of the RF. Figure 3.12 depicts the estimated spatiotemporal kernels of one complex, Type I_{fs} cell. The width of the CRF was estimated to be 7.5°, based on the magnitude of the first eigenvector of the STC matrix, 60 milliseconds (third row from the top, indicated by the filled triangle) before spikes.

The kernel width of 63 cells were estimated by the reverse correlation method. It ranged from 3.6° to 15.0°, with mean=7.4°, median=7.5° and standard deviation=2.3°. The distribution is plotted in Figure 3.6. The kernel width was in general larger than the MRF but smaller than d and d'. On average, the width was 1.5x the size of the MRF. d and d' were on average 2.2x the kernel width. The kernel width was weakly correlated with d (correlation=0.33, p=0.034), d' (correlation=0.14, p=0.36) and MRF diameter (correlation=0.22, p=0.15).

3.4.6 Dimension comparison: an example

To illustrate how the various measurements of RF size relate to each other, additional information about the cell whose RF profile was shown in Figure 3.12 is

given in Figure 3.13. The MRF of the cell was estimated to be 6.0° and the kernel width 7.5°. The grating subtraction curve of the cell had a long tail with $d' = 18.6$ (Figure 3.12a), meaning that an annulus grating completely outside the CRF was able to trigger spikes. The "non-silent" surround response was most likely orientation selective, like those shown in Figure 3.4. Since the reverse correlation kernels provided no information about the length of the CRF, a possible explanation was that the cell had a CRF whose length was much longer than its width and that the long tail was caused by the annulus stimulus entering the long CRF from the two ends. This hypothesis was proven false by the two-dimensional RF map shown in Figure 3.13b. The width and the length of the CRF were approximately 6° to 8° with no obvious elongation.

The surround direction modulation curve of this cell was shown in Figure 3.8b. The curve was measured with a concentric bipartite grating whose center was 12° in radius. The surround stimulus was clearly completely outside the CRF.

3.4.7 Relationships between summation properties and basic tuning properties

The numbers of cells for the three summation types are summarized in Table 3.1a. The figures are further broken down according to their simple/complex classification (Table 3.1b) and direction selectivity (Table 3.1c). The distribution of neither simple/complex classification, nor direction selectivity, was influenced by summation types (Two-way χ^2 tests. Simple/complex: $\chi^2 = 0.43$, $p = 0.80$. Direction selectivity: $\chi^2 = 0.73, p = 0.68$). Since the binary classification of simple/complex and direction selectivity involved thresholds that were arguably arbitrary, the distributions of F1/F0 and DI were also directly compared. Neither was influenced by summation type (One way Kruskal-Wallis test. F1/F0: Kruskal-Wallis χ^2=2.9, p=0.23. DI: Kruska-Wallis χ^2=0.75, p=0.68).

Basic statistics about the half-amplitude bandwidth of orientation tuning

curves are tabulated in Table 3.2, broken down according to (a) simple/complex classification and (b) summation type. Simple cells, in average, had slightly sharper orientation tuning curves than complex cells, although the difference was not significant (Kruskal-Wallis χ^2=3.54, p= 0.059). The distributions of bandwidth for the three summation types were significantly different (Kruskal-Wallis $\chi^2 = 20.92$, p= 2.859e-05). Type II cells had broader orientation tuning curves than Type I cells. Since the screening procedure of this study was intentionally biased toward selecting sharply orientation selective cells, it is possible that Type II cells were under represented in the data set. The difference between I_{fs} cells and I_f cell in bandwidth was not significant (Kruskal-Wallis χ^2=0.205, p=0.65), implying that the suppressive effect of I_{fs} was likely not related to sharpening of direction tuning curve. Furthermore, neither d nor d' correlated with orientation bandwidth.

Next, the relationships between d and d' and the basic tuning properties of Type I cells were compared. The small population of Type II cells was not included in the analysis because they clearly had much smaller d and d'. The joint distribution of d and d' is plotted in Figure 3.6a, with color code representing simple/complex classification. The distribution of d was not influenced by simple/complex types. There was a weak relationship between cell types and d': complex cells had larger d' than simple cells (Simple cells: mean=11.5°. Complex cells: mean=14.8°. Single-tailed Wilcoxon test: W=1464, p=0.038). Furthermore, neither d nor d' was influence by direction selectivity.

The joint distribution of d and d' is plotted in Figure 3.6b, with color code representing I_{fs}/I_f classification. Neither d nor d' significantly depended on I_{fs}/I_f classification. The numerical values for these statistics are tabulated in Table 3.3.

The distribution of $d-d'$ was not significantly different between Type I_{fs} and Type I_f. $d-d'$ was also not influenced by simple/complex classification, orientation bandwidth, or direction selectivity.

Table 3.1: (a) The number of cells for each summation type. The numbers are further broken down according to their (b) simple/complex classification, and (c) direction selectivity.

(a)

Summation	N	Percentage
I_{fs}	121	69.2%
I_f	34	19.4%
II	20	11.4%
Total	175	100%

(b)

Summation	Complex	Simple	Total
I_{fs}	76 (68.2%)	45 (37.2%)	121
I_f	21 (61.8%)	13 (38.2%)	34
II	14 (70.0%)	6 (20.0%)	20
Total	111 (63.4%)	64 (36.6%)	175

(c)

Summation	Dir selective	Dir non-selective	Total
I_{fs}	44 (36.4%)	77 (63.6%)	121
I_f	10 (29.4%)	24 (70.6%)	34
II	6 (30.0%)	14 (70.0%)	20
Total	60 (34.3%)	115 (65.7%)	175

Table 3.2: Statistics about half-amplitude direction bandwidth, broken down according to simple/complex classification and summation type.

Simple/complex	Median	Mean	Std. dev.
Simple	57.3°	68.8°	39.6°
Complex	66.4°	89.1°	70.0°
Summation	**Median**	**Mean**	**Std. dev.**
I_{fs}	57.6°	65.7°	30.2°
I_f	53.8°	74.6°	54.6°
II	110.0°	127.5°	82.6°

Table 3.3: Statistics about d and d' in (a) and (b) respectively. The population is divided according to simple/complex classification and summation type.

(a)

Simple/complex	Median	Mean	Std. dev.
Simple	13.4°	14.4°	2.8°
Complex	15.6°	16.0°	6.9°
Summation	Median	Mean	Std. dev.
I_{fs}	12.8°	15.2°	7.0°
I_f	13.5°	14.5°	4.2°

(b)

Simple/complex	Median	Mean	Std. dev.
Simple	10.6°	11.5°	4.1°
Complex	14.4°	14.8°	5.0°
Summation	Median	Mean	Std. dev.
I_{fs}	12.0°	13.0°	5.4°
I_f	13.6°	14.0°	5.7°

3.5 Discussions

3.5.1 Summary of findings

The 175 cells in the data set were classified into three types: Type I_{fs} (N=121, 69.2%), Type I_f (N=34, 19.4%) and Type II (N=20, 11.4%). The distinction between Type I and Type II was based on grating summation behavior: Type I cells responded with equal or greater firing rates when stimulated by bigger gratings, while the firing rates of Type II neurons begin to be suppressed when the diameter of the grating exceeded a certain size. Type I neurons were further divided into two subtypes, Type I_{fs} and Type I_f. When stimulated by concentrically bi-partitioned gratings, the center responses of Type I_{fs} cells were suppressed when the direction of the surround grating deviated from the that of the center grating. On the other hand, Type I_f neurons showed no suppression at all surround directions. The modulation effect of the surround was orientation selective for Type I_{fs} cells. The surround effect was not strongly orientation selective for Type I_f cells and Type II cells.

3.5.2 The measurement of RF size

Four different methods were used to estimate the size of V1 receptive fields: (i) A small moving bar (manually operated by the experimenter) was used to map the minimal response field (MRF) - the region in which the stimulus triggers spikes. (ii) Gratings with varying diameter were used to estimate the size of the grating summation field (GSF) - the grating diameter at which neural responses began to reach a plateau (for Type I cells) or start to decline (for Type II cells). (iii) Annular gratings with varying inner diameters and fixed outer diameters were used to estimate the annular minimal response filed (AMRF) - the region outside which a grating stimulus triggers no response. (iv) The reverse correlation method was used to estimate the width of the receptive field "kernels".

MRF diameter and kernel size The MRF (also known as the "hand-mapped" RF) estimated by (i) is the "original" definition of receptive field (Hartline, 1938, 1940; Kuffler, 1953; Barlow et al., 1967). Although it is used by many physiologists as the default definition of the CRF, the MRF can significantly underestimate the "true" CRF because weak or subthreshold regions of the CRF can easily be missed by the experimenter (see Chapter I for details). To address this problem, the reverse correlation method (iv) was used as a quantitative and systematic alternative. The CRF is often conceptualized as localized, oriented filters (the Gabor filters, see Daugman (1985)) and the "kernels" produced by the reverse correlation method are estimations of those filters (see Chapter IV for details about the reverse correlation method and calculation of the kernels).

Except for a few cases (N=8) where two-dimensional maps of the RFs were measured, the reverse correlation stimuli used in this study were composed of arrays of elongated bars (Figure 3.1e) and they only estimated the profiles, or cross-sections, of receptive fields. It follows that only the width of the RF was estimated directly. We believe that the full two-dimensional kernels can be reasonably assumed to be approximately squares because the two-dimensional maps

showed no obvious elongation (Figure 3.13b) and the hand-mapped MRFs were also approximately squares, even for cells with large GSF. The width of the receptive field as estimated by the reverse correlation method will be called the *kernel size* hereafter.

The estimated diameter of the MRF ranged from 2.0° to 10.0°, with mean=4.7°. The estimate is comparable (if slightly larger) to previous studies: average diameter about 2° to 4° (Hall et al., 1971; Sereno et al., 1991). The estimated kernel size ranged from 3.6° to 15.0°, with mean=7.4°. On average, the kernel size was 1.5x the MRF diameter. The kernel size seemed to be larger than expected and it is helpful to compare the numbers to that of the cats, an animal with slightly better visual acuity. The average MRF for cat's V1 neurons at low eccentricity (5°) is about 3.0° to 4.0° in diameter (Nelson and Frost, 1985), and the average kernel size about 3.0° to 6.0° (Jones and Palmer, 1987a; Szulborski and Palmer, 1990; DeAngelis et al., 1994; Ohzawa et al., 1996; Touryan et al., 2002, 2005). The kernel size of the ground squirrel is therefore slightly larger, but still comparable to the cat's.

Grating summation field The most surprising feature about the grating summation curves of the ground squirrel was that the majority (Type I) exhibited no suppression, and that the grating diameter at which neural responses plateaued (denoted by the symbol d) was quite large: mean d for Type I cells was 15.3°, which was about three times the size of the MRF and about twice the size of the reverse correlation kernel. The largest d recorded in the study was 38.4°.

In comparison, the average diameter of the GSF for cat V1 cells was estimated to be about 3.0° to 5.5° (Sengpiel et al., 1997; Walker et al., 2000). It is about twice the size of hand-mapped MRF and the same size as the reverse correlation kernel (DeAngelis et al., 1994; Walker et al., 2000). The average GSF diameter of monkey V1 cells is about 1° to 2°, roughly twice the size of the MRF (Jones et al., 2001; Levitt and Lund, 2002; Cavanaugh et al., 2002a; Angelucci et al., 2002b).

Cells in layer 6 of cat's V1 are known to integrate stimulus up to 8° (Gilbert, 1977) or even more (DeAngelis et al., 1994). However, those "long receptive fields" are flanked by suppressive sidebands (DeAngelis et al., 1994) and they might not produce Type I summation curves when stimulated by circular patches of gratings (Walker et al., 2000). Although in this study, no histological attempt was made to keep track of the laminar distribution of the RFs encountered, some cells with large d were recorded near the cortical surface and were definitely not in layer 6.

Cells in layer 2/3 of tree shrew's V1 exhibit strong length summation (Chisum et al., 2003) and their summation curves are comparable to Type I cells. A subtle difference is that the MRF of tree shrew's layer 2/3 neurons are clearly elongated, as opposed to the square MRFs found in the ground squirrels.

Annular minimal response field Annular gratings with fixed outer diameters and varying diameters were used to measure the annular minimal response field[4] (AMRF), the region which triggers no spikes above spontaneous level if it is excluded from the stimulus. The tuning curve is called the grating subtraction curve.

The most unusual feature of the grating subtraction curves was that Type I cells had large AMRF - on average 13.5°. This is in contrast to previous studies where the surround was much smaller: AMRF was estimated to be about 3° for cats and monkeys (Li and Li, 1994; Sengpiel et al., 1997; Cavanaugh et al., 2002a).

3.5.3 How large is the CRF?

All four measures discussed in the previous have been used as the definition of the CRF. The MRF is the original definition of the CRF (Hartline, 1938, 1940; Kuffler, 1953; Barlow et al., 1967) and is widely used by visual physiologists. For cat and monkey, the GSF is the diameter where iso-orientation gratings of the surround start to suppress center responses. It is proposed to be the proper defi-

[4]The term is from Cavanaugh et al. (2002a).

nition of the CRF by Sengpiel et al. (1997); Walker et al. (2000) and Cavanaugh et al. (2002a). The AMRF reflects the intuition that the surround only modulates the center responses and should be silent by itself. It is used by Li and Li (1994) as the center/surround boundary. The reverse correlation kernel captures the idea that the CRF generates the basic feature selectivity (ie. orientation and spatialtemporal frequencies) of a neuron and that it can be modeled mathematically by Gabor wavelets (Daugman, 1985; Jones and Palmer, 1987c). DeAngelis et al. (1994) estimated the kernel size of cat's V1 neurons to be similar to the GSF.

The reason why these four independent measures have been (and can be) used as the definition of CRF is because they are in general comparable to each other[5].

The four measures of RF size in this study did not agree with each other. The diameters of the GSF and the AMRF covered a very large range and they were in average too large (GSF: 15.3°, AMRF:13.5°) to be comfortably called the CRF for two reasons: First, the CRF of the cat is estimated be to less than 6° in diameter by any of the four methods. It seems unreasonable to conclude that the ground squirrel had much larger CRF, given the fact that the two species have similar visual acuity (cat: 6 c/d vs. ground squirrel: 4 c/d). Second, the CRF is thought be be mainly mediated by feedforward projections in the visual cortex and the nCRF by horizontal and/or feedback connections (see Chapter I for review). Receptive fields as defined by the GSF or the AMRF seemed to be too large for the spread of feedforward terminals. Furthermore, using AMRF as the CRF was problematic because the grating subtraction curves of many cells were smooth with no obvious discontinuity, indicating no discrete "silent" surrounds.

As pointed out by many authors, the MRF is most likely too small for the CRF because it is easy for the experimenter to miss weak or subthreshold RF subfields. Additionally, DeAngelis et al. (1992) and Walker et al. (2000) convincing

[5]As discussed in detail in Chapter I, there are systematic differences among them. The MRF is the smallest among them.

argued that the size of the MRF is too small to explain spatial frequency tuning of V1 neurons. For many cases in the current study, the estimated MRF was too small for gratings to trigger spikes.

Overall, the reverse correlation kernels seem to be the most appropriate operational definition for CRF among the four. It size covered a smaller range (3.6° to 15.0°), was more uniform (standard deviation=2.3°), and the average size (7.4°) was much closer to the estimated CRF size of the cat.

Using the reverse correlation kernel as the CRF, it is reasonable to say that the surround RF for squirrel Type I cells was (iso-directionally) facilitatory because the GSF was much larger than the kernel size. This is in contrast to a substantial number of previous studies where no surround facilitation was found (Fries et al., 1977; DeAngelis et al., 1994; Knierim and Van Essen, 1992; Sengpiel et al., 1997; Walker et al., 1999, 2000; Cavanaugh et al., 2002a). Sengpiel et al. (1997), for example, reported that the grating summation curves of 44% of cat's V1 cells did not show suppression, but the saturation point was about 3.0°, approximately the size of the MRF. The surround RF of those cells were un-suppressing, but not facilitatory.

3.5.4 Surround facilitation

Despite the large number of reports on surround suppression, facilitation has been reported by a few studies[6]. Using high-contrast drifting gratings similar to those used in this study, Li and Li (1994) reported that about 17% of cat's V1 neurons were facilitated by the surround. The reported GSF was about three times the size of the MRF - very similar to the ratio found in this study. Furthermore, discrete patches of iso-oriented stimuli (bars, gratings, or gabor functions) arranged colinearly (similar to Figure 3.1d at "end" position) reliably produced facilitation when the contrast of the center was low (Nelson and Frost, 1985; Polat et al., 1998;

[6]As discussed in Chapter I, some of those reported facilitatory effects probably were due to underestimation of the CRF and were therefore not genuine facilitation.

Kapadia et al., 1995; Toth et al., 1996; Kapadia et al., 2000; Mizobe et al., 2001).

Because the AMRF was significantly larger than the MRF and the kernel size, it is implied that although the regions immediately surrounding the MRF was silent when stimulated by a small, localized stimulus, they were not always silent when stimulated by the more extensive annular gratings. Figure 3.4a shows that, for Type I_{fs} cells, the non-sillent surround responses was orientation selective, even when the center was excluded from stimulation. Non-silent surround was reported previously by some researchers (Sillito et al., 1995; Knierim and Van Essen, 1992). Unlike the facilitation effects of the squirrels, the non-silent surrounds in those reports were suppressive when stimulated together with the center. Furthermore, the non-silent surrounds in Knierim and Van Essen (1992) were not orientation selective when stimulated alone.

3.5.5 Orientation and direction selectivity of the surround

The grating summation curves of Type II cells were similar to typical grating summation curves found in cats and monkeys. However, unlike those reports where surround suppression was typically orientation selective, Type II squirrels cell were suppressed by all surround orientations (Figure 3.10) and the suppression was not clearly orientation selective. Surround suppression with no orientation selectivity had been reported previously by Maffei and Fiorentini (1976); Fries et al. (1977); Knierim and Van Essen (1992); Sengpiel et al. (1997) and Jones et al. (2002). Except for Maffei and Fiorentini (1976), orientation non-specific suppression was found in only a small population of cells.

The majority cell type, Type I_{fs}, was found to be facilitated by iso-orientation stimulus. This is in stark contrast to a large number of studies reporting iso-orientation suppression (Blakemore and Tobin, 1972; Nelson and Frost, 1978; Knierim and Van Essen, 1992; DeAngelis et al., 1994; Li and Li, 1994; Sillito et al., 1995; Sengpiel et al., 1997; Jones et al., 2002; Cavanaugh et al., 2002b). However, the

ground squirrel pattern was similar to a class of cells, called peak-facilitatory surround, in cat's V1 reported by Li and Li (1994)[7].

Surround suppression for Type I_{fs} cells occurred when the surround orientation was non-optimal. Maximal suppression typically occurred at the orientation orthogonal to the optimal orientation but not always. This was in contrast to the large number of studies showing minimal suppression or even facilitation at ortho-orientation. A notable exception was the peak-facilitatory surround cells reported by Li and Li (1994).

Ortho-orientation suppression for V1 neurons has been reported by a number of studies (Morrone et al., 1982; Bonds, 1989; DeAngelis et al., 1992), although those effects were obtained under very different conditions: when a ortho-orientation grating is superimposed on a grating driving a cell, the response is suppressed. The suppression is orientation non-specific and originated inside the classical receptive field.

Direction selectivity of a cell was determined by a large grating which certainly covered some, if not all, of the surround RF. Since direction selectivity of the center RF by itself was not measured, it was not possible to decide if the center and the surround had the same direction selectivity. As measured this way, Type I_{fs} cells that were direction nonselective mostly (91%) had surrounds that were also direction nonselective. A small number of cells displayed slight direction selectivity, such as the cell shown in Figure 3.8a.

Surround modulation of Type I_{fs} cells that were direction selective could be either direction selective or nonselective. Figure 3.8c illustrates an example of the former, where the surround was suppressive in the anti-direction but facilitative in the iso-direction. This type of cells accounted for 43.6% of the Type I_{fs} popu-

[7]It is curious that the grating summation curves and surround modulation curves found in the ground squirrel were most similar to (although not completely the same as) the results of Li and Li (1994), using cats. It is even more puzzling that the results by Li and Li (1994) were not duplicated by other cat studies. A highly speculative explanation is that Li and Li (1994) used urethan in anesthesia, which is seldom used by other cat researchers but used in this study.

lation. Similar behavior was reported by Li and Li (1994). Figure 3.8d illustrates an example of the latter, where the surround was facilitative in both directions. Previous studies also demonstrated that direction selectivity of the surround did not necessarily match that of the center (Fries et al., 1977; Nelson and Frost, 1978, 1985; DeAngelis et al., 1994; Li and Li, 1994; Jones et al., 2001; Cavanaugh et al., 2002b).

The surround of Type I_f was always direction nonselective, even for direction selective cells.

3.5.6 Inhomogeneity of the surround RF

As reviewed in detail in Chapter II, earlier researchers of surround suppression concentrated on fixed positions such as the end-zones and the sidebands. More recent work using stimuli similar to what was used in this study (Figure 3.1d) showed that the loci of surround suppression were not necessarily limited to those positions and the distributions were not necessarily symmetrical (Walker et al., 1999; Jones et al., 2001, 2002).

Despite that surround suppression was found to be not necessarily symmetrical, the surround stimulus in this study was always symmetrical in order to increase the magnitude of the surround effect and decrease the number of testing conditions.

Only one Type II cell was tested for surround homogeneity and the surround was suppressive at all positions. More data are needed to conclude if surround is homogeneous for all Type II cells.

Among the Type I cell tested, facilitation always occurred at the end position. Additional evidences to support the observation will be given in Chapter V. Facilitation at end position was reported by Nelson and Frost (1985); Kapadia et al. (1995); Polat et al. (1998) and Mizobe et al. (2001) at low center stimulus contrast.

The orientation of the surround discs in this study was always the same as the center. It followed that the loci of surround suppression for Type I_{fs} cells unfortunately could not be revealed. A few experiments using ortho-orientation was tested in the pilot study but the strength of surround suppression was weak and unreliable. It is possible that the suppressive loci was more extensively distributed in the surround.

3.5.7 Functional considerations

Sharpening orientation tuning Ortho-orientation suppression has long been theorized as a mechanism for sharpening the orientation tuning of V1 neurons (see Ferster and Koch (1987) and Ferster and Miller (2000) for review). Although the hypothesis was not tested directly in the currently study, the lack of correlation between the orientation tuning bandwidth and Type I_{fs}/Type I_f distinction seems to suggest that sharpening orientation tuning is not the main function for ortho-orientation suppression.

Illusory contour Feature selective responses (see Figure 3.4, as well as the results presented in Chapter V) triggered by annular gratings are useful for detecting objects under occlusion, and can be seen as a form of response to illusory contours[8]. Neural correlates of the perception of illusory contour are usually found in extrastriate visual areas, such as V2 (von der Heydt et al., 1984; Peterhans and von der Heydt, 1989), although some observations were made in V1 as well (see von der Heydt (2003) for review). Since the ground squirrel, a rodent, has a more compact visual cortex and fewer number of visual areas than the cat or the monkey, it is plausible that some physiological functions found in cat's or monkey's V2 are found in squirrel's V1. Surround facilitation as a form of illusory contour detection was also suggested by Nelson and Frost (1985).

Contour integration Detection of continuity of visual feature is an im-

[8]Note that the data presented in this report does not necessarily meet all the criteria for "illusory contour", hence "a form of illusory contour".

portant part of Gestalt psychology. Psychophysical experiments demonstrated several phenomena showing improvement in visual detection tasks in the presence of extended features (Field et al., 1993; Polat, 1999). The iso-orientation, co-axial facilitation effect as described in this study is suitable for integration continuous line segments.

Detecting small objects The large integration fields found in most of the neurons in squirrel's V1 seems to imply that the animal would have problems detecting small objects, which is unlikely to be true given the food-gathering behaviors of the ground squirrels in the wild. There are a few possible explanations. First, the size of the integration field does not necessarily determine the ability to detect small features. The large receptive fields of visual area MT, for example, does not entail the lack of resolution in motion detection. Second, although small in number, cells with iso-orientation suppression (Type II) do exist and they can provide tuning for small sizes. Finally, it is possible that the number of Type II cell was under-estimated due to sampling bias. It is possible that Type II cells have distinctive morphology (such as smaller cell body) which makes them difficult to be picked up by sharp electrodes. Cell selection in this study is biased toward sharp tuning in orientation (important for the reverse correlation stimuli in the following chapters), which would undersample the number of Type II cells because they tend to have broader orientation tuning.

Pop-out It is a lot easier to detect a target embedded in a complex background, if the visual features of the target differ from that of the distractors (Nothdurft, 1991, 1993). The phenomenon is called "pop-out", and it is commonly believed to be associated with the iso-orientation suppressive behavior of the surround found in cat and monkey (Knierim and Van Essen, 1992; Kastner et al., 1997). For a neuron to response in a way that parallels psychophysical experiments, the surround receptive field needs to be suppressive selectively at iso-orientation. It is puzzling that such behavior was not found in ground squirrel V1. The straight forward explanation, that the ground squirrel is incapable of per-

forming pop-out tasks, is unlikely since the animal is highly visual and must forage for food in complex environments. A speculative answer is that pop-out related mechanisms are found in other visual areas, such as V2. The large facilitatory summation fields can become the basis of iso-orientation suppression if they are connected to suppressive interneurons.

3.5.8 Implications about cortical circuitry

The stark discrepancy between surround facilitation observed in this study versus suppression reported on cats and monkeys might imply a radical difference in the underlying circuits. However, it is not necessarily the case. Intracellular recording in V1 of the cat revealed (facilitatory) depolarization fields as large as 11° in diameter when stimulated by annular gratings (Bringuier et al., 1999). Iso-orientation surround suppression therefore hinges on the balance of subthreshold facilitation (depolarization) and suppression (hyperpolarization), which explains why the GSF can be altered dynamically by stimulus parameters such as contrast (Levitt and Lund, 1997; Polat et al., 1998; Sceniak et al., 1999; Mizobe et al., 2001; Anderson et al., 2001). It follows that the facilitatory behavior found in the squirrel is not necessarily incompatible with existing literature on the neural circuits underlying RF organization.

Facilitation found in this study is compatible with the popular theory linking center/surround interaction to the horizontal axons in layer 2/3 of the visual cortex (reviewed in Chapter II). The horizontal connections are proposed to be the neural substrate for the large depolarization field by Bringuier et al. (1999), and they are known to make orientation-specific connections with other neurons in cats and monkeys. Under the assumption, it follows that the horizontal connections of the ground squirrel are also orientation selective, even though the anatomical study by Van Hooser et al. (2006) found no discrete clusters of synaptic terminals. This is not a contradiction because V1 of the squirrel seems to lack columnar orga-

nizations for orientation, and therefore the terminals would not form clusters even if they are selective to orientation.

The results discussed in Section 3.4.4 showing that facilitation originated from the end-positions, and not the side-position, of the CRF. The finding is consistent with the physiological and anatomical data obtained in the tree shrew (Bosking et al., 1997; Chisum et al., 2003) and new world monkeys (Sincich and Blasdel, 2001).

More discussions about cortical circuitry can be found in Chapter V.

3.5.9 Basic tuning properties

Tuning properties of V1 neurons of the gray squirrel (*Sciurus carolinensis*), a closely related species, were studied in detail by Heimel et al. (2005). Using the same criterion for simple/complex classification, Heimel et al. (2005) reported a higher percentage of complex cells (75.2%) than the percentage found in this study (63.4%). Complex V1 cells in grey squirrel, cat, monkey, and other animals are reported to be more sharply tuned in orientation selectivity than simple cells. This was also found to be true by the current study although the difference was not statistically significant.

The median half-amplitude orientation bandwidth of the gray squirrel was estimated to be 50° (Heimel et al., 2005), which was comparable to the estimation of this study (61.3°). Only five cells in this study were not orientation selective, although (Heimel et al., 2005) reported the percentage of orientation non-selective cell in the grey squirrel to be 25%. The discrepancy was expected: the screening procedure in this currently was intentionally bias toward orientation selective cells because orientation selectivity is highly desirable for the dynamic stimuli used in the experiments that will be described in later chapters.

The percentage of direction selective cell, defined as $DI > 50$, was 34.3% in this study. If the DI threshold were raised to 66.6, the percentage was 18.0%.

The percentage was about twice as high as reported by Heimel et al. (2005) (10%, DI threshold at 66.6). It is uncertain if the discrepancy was due to the orientation selectivity bias in this study.

3.6 Acknowledgements

Parts of this chapter are being prepared for submission as "Integration of visual information in V1 of the California ground squirrel (*Spermophilus beecheyi*)" by Hsin-Hao Yu, Virginia R. de Sa, and Martin I. Sereno, as well as "Spatialtemporal properties of classical/non-classical interaction in the orientation domain of V1 neurons of the California ground squirrel (*Spermophilus beecheyi*)" by Hsin-Hao Yu, Virginia R. de Sa, and Martin I. Sereno.

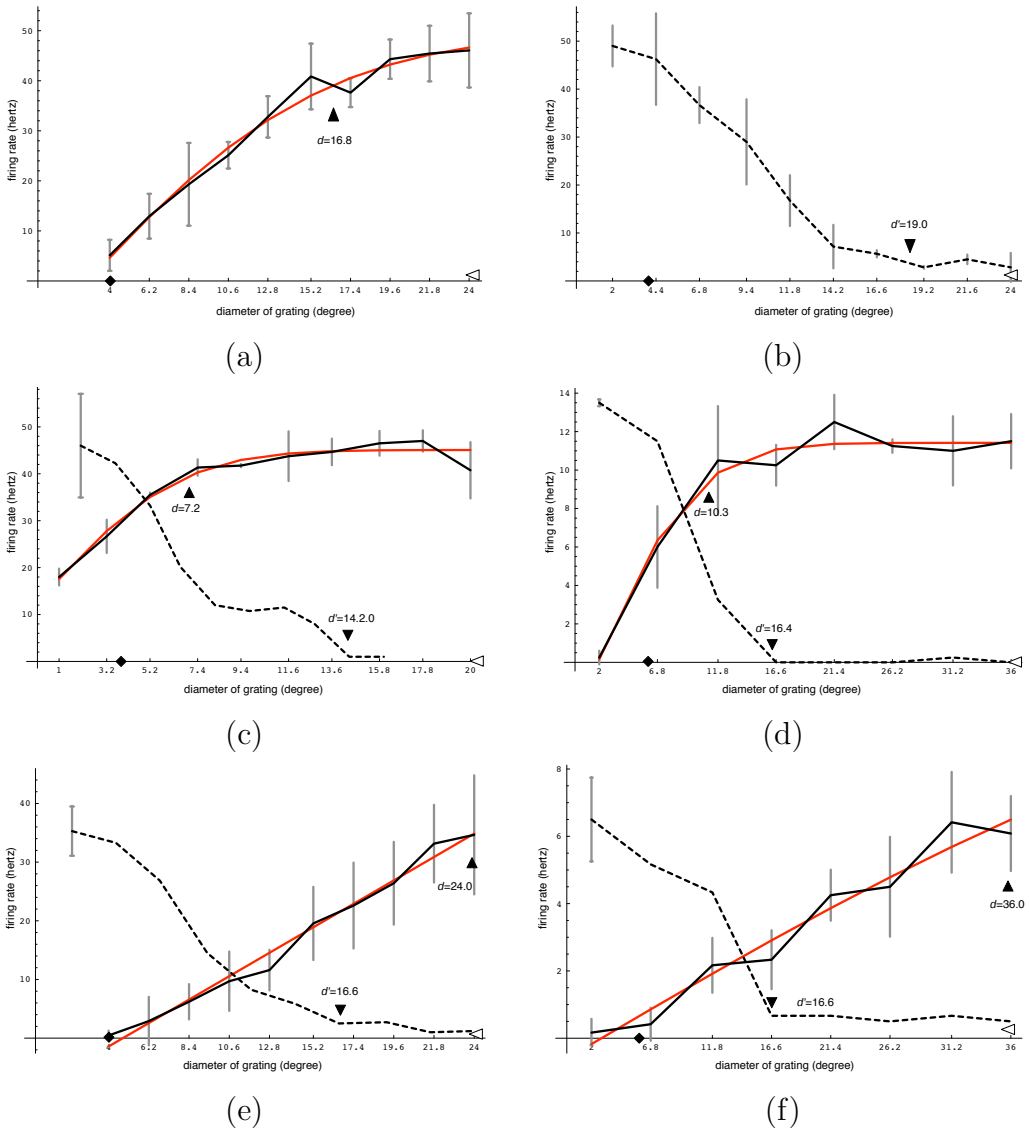

Figure 3.2: Grating summation curves (solid lines) and grating subtraction curves (dashed lines) of five representative Type I cells. Unfilled arrows indicate spontaneous firing level, filled arrows indicate the size estimation, and the diamonds represent the size of the MRF. The grating summation curves were fitted to an integral-of-gaussian model, and the optimally fitted curves are in red. (a) and (b) are the grating summation curve and grating subtraction curve of the same cell. (c-f) are four additional examples where the two curves are plotted together in the same diagram. Only the mean standard deviation of the grating subtraction curves were indicated in (c-f) to avoid clutter. (a-b) Complex, Type I_{fs}, 87% variance explained by the fitted model. (c) Complex, Type I_f, 90% variance explained. (d) Direction selective, complex, Type I_{fs} 88% variance explained. (e) Complex, Type I_{fs}, 80% variance explained. (f) Complex, Type I_f, 82% variance explained.

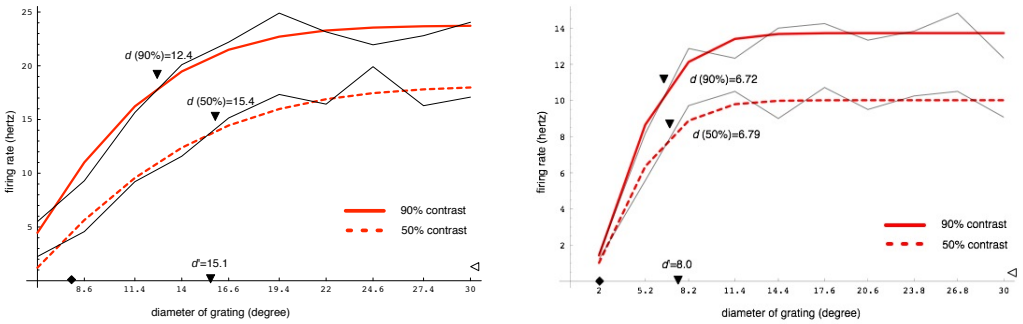

(a) (b)

Figure 3.3: Grating summation curves of two representative cells, measured by gratings of two contrast levels (90%, represented by solid lines, and 50%, represented by dashed lines). The 90%-contrast curves were higher than 50%-contrast curves at all grating sizes, indicating that the 50%-contrast curves reached plateaus not because of firing rate saturation, but were influenced by a mechanism similar to contrast normalization. (a) Complex, Type I_{fs}. (b) Simple, Type I_{fs}.

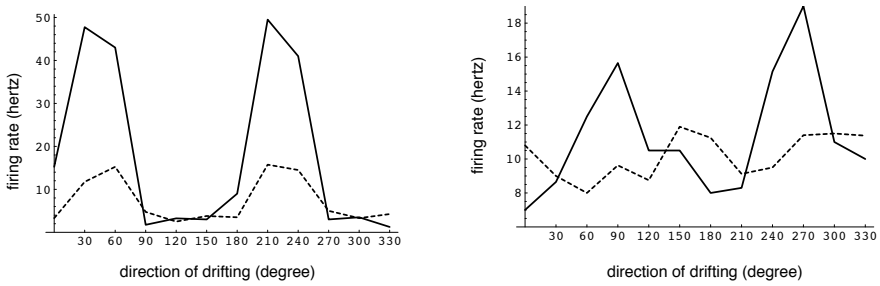

(a) (b)

Figure 3.4: Orientation tuning curves of two cells, measured in two ways: by a $24°$-by-$24°$ grating (solid line), and by an annular grating patch (dashed line). (a) A Type I_{fs} cell. The grating summation curve and subtraction curve of the same cell are plotted in Figure 3.2 (a) and (b), with $d = 16.8°$ and $d' = 19.0°$. MRF diameter=$4.0°$. The inner diameter of the annulus was $12°$ and outer diameter was $30°$. Even when the center of the RF was excluded from stimulation by the annular grating, the responses were still selective to stimulus direction. (b) A Type I_f cell. Complex. $d = 18.4°$, $d' = 18.6°$, MRF diameter=$5.0°$. The inner diameter of the annulus was $12°$ and the outer diameter was $30°$. Unlike the Type I_{fs} cell, this cell did not show orientation selectivity when stimulated by the annular grating. The classification of Type I_{fs} and Type I_f is described in Section 3.4.3.

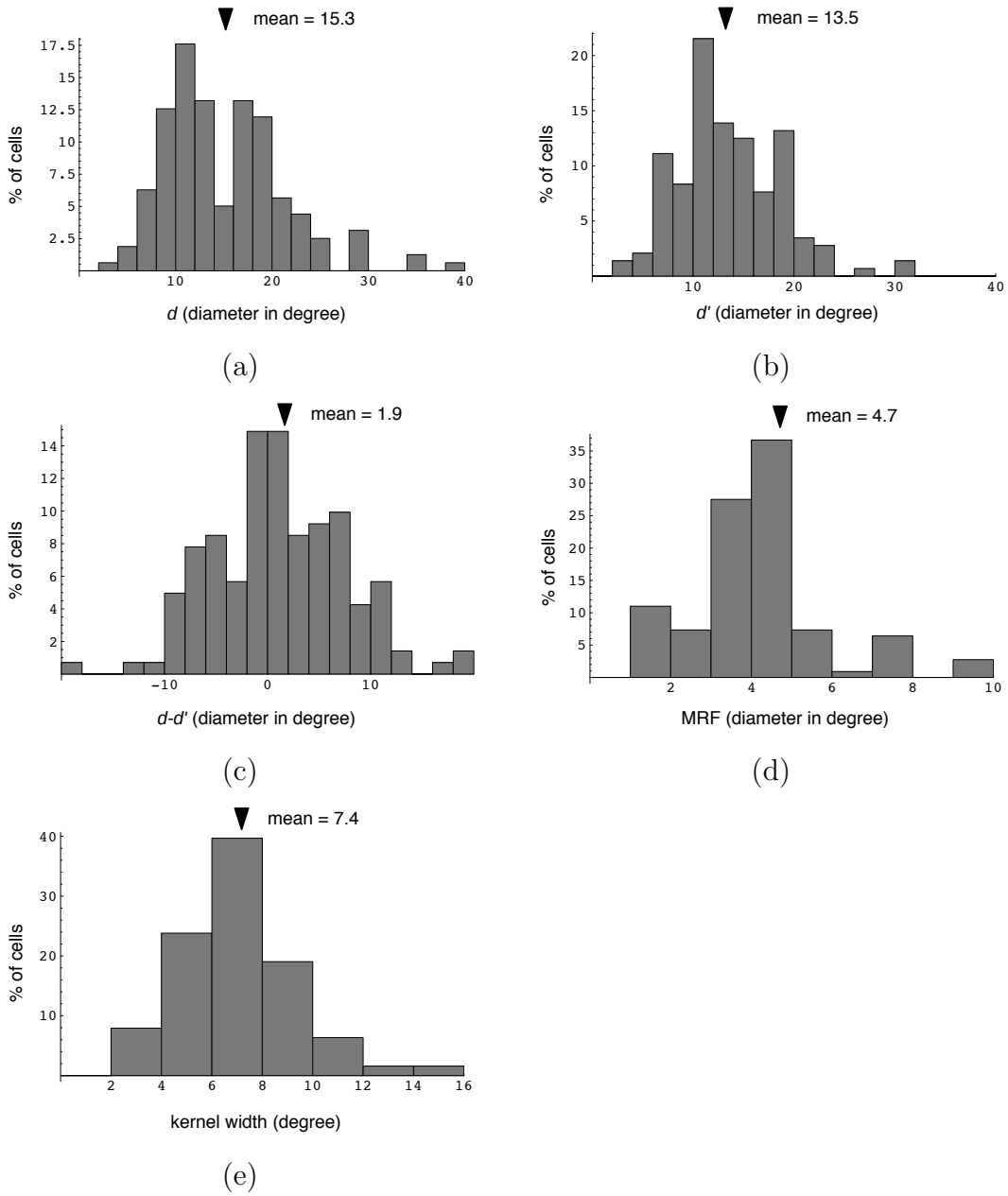

Figure 3.5: The distributions of (a) d, (b) d', (c) $d - d'$, and (d) the diameter of the MRF for Type I cells. (e) The distribution of the width of reverse correlation kernels.

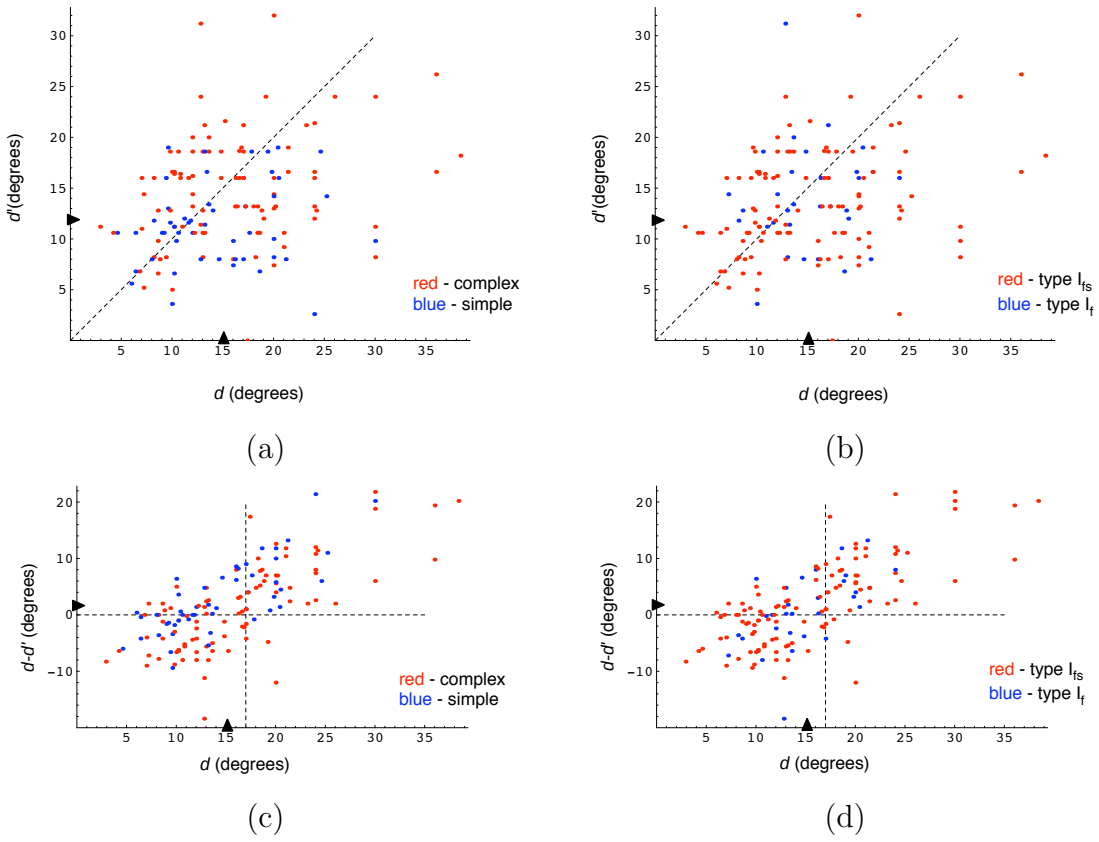

Figure 3.6: (a) and (b): The joint distribution of d and d' for Type I cells. (c) and (d): The same information, plotted as d-vs-$d - d'$. The filled arrows on the axis indicate the means of d and d'. In (a) and (c), red dots represent complex cells and blue, simple cells. In (b) and (d), red dots represent Type I_{fs} cells, and blue dots, Type I_f cells. Dashed vertical lines in (c) and (d) represent $x = 17$.

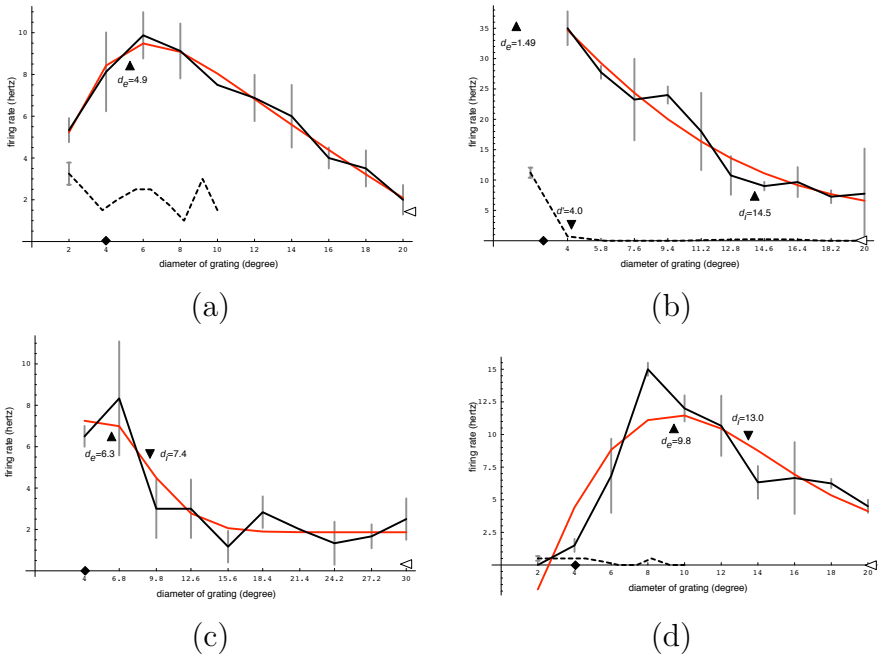

Figure 3.7: Grating summation curves (solid line) and grating subtraction curves (dashed lines) for four representative Type II cells. The grating summation curves were fitted to a model of the difference of a facilitatory mechanism (a gaussian envelop with spread d_e) and a suppressive mechanism (a gaussian envelop with spread d_i). (a) Complex, 86% variance explained by the fitted model. The estimated d_i $=40.2^\circ$ was outside the range of tested grating diameter. (b) Complex, 88% variance explained. (c) Simple, 73% variance explained. The grating subtraction curve was not measured. (d) Complex, 73% variance explained.

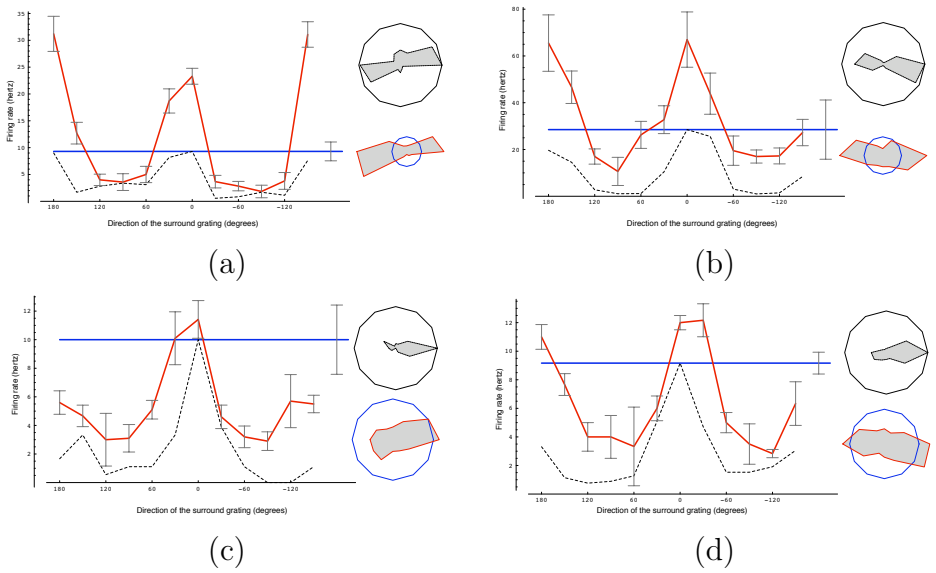

Figure 3.8: Orientation modulation curves of four representative Type I_{fs} cells. The same information about each cell is displayed in two different formats - in cartesian coordinates (left) and in polar coordinates (right). The dashed lines (curves in cartesian plots and polygons in polar plots) represent the direction tuning curves of the cells; the blue lines (straight line in the cartesian plots and circles in polar plots) represent firing rates in response to the center gratings alone; and the red lines represent the firing rates in response to the center and surround gratings. The direction of the surround grating was measured as the angle relative to the center grating. In polar plots, the 3 o'clock direction represents the preferred direction of the cell. The size of the grating used for establishing the orientation tuning curves was not necessarily the same as the diameter of the center grating in the surround modulation experiments. The orientation tuning curves were scaled such that their peaks matched the firing rates of the center-alone conditions of the surround modulation experiments. (a) Simple, d =20.0°, d' =14.4°, b =16.0°. (b) Complex, d =16.6°, d' =18.7°, b =12.0°. (c) Simple, d =9.2°, d' =10.6°, b =9.0°. (d) Simple, d =9.6°, d' =19.0°, b =11.4°.

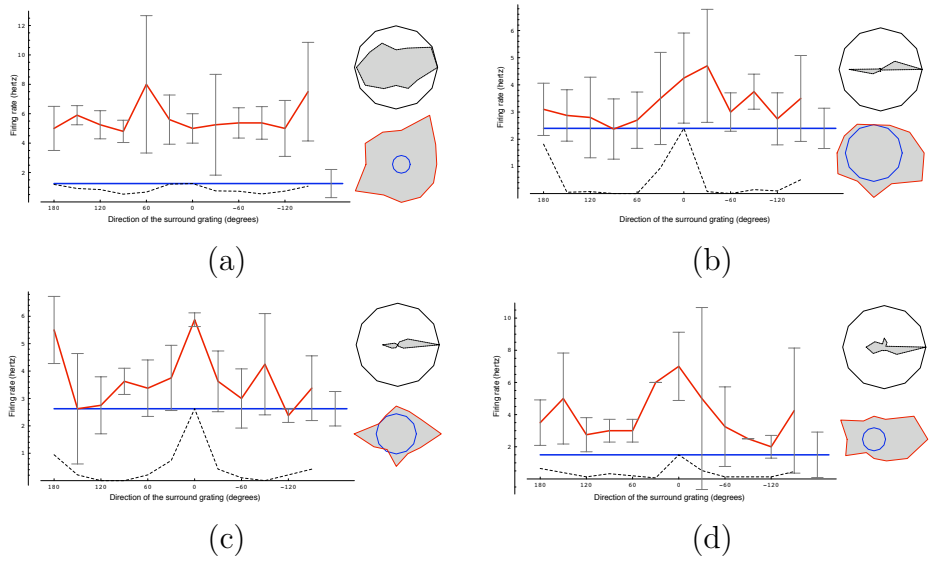

Figure 3.9: Orientation modulation curves of four representative Type I_f cells. (a) Complex, d =7.2°, d' =14.0°, b =6.0°. (b) Complex, d =13.0°, d' =12.8°, b =12.8°. (c) Simple, d =20.4°, d'=19.0°, b =16.0°. (d) Simple, d =10.6°, d' not measured, b =8.0°.

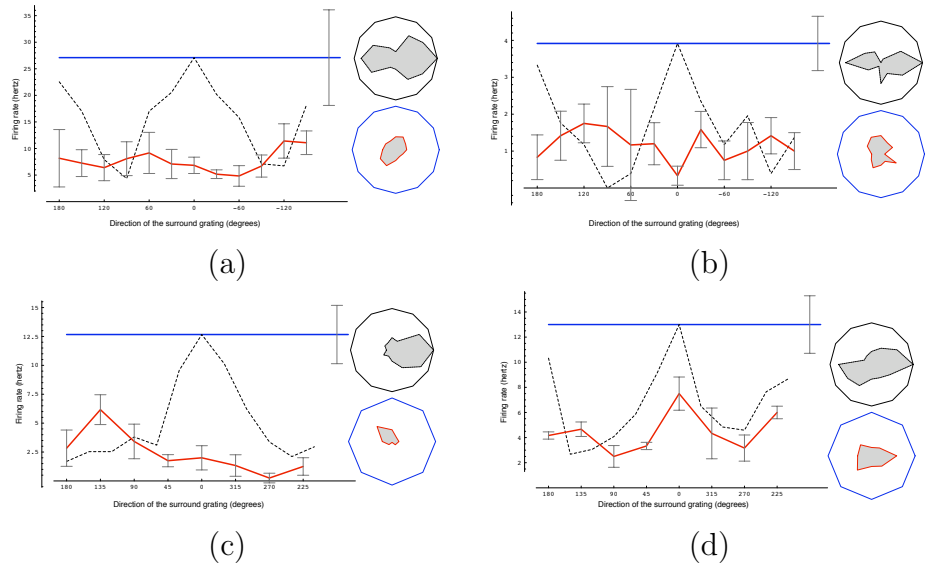

Figure 3.10: Orientation modulation curves of four representative Type II cells. The center responses were suppressed by the surround gratings at all directions. (a) Complex, d_e =1.4°, b =4.0°. (b) Simple, d_e =1.9°, b=4.0°. (c) Complex, d_e =9.6°, b =6.0°. (d) Simple, d_e =3.0°, b =4.8°.

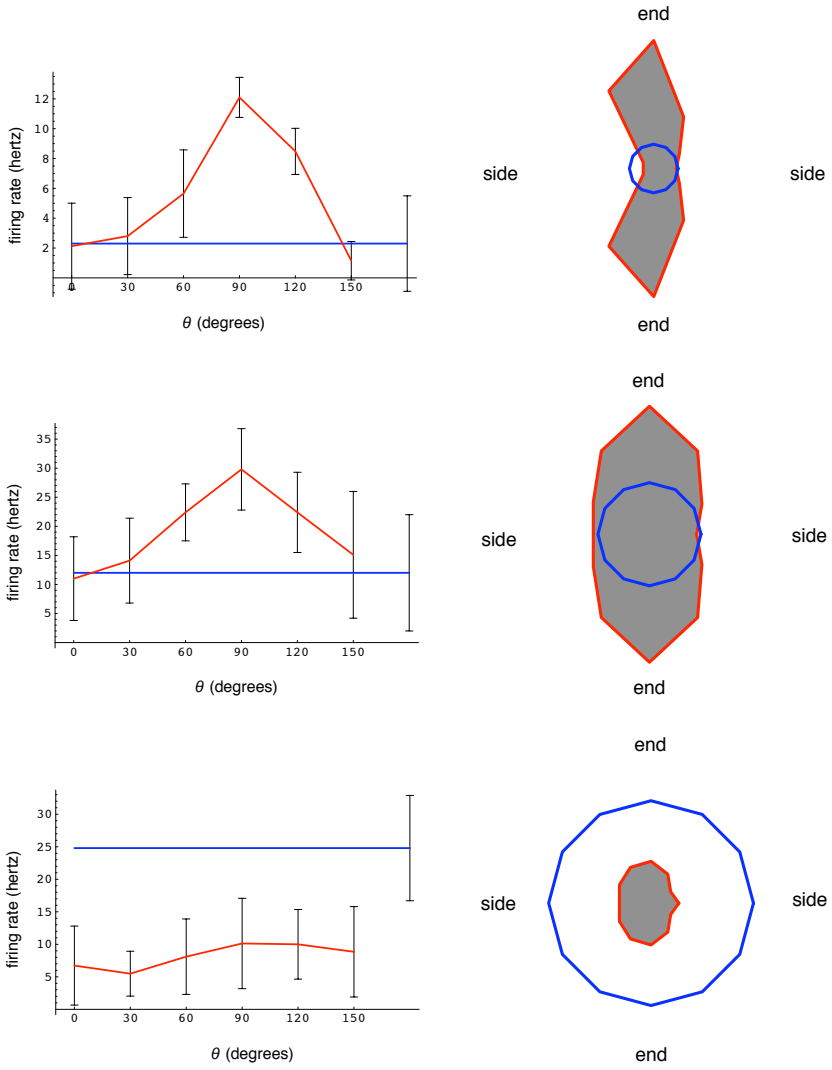

Figure 3.11: Stimuli as illustrated in Figure 3.1d were used to examine if the surround RF was homogeneous. The diameter of the center disc is symbolized by b. (Left column) The blue line represents the firing rate of the cell when only the center was stimulated. The red line represents the firing rate of the cell, as a function of θ, the parameter characterizing the position of the two discs in the surround (side position: $\theta = 0°$; end position: $\theta = 90°$. The same information is displayed in polar plot form in the right column). (Top row) A Type I_{fs} cell. The facilitatory effect of the surround originated mainly from the end position. Complex cell, direction selective, $d = 20.0°$, $d' = 8.2°$, MRF diameter=$3.0°$, $b = 8.0°$. (Middle row) A Type I_f cell. Complex. $d = 18.4°$, $d' = 18.7°, MRFdiameter = 5.0°$.b=$12°$. (Bottom row) A Type II cell. The surround RF was suppressive in all positions. The same cell as Figure 3.7(b). $b = 4.0°$.

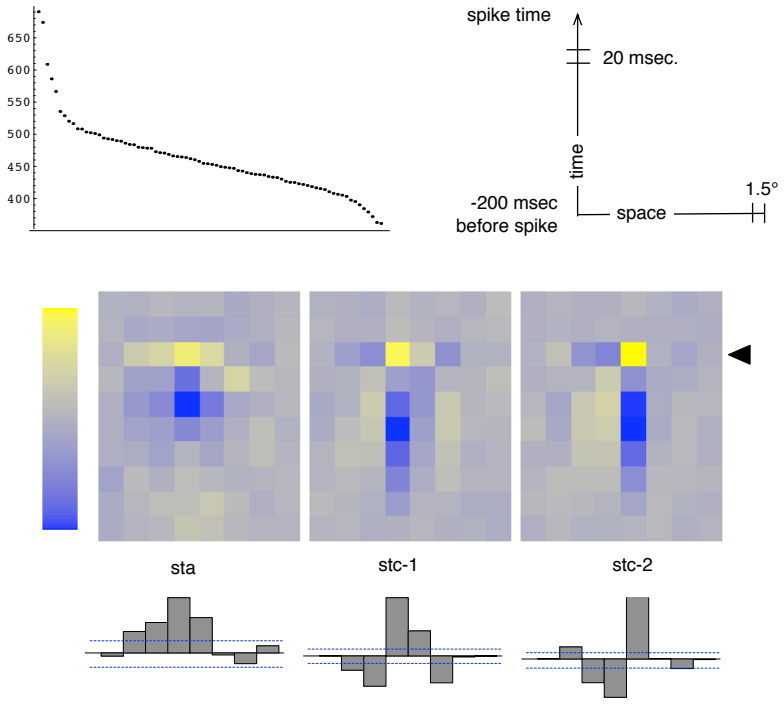

Figure 3.12: Estimating the width of the CRF by the reverse correlation method. The stimulus is illustrated in Figure 3.1e. Results from a complex, Type I_{fs} cell are shown. First row left: the distribution of the eigenvalues of the spike-triggered covariance (STC)matrix. First row right: the format for depicting spatialtemporal kernels. Rows represent space (the eight divisions represent the eight bars in the stimulus) and the columns represent time. The spatial resolution was 1.5° and the temporal resolution was 20 milliseconds. The top of the diagram represents spike time. Second row: the estimated spatialtemporal kernels. (Left) The spike-triggered average (STA). (Middle) The largest eigenvector of the STC matrix. (Right) The second largest eigenvector of the STC. The magnitude was arbitrary, with yellow representing bright and blue representing dark. Third row: the magnitude of the kernels, at -60 milliseconds before spike (third rows from the top in the spatialtemporal kernel, indicated by the filled triangle). The blue dashed lines represent base-line magnitude. The width of the RF was estimated to be 7.5°, based on the magnitude of the first eigenvector of the STC matrix, 60 millisecond before spikes.

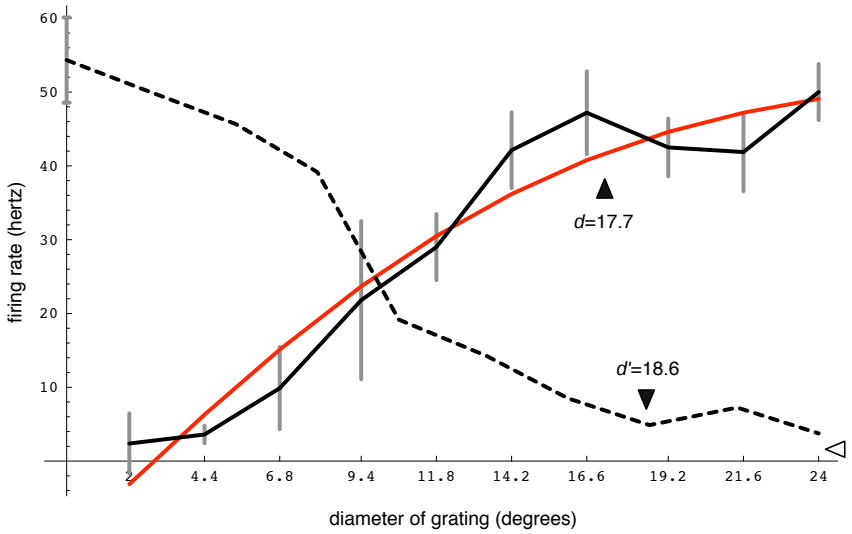

(a)

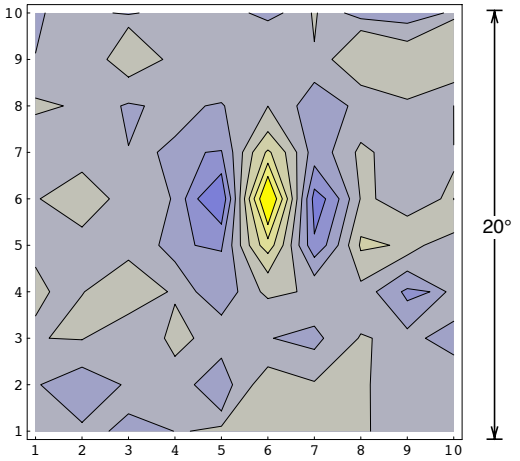

(b)

Figure 3.13: The summation curves (a) and the two-dimensional subfield map (b) of the same cell whose subfield profile was shown in Figure 3.12 and whose surround direction modulation curve was shown in Figure 3.8b. The two-dimensional subfield map was the first eigenvector of the spike-triggered covariance matrix. Unlike the spatialtemporal maps in Figure 3.12, the map was a spatial representation calculated 50 milliseconds before spike. The whole map represented a space of $20°$-by-$20°$ and one pixel represented a space of $2°$-by-$2°$. The size of the CRF was about $6°$ to $8°$ in diameter with no evidence for elongation. The two dimensional map was consistent with the subfield profile.

Chapter 4

Spatialtemporal structure of the classical receptive fields

4.1 Introduction

The stimuli used in Chapter III were mostly based on slowly drifting gratings. A more sophisticated experimental paradigm, the reverse correlation method, was used to reveal the nature of center/surround receptive field that went beyond the power of grating-based experiments. This chapter reports the results concerning the organization of the classical receptive field. The surround (non-classical) receptive field is analyzed in Chapter V and VI.

Drifting gratings are low dimensional stimuli in the sense that they can be completely specified by a small number of variables: direction, spatial frequency and temporal frequency. They are widely used in visual neuroscience because of their simple spatialtemporal structure. The reverse correlation stimuli, on the other hand, are high dimensional. They do not assume a periodic structure spatially or temporally. Furthermore, the stimuli are update at a much higher rate than the gratings (50 hertz vs. 3 hertz) and the analysis technique is sensitive to the precise timing of spikes so that dynamic, rapid events can be unveiled. The

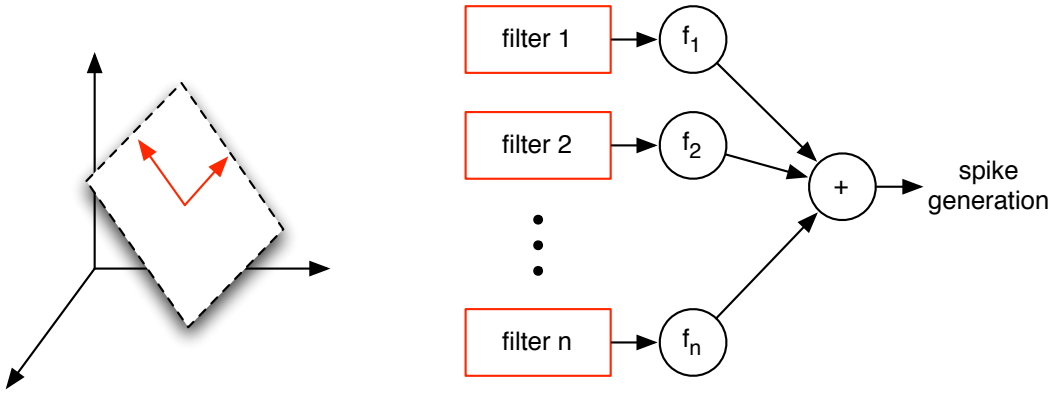

Figure 4.1: The reverse correlation can be interpreted in two ways. (left) A geometrical interpretation: The three dimensional space is an abstract representation of the high-dimensional stimulus space. The spike-triggering ensemble is assumed to lie on a low-dimensional subspace. The STA (not shown in the diagram) and the significant eigenvectors of the STC (represented by red arrows) are used to capture the geometry of the subspace. (right) An algebraic interpretation: the firing of a neuron is assumed to be be determined by a set of orthogonal linear filters, represented by red boxes. The outputs of the filters are modified by nonlinear functions (f_1 to f_n) and their sum is passed to poisson spike generator. The STA and the eigenvectors are estimates of the filters in this interpretation.

next section provides a brief introduction to the methodology. The rest of the chapter reports a reverse correlation analysis of the CRF of squirrel neurons, and compares the results to previous studies using similar methodology.

4.2 The reverse correlation method

Reverse correlation is a framework of experimental design and data analysis that has been applied successfully in the study of sensory coding in the visual, auditory, and tactile systems. The technique originated from the mathematical framework of Volterra series, a generalization of the Taylor expansion to the domain of stochastic processes, which approximates nonlinear systems of arbitrary complexity by a series of orthogonal functions called "kernels". It is proved that the kernels can be estimated individually by subjecting the system to a input of

Gaussian white noise, which is why the method is also known as white noise analysis. Although the full mathematical treatment seems daunting[1], the formulation can be greatly simplified when they are applied to the study of V1 neurons by adopting some assumptions of the system (Chichilnisky, 2001; Ringach, 2004). Intuitively, the basic idea can be explained thusly: the stimulus consist of "white noise", that is, pixels whose intensity are statistically independent from each other, both spatially and temporally. Since this is a high entropy stimulus, a neuron typically responds sparsely. The spatialtemporal patterns of the stimulus preceding each spikes are collected into what's called the *spike-triggering ensemble*. Since there is no statistical structure in the original stimulus, any structure in the spike-triggering ensemble reflects the processing of the neuron.

The key to understanding neural processing thus relies on discovering statistical structures in the spike-triggering ensemble. Multivariate statistics proved to be very useful in this regard. The mean of the ensemble, called the *spike-triggered average* (STA), corresponds to the linear term in the Volterra series and captures the linear behavior of the neuron. STA has been used successfully to reveal the spatialtemporal receptive fields of simple cells, a type of cell in V1 which is more linear in its spatial summation than other cells (Jones and Palmer, 1987a,c; DeAngelis et al., 1993a; Ohzawa et al., 1996). However, other types of cells, such as complex cells, are more nonlinear and requires higher order kernels to account for their behavior (Szulborski and Palmer, 1990). In terms of the geometry of the spike-triggered ensemble, the distribution is no longer a simply isotropical cloud but requires higher order statistics, such as the covariance matrix, to specify. A technique that proves to be very useful in the study of complex cells is to visualize the eigenvectors of the covariance matrix of the spike-triggered ensemble, called the *spike-triggered covariance* (STC) (de Ruyter van Steveninck and Bialek, 1988; Schwartz et al., 2002; Touryan et al., 2002; Rust et al., 2005). It is an application of the Principal Component Analysis (PCA), a standard tool in multivariate

[1]See Marmarelis and Marmarelis (1978); Rieke et al. (1999); Dayan and Abbott (2001).

statistics whose goal is to reduce the dimensionality of high dimensional data to a subspace of lower dimensionality which most efficiently explain the variance in the data. The PCA method works entirely on the covariance matrix and therefore is blind to high-order statistical relationship in the data[2], essentially assuming the spike-triggered ensemble to be gaussian distributed. Alternatively, the STA and STC techniques can be understood as fitting the data to a model which assumes the spike-response as a nonlinear function of the outputs of multiple, orthogonal filters (Rust et al., 2005). The concepts are illustrated in Figure 4.1.

Although the mathematics requires Gaussian white noise, approximations of white noise, usually binary, are used in practice. Various techniques have been developed such that stimuli with statistical regularities, such as natural images, can also be used (Ringach et al., 2002; Smyth et al., 2003; Sharpee et al., 2004; David et al., 2004; Touryan et al., 2005). There are also numerous extensions to the analysis techniques (citation.)

4.3 Methods

4.3.1 Data collection

The methods of animal preparation and data collection were identical to those described in Chapter III.

4.3.2 Stimulus

The reverse correlation stimulus consisted of a circular patch, which was divided into 6 to 10 bars in parallel. The orientation of the bars paralleled the optimal orientation of the cell, as measured by gratings. The color of each bar was randomly and independently turned bright or dark, updated at 50 hertz. The

[2]The Independent Component Analysis (ICA) is an algorithm that works on non-gaussian distributions. See Bell and Sejnowski (1995).

contrast was 50%. The diameter of the stimulus was typically larger than 10°. For most of the cells, a short reverse-correlation sequence covering a larger space (Chapter III) was ran to make sure that the size of the circular stimulus was sufficiently large.

4.3.3 Data analysis

Recovering STA and STC The spatialtemporal vector of the stimulus 200 msec before each spike was collected into the spike-triggering ensemble. The STA was the estimated mean of the ensemble. Each vector in the spike-triggering ensemble was orthogonalized with respect to the STA before the calculation of the STC matrix. This was done to ensure that the eigenvectors would also be orthogonal to the STA vector. It was verified that the eigenvectors of the orthogonalized STC were very similar to that of the unbiased covariance estimator in standard multivariate statistics.

The matrix was analyzed by eigenvalue decomposition (a la the Principal Component Analysis). The eigenvectors corresponding to the largest and smallest ten eigenvalues were visualized as a two-dimesnional spatialtemporal array in pseudo color with yellow representing positive values and blue negative values. For the STA, positive values correspond to brightness and negative values correspond to darkness. For the eigenvectors, the sign was arbitrary. The yellow/blue color scale only represent contrast.

Estimating the dimensionality of the spike-triggered ensemble The distribution of the eigenvalues was compared against that simulated under the null assumption: the spikes were completely random in their relationship to the stimulus. The spikes were randomly shifted, and the eigenvalue calculated for 500 times (Rust et al., 2005). The upper bound and the lower bound of the eigenvalues in those simulations were plotted as two black lines in Figure 4.2, Figure 4.4. Figure 4.6 and Figure 4.7.

Picking significant eigenvectors by comparing the eigenvalues to the null hypothesis proved to be helpful for the big (or "excitatory") eigenvectors but inadequate for the small (or "suppressive") ones. An alternative procedure was used: For each eigenvectors, as well as the STA, two probability density functions were estimated: the projection of the spike-triggered ensemble to that vector, and the projection of the entire stimulus space. The functions were calculated by dividing the projected values into ten discrete bins. The difference of the two distribution was quantified by the KL-divergence (Sharpee et al., 2004). A vector was considered significant if the KL-divergence was greater than 0.025. The procedure was illustrated in Figure 4.8.

The relationship between the KL-divergence and the eigenvalue was not straightforward and KL=0.025 threshold did not correspond to a fix threshold on the eigenvalue. The threshold was selected such that big eigenvalues that "stood out "from the rest were considered significant and that significant eigenvectors were clearly not noise. The eigenvectors were calculated using only half of the spikes to verify that the spatialtemporal structures of the significant eigenvectors were stable in convergence.

The KL=0.025 threshold was arguably chosen arbitrarily. However, it has the advantage of being a uniform criterion with a straightforward interpretation in terms of modeling.

Recovering nonlinearity Bla! say something about bayesian inferencing.

4.4 Results

The report is based on 41 cells, among them 11 were classified simple and the rest complex. The simple/complex classification was based on F1/F0 ratio of the cell's response to an optimally-tuned square-wave grating, at 1.0 cut-off.

4.4.1 Spike-triggering features

V1 neurons are selective to stimulus features, responding only to a small subset of the high-dimensional stimulus space. The spike-triggering ensemble was assumed to lie on a subspace. The STA (spike-triggered average) and STC (spike-triggered covariance) estimates were used to give an economical description of the feature subspace. The STA and the eigenvectors of the STC corresponding to significant eigenvalues are collectively called *kernels*[3]. Eigenvectors corresponding to the top eigenvalues are called "excitatory" kernels[4] and those corresponding to the bottom eigenvalues are called "suppressive kernels".

A few examples of STA/STC analyses are illustrated here to demonstrate the variety of neural behaviors found in the the dataset.

Figure 4.2 illustrates a complex cell. The top row in the figure shows the distribution of the eigenvalues of the spike-triggered covariance in red. The STA and the eigenvectors of the STC are displayed as two-dimensional rasters. The kernels are displayed in the following format: one row represents the spatial kernel at a fix time delay with respect to the spike time. The top of each diagram represents no time delay (ie. spike time). The time resolution is 20 millisecond for one row. The kernels are displayed in pseudo color. The upper (lower) rasters under the STC label in the figure display eigenvectors corresponding to the biggest (smallest) six eigenvalues in decreasing (increasing) order from left to right. The significance of the kernels was estimated by a procedure described in the next section. Those that were selected as significant are indicated by a red dot in a small circle. For this particular cell, the STA, the top two eigenvectors and the bottom eigenvector were significant.

The STA of the cell was vague with no clear subfields. The subfields,

[3]Note that kernels in this sense are closely related, but not mathematically equivalent, to the Wiener or the Volterra kernels used in the context of system identification.

[4]This violates the convention set in the previous chapter, which reserves the word excitation for describing change of membrane potential. However, an exception is allowed this this case to be consistent with Rust et al. (2005).

however, were revealed by the two excitatory kernels. The eigenvectors were spatialtemporally inseparable and tilted, indicating direction selectivity, which was consistent with results from grating experiments. They resembled the quadrature filter pair in the energy model of complex cell (Adelson and Bergen, 1985) . Note that one suppressive kernel was significant, which showed no spatial subfield and was not direction selective like the excitatory kernels. Among the 30 complex cells, 16 had this energy-model-like structure. Two more examples were shown in Figure 4.3.

Figure 4.4 illustrates a complex cell whose kernel structure did not resemble the energy model. The biggest two eigenvalues were not as close to each other as the cell analyzed in Figure 4.2, and the corresponding eigenvectors did not look like a quadrature pair. This type of STC structure was found in six additional complex cells in the dataset. Two are shown in Figure 4.5.

Figure 4.6 illustrates a simple cell. Like the complex cells, simple cells usually had significant excitatory and suppressive kernels. Unlike the complex cells shown in Figure 4.2 to Firgure 4.5, however, the STA had clear spatial subfields. Subfield structure in the STA alone was not a sufficient condition for simple/complex classification. Figure 4.7 shows a cell that was classified as a complex (F1/F0=0.1), which nonetheless had kernel structure similar to that of a simple cell. The STA clearly exhibited subfields.

4.4.2 The dimensionality of the spike-triggering ensemble

The goal of the STC technique was to search for a low-dimensional subspace where the spike-triggering ensemble lies. To estimate the dimensionality of the subspace, the distributions of the eigenvalues of the spike-triggered covariance matrix were compared to that of the null-hypothesis, ie. that spikes were unrelated to the stimulus (Rust et al., 2005). Spikes were shifted randomly and the eigenvalues of the covariance matrices were calculated. The upper bounds and the lower

bounds of the eigenvalues of 500 such simulation were plotted as two black lines in Figure 4.2, Figure 4.4. Figure 4.6 and Figure 4.7. The eigenvalues of the original covariance matrices were plotted in red. As can be seen in the figures, although a few big eigenvalues clearly "stood out" from the rest, the smaller eigenvalues tended to drift gradually from the null hypothesis and it was not always obvious which were significant.

An alternative procedure was used. Let v be any vector in the stimulus space. Let $f_v(x)$ be the probability density function of the projection of the spike-triggering ensemble to v, and $f'_v(x)$ be the probability density function of the projection of the whole stimulus space to v. If v did not contribute to the firing of a neuron, the two density functions should be indistinguishable. It follows that the effectiveness of a filter can be measured by how the two distributions differ from each other. Indeed, Sharpee et al. (2004) proposed a method to search for spike-triggering features by maximizing the difference of the two distributions.

To quantify the difference between $f_v(x)$ and $f'_v(x)$, the KL-divergence was used. Figure 4.8 illustrates the procedure applied to the same complex cell as in Figure 4.2. The significance of the STA, the top three excitatory kernels (E1, E2, and E3) and the bottom two suppressive kernels (S1 and S2) was evaluated. For each vector, $f_v(x)$ was plotted in red and $f'_v(x)$ in black. The KL-divergence of the two curves was also displayed in each plot. The distributions of the projection to the third eigenvector (E3) was practically indistinguishable and it was reflected by the small KL-divergence. It is therefore considered insignificant. The threshold of significance was set at KL=0.025. Significant vectors are indicated by a red dot enclosed by a red circle in the spatialtemporal raster plot of each vector.

The estimated dimensionality of the spike-triggering ensemble (ie. the number of significant kernels) is shown in Figure 4.9 as histograms. Overall, the median number of significant excitatory kernel is 2 and the median number of significant suppressive kernel is 1.

4.4.3 Nonlinearity

The nonlinear function associated with each kernel (represented by f_1 to f_n in Figure 4.1) was calculated by the ratio of two probability density functions: the projection of the spike-triggering ensemble to the kernel, and the projection of the whole stimulus space to the kernel. The nonlinearities of the same complex cell as shown in Figure 4.2 were depicted in Figure 4.10. The nonlinearities of the two excitatory kernels resembled the full-wave rectification functions in the energy model.

The nonlinearities of the same simple cell shown in Figure 4.6 were depicted in Figure 4.11. Compared to complex cells, the nonlinear function associated with the STA had similar (or bigger) magnitude as the eigenvectors.

4.5 Discussion

The geometry of the spike-triggering ensemble

STC analysis is a form of dimension reduction technique (namely, the Principal Component Analysis) which assumes that the spike-triggering ensemble falls on a low-dimensional subspace. Ideally, only a small number of eigenvalues of the STC matrix deviate from the null hypothesis (ie. spikes are randomly generated and are independent of stimulus). While this seems to be true for the top eigenvalues, bottom eigenvalues tend to drift gradually from the distribution of the null hypothesis. This could indicate that the spike-triggering ensemble was not distributed as a gaussian cloud, as assumed by PCA. Algorithms which are sensitive to higher-oder statistics, such as the Independent Component Analysis (Bell and Sejnowski, 1995), might be more appropriate. Alternatively, the ensemble might be composed by disjointed clusters and clustering algorithms might be helpful to elucidate its structure.

The dimensionality of the spike-triggering ensemble

The dimensionality of the ensemble was estimated by measuring how much the projection of the ensemble deviate from the projection of the whole stimulus space. As determined by this procedure, the dimensionality of the ensemble was low, typically two. This is similar to the number reported by Touryan et al. (2002) for the cat, although Rust et al. (2005) reported a much higher number for primates. The difference can probably be explained by the fact that Rust et al. (2005) was able to record much more spikes.

The shape of excitatory kernels

The excitatory kernels of about half of the complex cells resembled the classical energy model by Adelson and Bergen (1985), having two kernels with eigenvalues close to each other. The kernels resembled spatially shifted version of each other (Figure 4.2 and Figure 4.3).

A number of complex cells, however, did not seem to conform to the quadrature structure of the energy model. Some of those are shown in Figure 4.4 and Figure 4.5. The second excitatory kernel of them corresponded to a much smaller eigenvalue than the first, and the second kernel looked like duplicated version of the first. Although this might reflect an alternative organizing principle of complex cells, a more mundane explanation is that those cells actually were energy-model complex cells but the kernels were corrupted, possibly because the bars of the reverse correlation stimulus did not align with the subfields or the bars were too wide. Further investigation is required to interpret the results.

The shape of suppressive kernels

The suppressive kernels typically did not have spatial subfields, even for those cells showing clear subfields in the excitatory kernels. This might reflect a suppressive mechanism in the spatial frequency domain.

Suppressive kernels for direction selective cells showed no direction selectivity, which was in contrast to Rust et al. (2005) where direction selective cells were suppressed by the anti-preferred direction. This might indicate a difference in the underlying circuits of direction selectivity.

4.6 Acknowledgements

Parts of this chapter are being prepared for submission as "Integration of visual information in V1 of the California ground squirrel (*Spermophilus beecheyi*)" by Hsin-Hao Yu, Virginia R. de Sa, and Martin I. Sereno

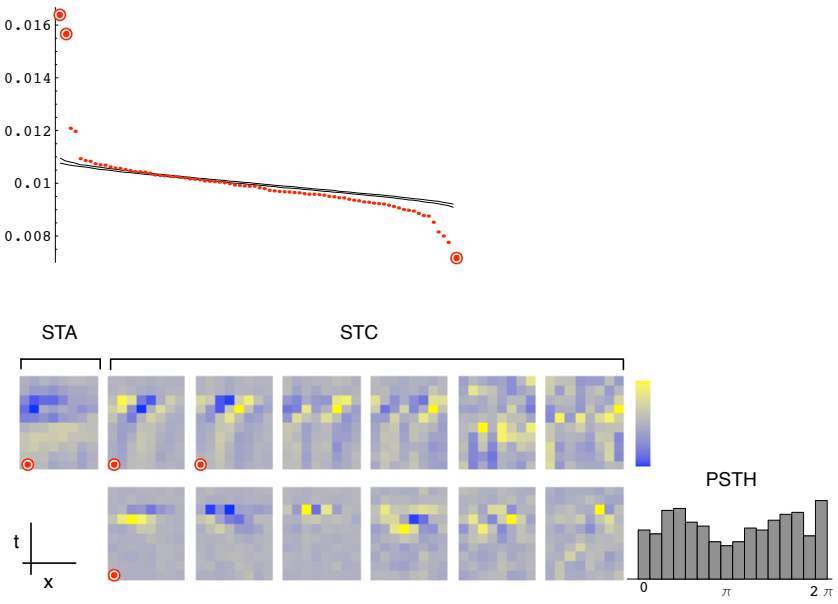

Figure 4.2: STA/STC analysis of a complex cell (F1/F0=0.1). Top: The distribution of the eigenvalues of the spike-triggered covariance matrix, in red. The two gray lines represent the upper bound and lower bound of the eigenvalues when the spikes were randomly shifted for 500 times. They represent the eigenvalue distribution under the hypothesis that spikes were independent of the stimuli. Bottom: the STA and the eigenvectors of the STC. They are represented as two-dimension rasters. One row in a raster represents the spatial kernel at a fixed time delay with respect to spike time. The top row represents no time delay. The time resolution is 20 millisecond for each row. One row represents the eight bars covering a circular region of 10° in diameter. The rasters under the STC label are the eigenvectors of the spike-triggered covariance. The upper (lower) rasters are the eigenvectors corresponding to the biggest (smallest) six eigenvalues in decreasing (increasing) oder from left to right. The peristimulus time histogram (PSTH) of the neural response to a full cycle of a optimally tuned, square-wave, drifting grating was also shown. The significance of the eigenvectors was evaluated by a procedure described in Methods. The procedure applied to this particular cell was illustrated in Figure 4.8. Eigenvectors and eigenvalues that were selected as significant are indicated by a red dot enclosed by a small circle. The calculation was based on 51236 spikes.

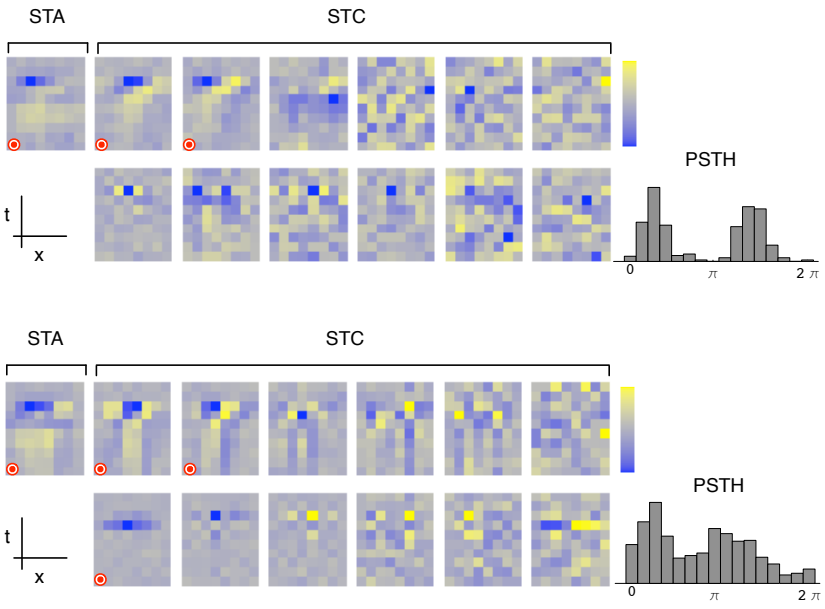

Figure 4.3: Two complex cells with kernel structures similar to the one shown in Figure 4.2. Top: F1/F0=0.05. Stimulus diameter=10°. 16867 spikes. Bottom: F1/F0=0.4. Stimulus diameter=12°. 49567 spikes.

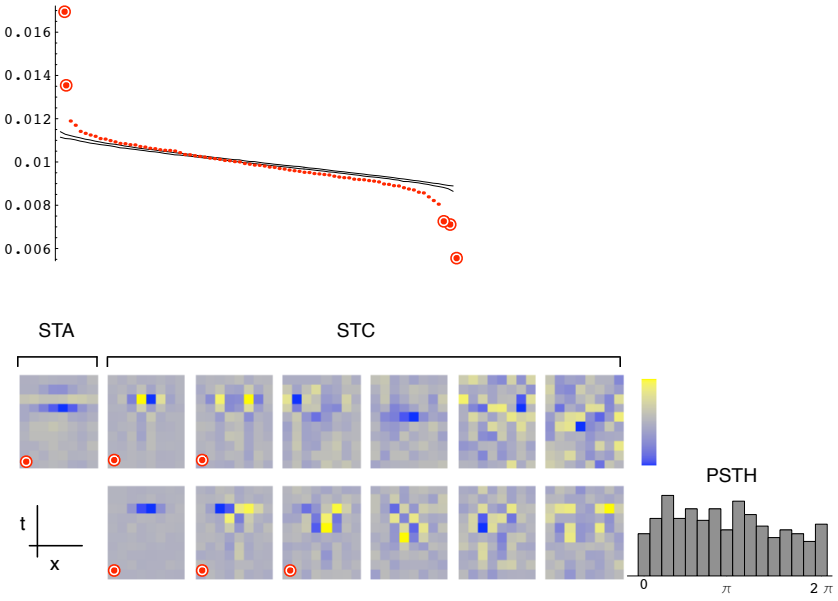

Figure 4.4: STA/STC analysis of a complex cell (F1/F0=0.2). Unlike the cell shown in Figure 4.2, the kernel structure did not resemble the energy model. Stimulus diameter=12°. Calculation based on 35444 spikes.

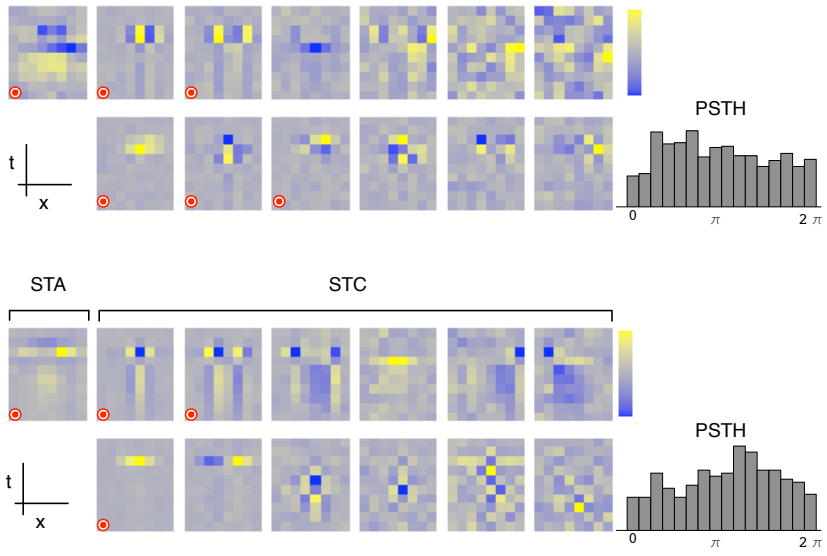

Figure 4.5: Two more examples of complex cells whose kernel structure were similar to the one shown in Figure 4.4 and did not resemble the energy model. Top: F1/F0=0.2. Stimulus diameter=12°. 15331 spikes. Bottom: F1/Fo=0.04. Stimulus diameter=12°. 87603 spikes.

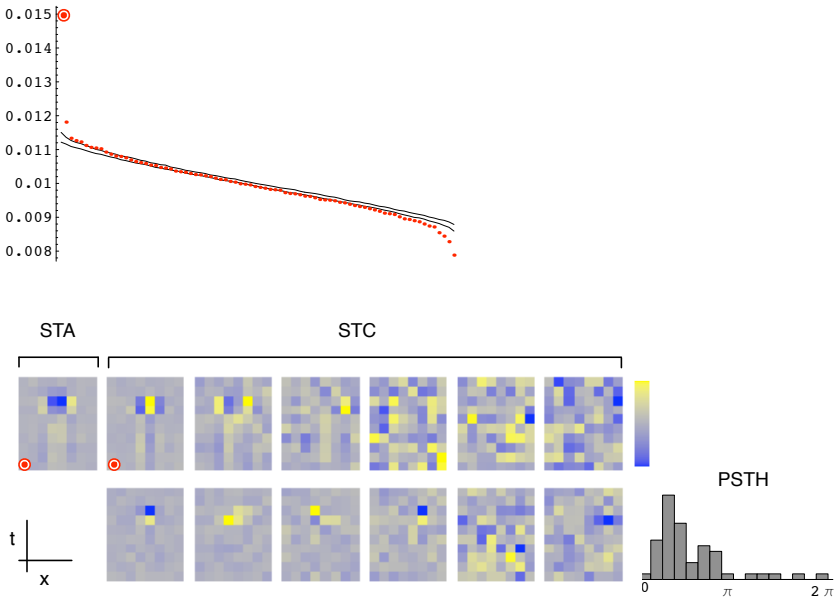

Figure 4.6: STA/STC analysis of a simple cell (F1/F0=1.3). The diameter of the stimulus patch was 10°. Calculation based on 19893 spikes.

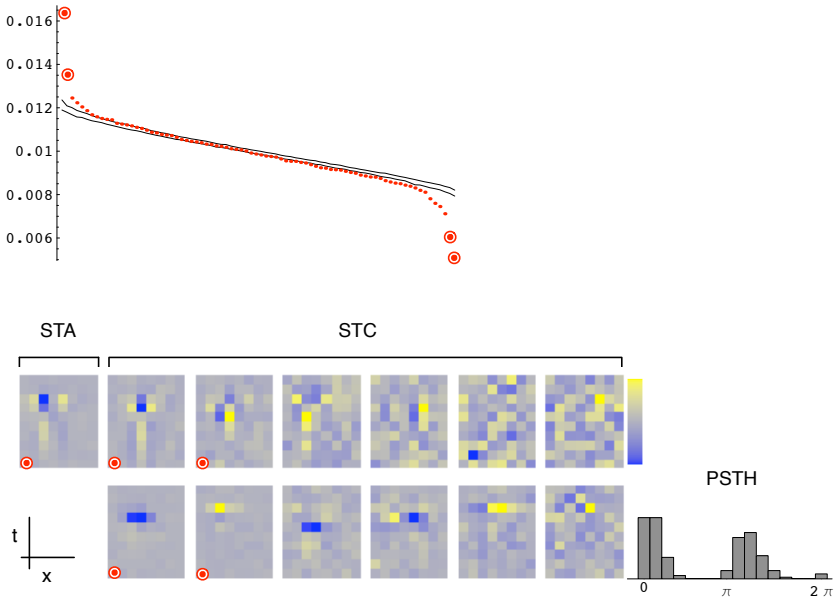

Figure 4.7: A cell that was classified as a complex cell (F1/F0=0.1). However, unlike the complex cells shown in Figure 4.2 to Firgure 4.5, the STA had clear subfields. In this regard, the kernel structure of this cell was more similar to the simple cell shown in Figure 4.6. Stimulus diameter=14°. 8174 spikes.

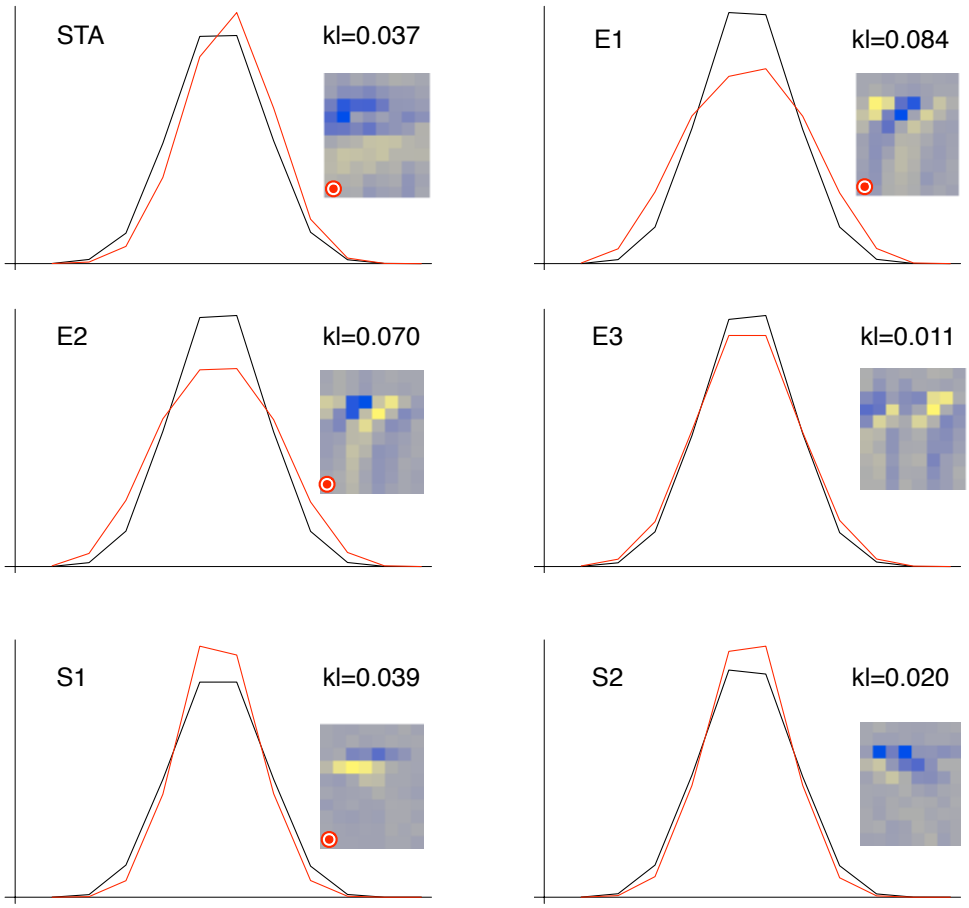

Figure 4.8: Estimating the dimensionality of the spike-triggering ensemble. The procedure was applied to the same cell as shown in Figure 4.2. The significance of the STA vector, the top three (E1 to E3) , and the bottom two (S1 and S2) eigenvectors of the STC matrix were evaluated. For each vector, the probability density function of the projection of the spike-triggering ensemble was plotted in red, and that of the projection of the whole stimulus space was plotted in black. The difference between the two distributions was quantified by the KL-divergence. A vector was considered significant (indicated by the red circle in the spatialtemporal raster plot of the vector) if the KL-divergence was greater than 2.5.

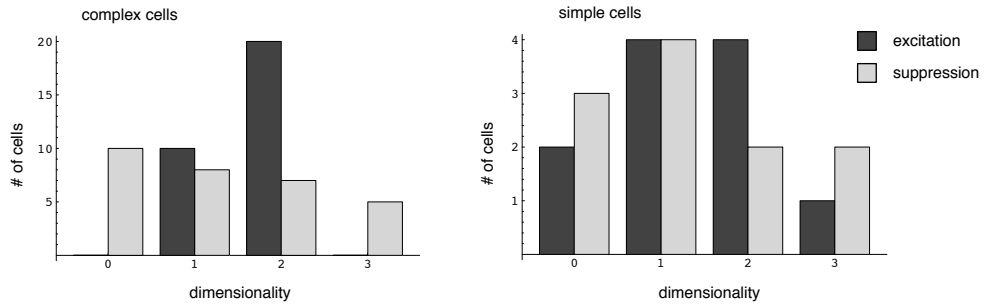

Figure 4.9: The histograms of estimated dimensionality of the spike-triggering ensemble. The number of significant excitatory (suppressive) kernel is represented by the dark (light) bars. Complex cells are charted on the left, and simple cells on the right.

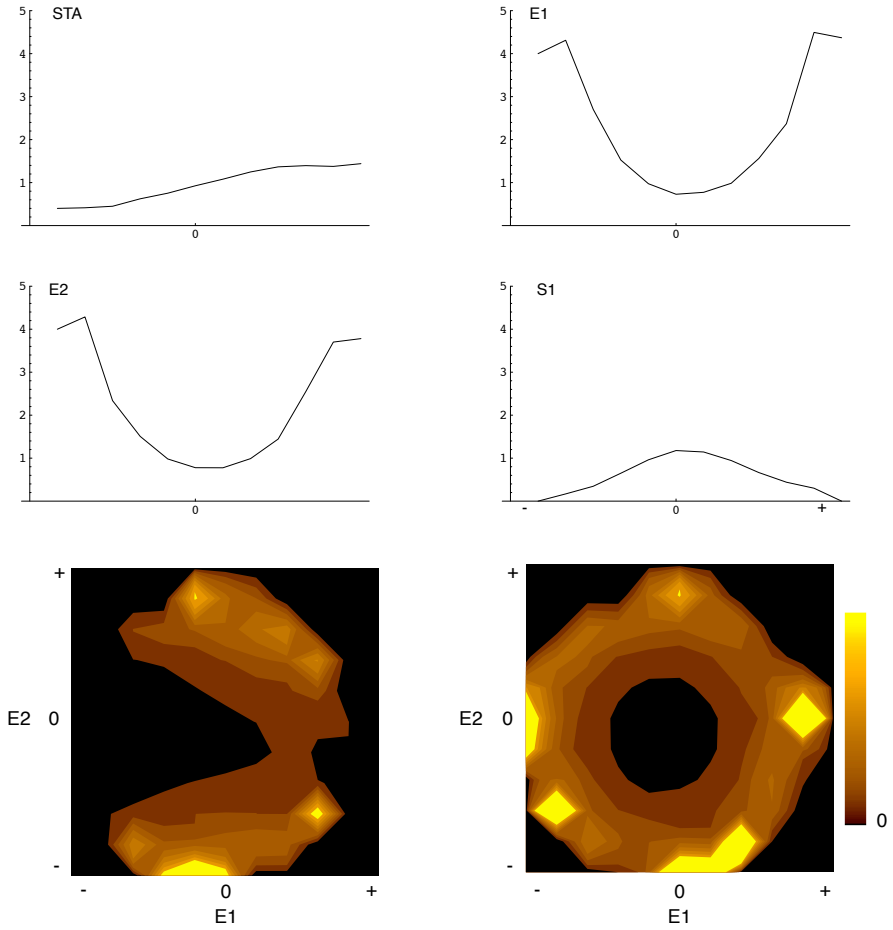

Figure 4.10: The nonlinear functions associated with of the the STA, the first two excitatory kernels (E1 and E2) and the suppressive kernel (S1) of the same complex cell as shown in Figure 4.2. The two-dimensional density plots depict the joint function of STA-vs-E1 and E1-vs-E2.

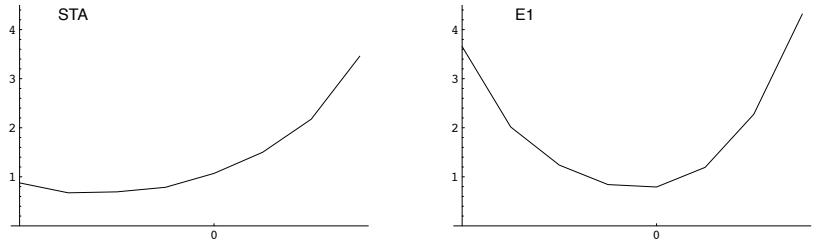

Figure 4.11: The nonlinear functions associated with of the the STA and the first excitatory kernels (E1) of the same simple cell as shown in Figure 4.6.

Chapter 5

Spatialtemporal structure of the non-classical receptive fields

5.1 Introduction

In the previous chapter, the reverse correlation method was used to characterize the structure of the center (classical) receptive field. This chapter focuses on the surround (non-classical) RF. Center/surround effects, originally demonstrated by slow, drifting gratings in Chapter III, were further examined by the reverse correlation paradigm.

The reverse correlation technique potentially could provide information about the surround RF beyond the capability of the grating stimulus for two reasons: First, the dynamic (ie. rapidly changing) nature of the stimulus made it possible to resolve transient events that lasted for only a fraction of the temporal period of the drifting gratings. Second, the reverse correlation stimulus was much richer and did not assume a periodic structure. Grating parameters that were not manipulated in Chapter III (such as the spatial phase) could potentially be inferred from the reverse correlation data.

Two aspects of the surround RF were investigated. First, ortho-orientation

facilitation was studied by an extension of the stimulus used in Chapter IV. Similar to what was described in the previous chapter, the new stimulus consisted of paralleled bars who brightness was determined randomly. However, the center RF and the surround RF were stimulated independently, so that their interaction can be analyzed. The orientations of the center component and the surround components were kept fixed.

To examine the dynamic interaction of the center and the surround RFs in the orientation domain, a second stimulus was used. The stimulus was divided concentrically into two components, each composed by gratings of optimal spatial-frequency. The orientation of the center was fixed, but the orientation of the surround was changed randomly at high refresh rate.

The results showed that, at iso-orientation, the kernel structure of the surround RF was very similar to that of the center RF, contradicting reports claiming broader tuning properties of the surround. No timing difference between the center and the surround was observed. The orientation dynamics stimulus, however, revealed a subtle difference in timing between surround facilitation and suppression. The results suggested a model of center/surround organization where facilitation was orientation selective but suppression was not.

5.2 Methods

5.2.1 Data collection

The methods of animal preparation and data collection were identical to those described in Chapter III.

5.2.2 Stimulus

Stimulus 1 The stimulus is illustrated by the upper row of Figure 5.1. One frame in the stimulus consisted of two concentrically arranged components, each

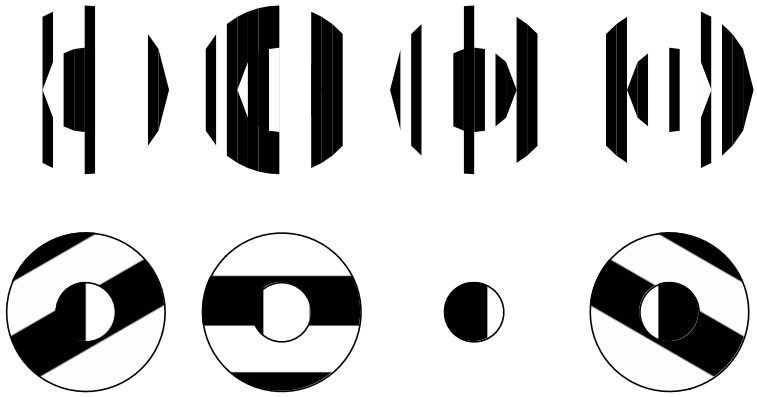

Figure 5.1: Two types of reverse correlation stimulus were used to examine the dynamic interaction by the center and the surround. Upper row: the stimulus used to study the surround RF structure in the iso-orientation facilitation condition. Lower row: the stimulus used to study surround effect in the orientation domain. Four frames in each type were illustrated. See text for details.

divided into an array of paralleled bars of equal width. The bars in the center component and the surround component were aligned. The brightness of the bars was randomly and independently turned bright or dark at 50% contrast. The orientations of both components were set to the the optimal orientation of the cell, as measured by a large patch of drifting grating. Care was taken to make sure that center component was large enough to cover the width of the CRF kernel (as in Chapter IV). The frames were updated at 50 hertz refresh rate unless stated otherwise.

The stimulus was run under three conditions: i). Only the center stimulus was displayed. In this condition, the stimulus was the same as described in Chapter IV. ii). Both the center and the surround were displayed. iii). Only the surround stimulus was displayed. Condition iii.) was not run for those cells whose surround was silent by itself.

Stimulus 2 The stimulus is illustrated by the lower row of Figure 5.1. One frame in the stimulus consisted of two concentrically arranged components, each

made up by a square-wave grating of optimal spatial frequency (as measured by a large, drifting grating). The spatial phase of the center grating, the spatial phase of the surround grating, and the orientation of the surround grating were randomized. The orientation of the center grating was fixed to the optimal orientation of the cell. The spatial phases and the surround orientation were sampled at 15° interval. At the probability of $\frac{1}{13}$ (or 7.7%), the surround grating was not displayed (as illustrated by the third frame in the bottom row of Figure 5.1). This condition was used to establish if the surround was facilitatory or suppressive. The frames were typically updated at 50 hertz refresh rate. In a few cases 100 hertz refresh was used. The stimulus was a direct extension of Ringach et al. (1997), which used a single component stimulus to study the dynamics of orientation tuning of the classical receptive field.

Except for one Type II cell, the stimulus was only used for Type I_{fs} cells. The diameter of the center stimulus was set to the size such that a surround modulation curve with clear facilitation and suppression could be found.

5.2.3 Data analysis

Stimulus 1 STA and STC analyses (as described in Chapter IV) were performed. The following labels were used to designate the calculation of kernels under different conditions:

- C/C: center kernels, calculated under the condition when only the center component was presented.
- CS/C: center kernels, calculated under the condition when when both the center and the surround components were presented.
- CS/S: surround kernels, calculated under the condition when both the center and the surround components were presented. The center component was ignored in the calculation.

- S/S: surround kernels, calculated under the condition when only the surround component was presented.

Stimulus 2 For each spike in the spike-train, the parameters of the stimulus (center phase, surround phase, surround orientation) at τ milliseconds prior to the spike were looked-up. The probability distributions of each of the three parameters was calculated individually by normalizing the occurrence histogram. The condition where the surround was not displayed was considered the 13th surround "orientation", so that the probability of the presence of the surround at any orientation could be compared directly to that of the absence of the surround. τ was sampled from 200 ms to 0 ms at 10 ms resolution.

The reliability of the probability estimation was validated by performing the same analysis using only half of the recorded spikes.

5.3 Results

5.3.1 Spatialtemporal structure of the surround

Concentric, bipartite reverse-correlation stimuli (as illustrated in top row of Figure 5.1) were used to explore the subfield structure of the center and the surround. Figure 5.2 displays the grating summation curve and the grating subtraction curve (Chapter III) of a representative complex cell. The GSF was much larger ($d = 18.4°$) larger than the hand-mapped MRF (4° in diameter). The grating subtraction curve had long tail and was never silent when stimulated by an annulus grating, for the entire range of inner diameter tested. Reverse correlation kernels of the same cell are displayed in Figure 5.3. Since it was a complex cell, subfield structures are revealed by the top eigenvectors (E1 and E2) of the STC matrices. The C/C kernel (center kernel when only the center stimulus was presented) and the CS/C (center kernel when the surround stimulus was presented

as well) had almost identical structure[1] The estimated width of the center kernels was 5.6° in diameter, which was slightly bigger than the MRF, but covered only a small fraction of AMRF. Indeed, the presentation of only the surround component of the stimulus (the S condition) elicited many spikes. The kernels of the S condition (STC:S/S) had the same width as the center kernels (STC:C/C and STC:CS/C), despite that a large spatial extent was stimulated. The result was consistent with the finding that facilitation mainly came from the "end" position and not from the "side" position (Chapter III. Section 4.4.). When the center and the surround were stimulated simultaneously (the CS condition), the surround kernels (STC:CS/S) were also very similar to the S condition. Note that there was no obvious timing difference between STC:CS/C and STC:CS/S.

Two further examples of center/surround STC analysis are provided in Figure 5.4 and Figure 5.5. Note that: i.) The stimulus presentation rate in Figure 5.4 was 100 hertz rather than the usual 50 hertz, and one row in the raster plot represents 10 ms. Even with higher refresh rate, STC:CS/C and STC:CS/C kernels still had similar time courses. No obvious delay in the surround was observed. ii.) The surround kernels were slightly mis-aigned with the center kernels. While this could imply a difference in spatial-phase between the center and the surround, it could also be attributed to small errors in the estimation of the preferred orientation of the cell, given that orientation tuning curves were limited to 30° sampling resolution. Further investigation is required to resolve this issue.

[1]Except that their signs were reversed. The signs of eigenvectors are arbitrary and does not reflect a real difference in the structure of the spike-triggering ensemble.

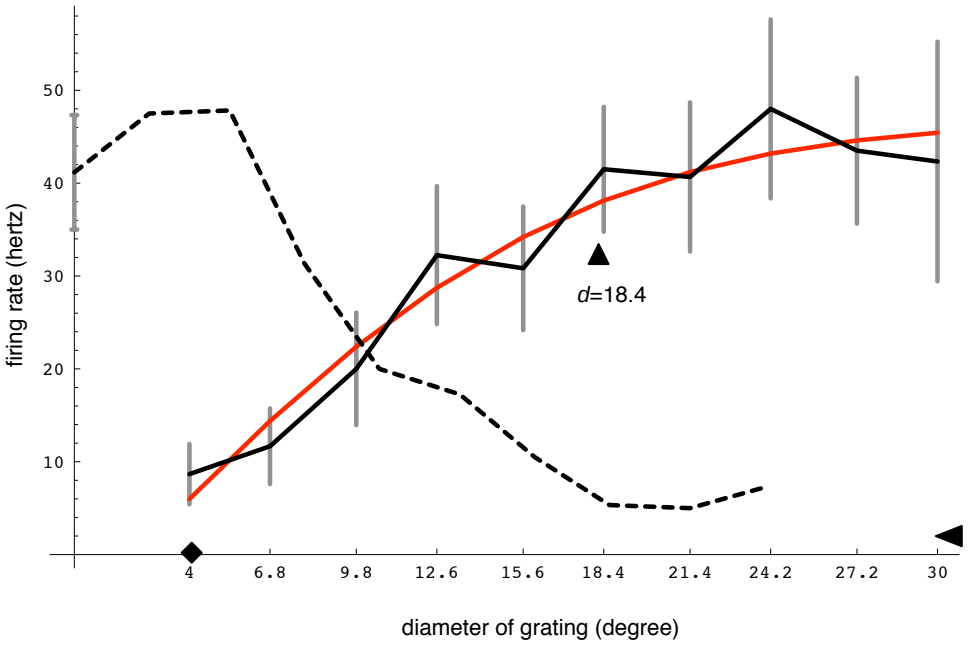

Figure 5.2: Grating summation curves of a representative complex cell, whose reverse correlation kernels are display in Figure 5.3.

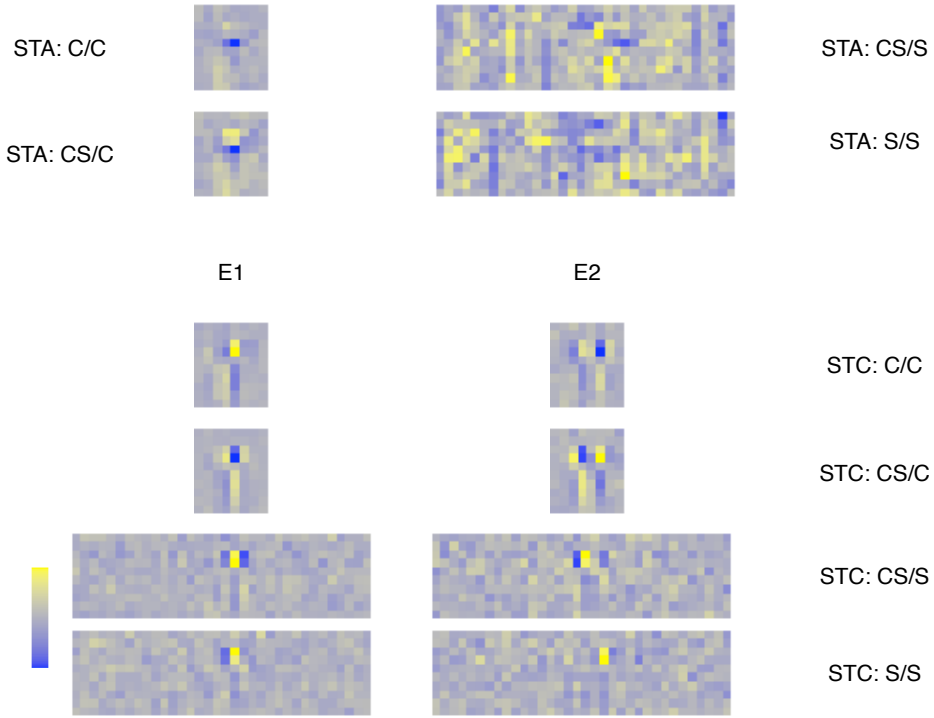

Figure 5.3: Reverse correlation kernels of the cell whose grating summation behavior is shown in Figure 5.2. Diameter of the center stimulus: 9°. Kernels are labeled as described in the Data Analysis section. E1 and E2 are the first and the second eigenvector of the covariance matrix. Note that the signs of the eigenvectors are arbitrary, and the color code for the eigenvectors only represents brightness contrast and does not represent absolute brightness. C condition: 25552 spikes. S condition: 33928 spikes. CS condition: 77595 spikes.

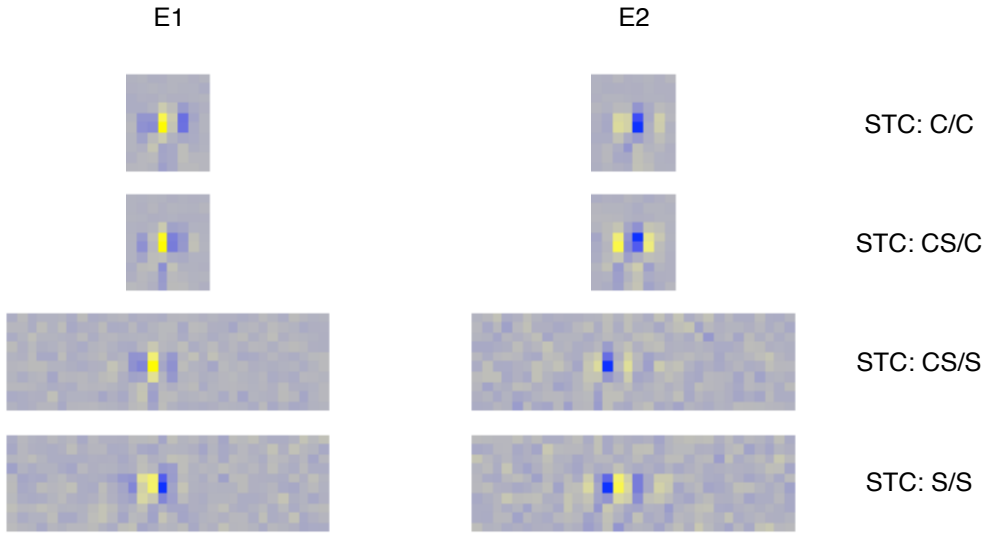

Figure 5.4: Center/surround STC analysis of another complex cell. Center stimulus diameter: 10°. Estimated kernel width: 6.25°. MRF diameter: 5°. $d = 16.6^\circ$. $d' = 16^\circ$. Stimulus refresh rate: 100 hertz and therefore one row in the raster represents time duration of 10 ms instead of the usual 20 ms. C condition: 23260 spikes. S condition: 7733 spikes. CS condition: 27350 spikes.

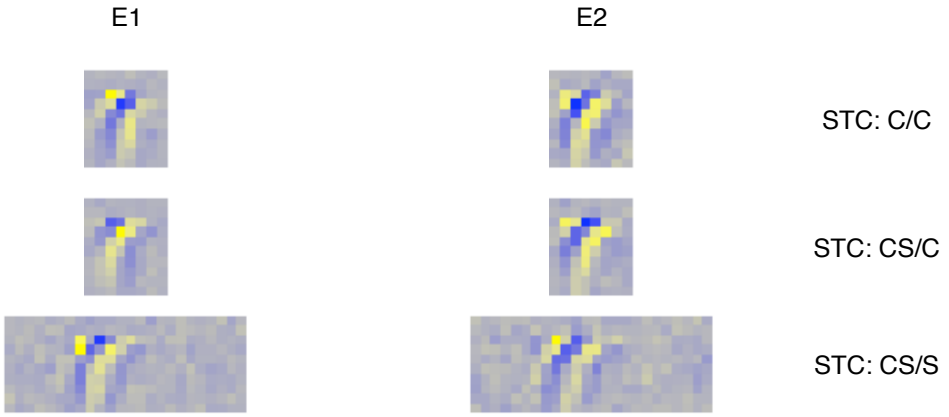

Figure 5.5: Center/surround STC analysis of an direction-selective, complex cell. Center stimulus diameter: 10°. Estimated kernel width: 7.5°. MRF diameter: 5°. $d = 12^\circ$. $d' = 13.2^\circ$. C condition: 13698 spikes. CS condition: 42332. The surround was not silent but unfortunately S condition was not collected.

5.3.2 Dynamics of surround orientation

The stimulus illustrated in the bottom row of Figure 5.1 was used to explore the temporal dynamics of the surround RF in the orientation domain. Each frame in the stimulus was divided into a center and a surround component, each made up of a grating of optimal spatial frequency. The orientation of the center was fixed to the optimal, while the orientation of the surround was randomly sampled at each frame. The spatial phases of the two components were also randomized. The orientation of the surround ranged from 0° to 165° and was sampled at 15° interval. Instead of the 12 orientations, the surround could also be absent from display. This "no-surround" condition was to used to infer if the surround effect was facilitatory or suppressive. The stimulus design was a direct extension of Ringach et al. (1997).

The result of one representative Type I_{fs} cell is displayed in Figure 5.6. The second row in the figure illustrates the probability distributions of the spatial phase of the center, at a few selective time points before spikes. This was used as an estimate of temporal evolution of the selectivity of the center RF[2]. The center RF of the illustrated cell became "active" (ie. modulated by the spatial phase of the grating) from -80 to -40 ms. The time window is highlighted by red boxes in the figure.

The probability of the surround stimulus being absent is shown in the top row, as a function of time (τ). Outside the red box, the probability was at the baseline ($\frac{1}{13}$). However, in the time window from -80 to -40 ms, the probability clearly went through a bi-phasic modulation. The probability was increased for 20 ms and then was decreased for 20 ms.

The probability distributions of the orientation of the surround at selected time points are displayed in the bottom row of the diagram. The "no surround"

[2]Although the ideal complex cells is phase invariant, real complex cells are not completely phase invariant. Modulations of the spatial phase tuning curve could be seen for the complex cells recorded.

condition was treated as the 13th "orientation" so that it could be compared directly with the 12 orientations. The "no surround" probabilities are indicated by blue horizontal lines in the diagrams. If the probability of a particular surround orientation was higher than that of no surround at all, the surround orientation was facilitatory. If lower, suppressive. As can be seen in the figure, at -70 ms, the surround was suppressive at all orientations. On the other hand, at -50 ms, the surround was facilitatory at all orientations. At -60 ms, facilitation and suppression was mixed but the facilitation had the same orientation selectivity as the center. The pattern resembled the orientation modulation curves measured by slow gratings. Figure 5.7 illustrates a second cell showing similar patterns.

Figure 5.8 illustrates the results of a Type II cell. Peak suppression occurred at -80 ms and the suppression was not orientation selective, just like Figure 5.6. However, facilitation did not occur at the time point (-50 ms) where center responses peaked.

Twenty-eight cells were studied with this type of experiment. Among them, twelve were found to exhibit similar patterns as shown in Figure 5.6 to Figure 5.8. Two cells in the 28 behaved differently, showing mixed facilitation/suppression at all time point during center activation. Figure 5.9 illustrates such a cell. For the rest of cell studied, the stimulus failed to elicit clear surround effects. That is, the "no-surround" probability showed no clear modulation and/or the orientation of the surround showed no selectivity.

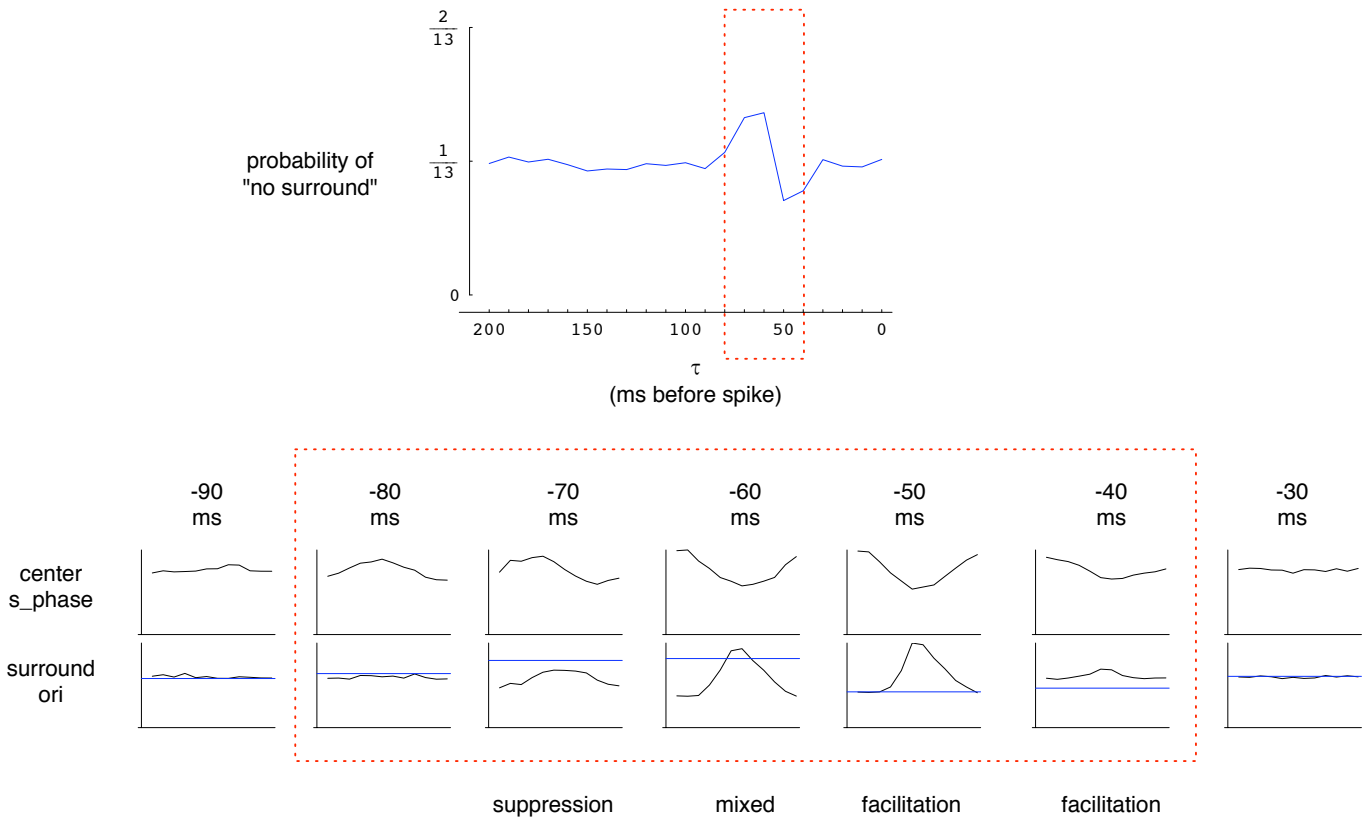

Figure 5.6: Orientation dynamics of the surround of a representative Type I cell. Upper row: the probability of the cell preferring the surround stimulus to be not displayed at τ millisecond before spikes. Second row: the probability of the spatial phase of the center stimulus at a few selected time points before spikes. Third row: the probability of the orientation of the surround at selected time points. The blue lines represent the probability of the "non-surround" condition. The center of the x-axis represents the same orientation as the center. Calculation based on 22480 spikes. Complex Type I_{fs} cell. $d = 20°$. $d' = 14.4°$. Diameter of center=$11.4°$. Diameter of surround=$34°$. Display frame rate was 100 hertz.

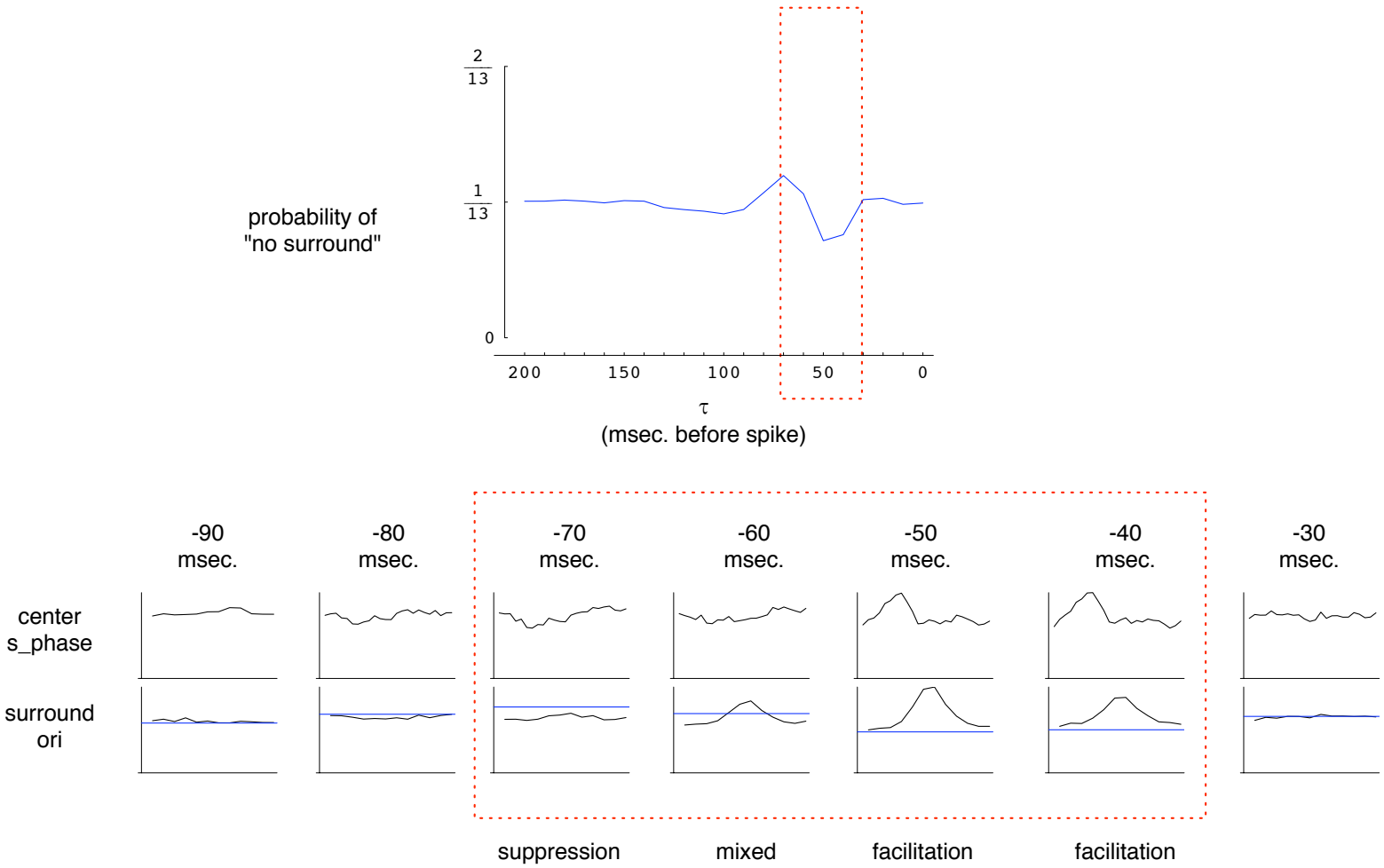

Figure 5.7: Another example of surround orientation dynamics. Same display format as Figure 5.6. Calculation based on 63393 spikes. Complex Type I_{fs} cell. $d = 16.4°$. $d' = 24.0°$. Diameter of center=$14°$. Diameter of surround=$30°$. Display frame rate was 50 hertz.

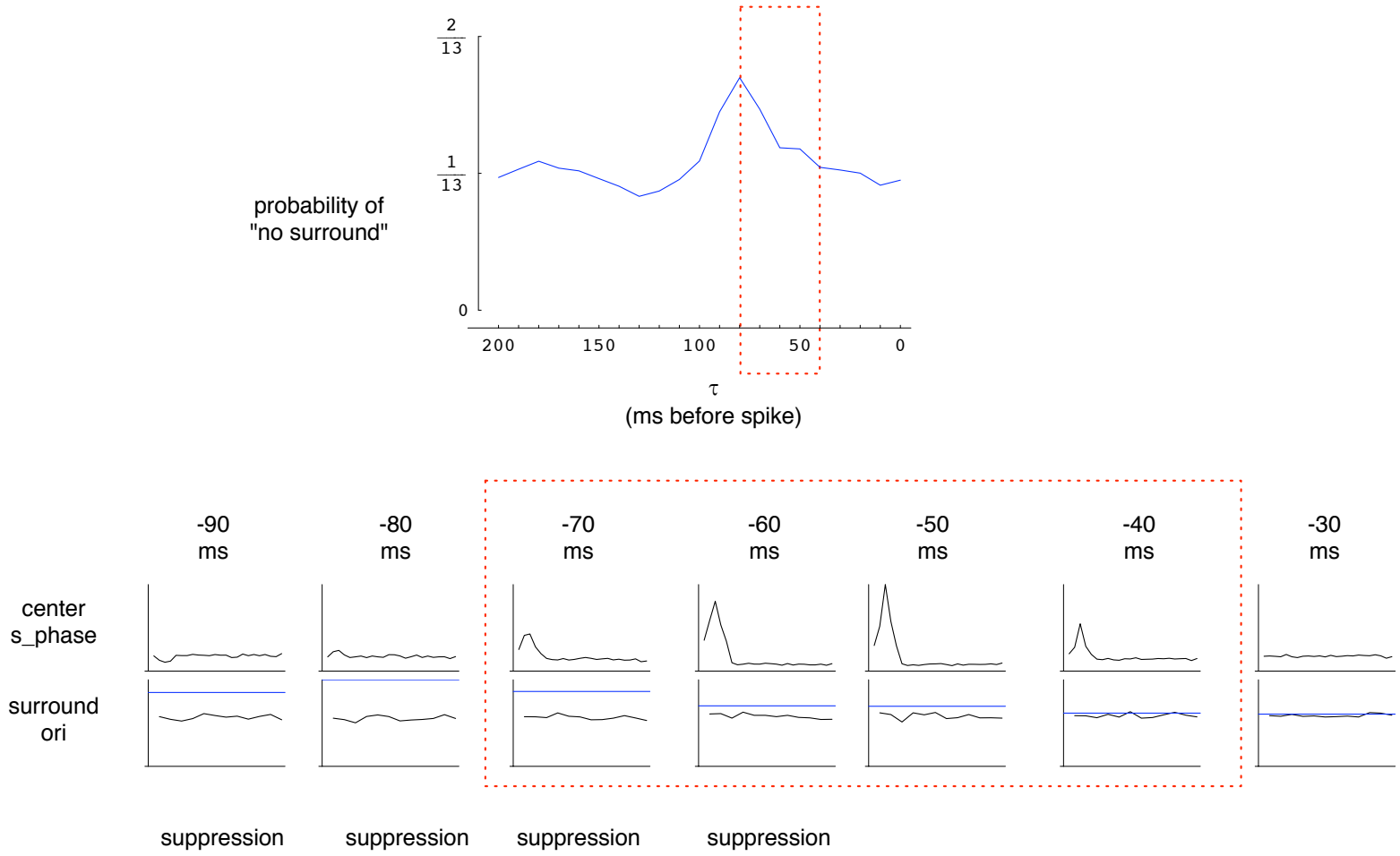

Figure 5.8: A third example of surround orientation dynamics. Same display format as Figure 5.6. Calculation based on 7367 spikes. Complex Type II cell. $d = 6.2°$. Diameter of center=$4°$. Diameter of surround=$20°$. Display frame rate was 50 hertz.

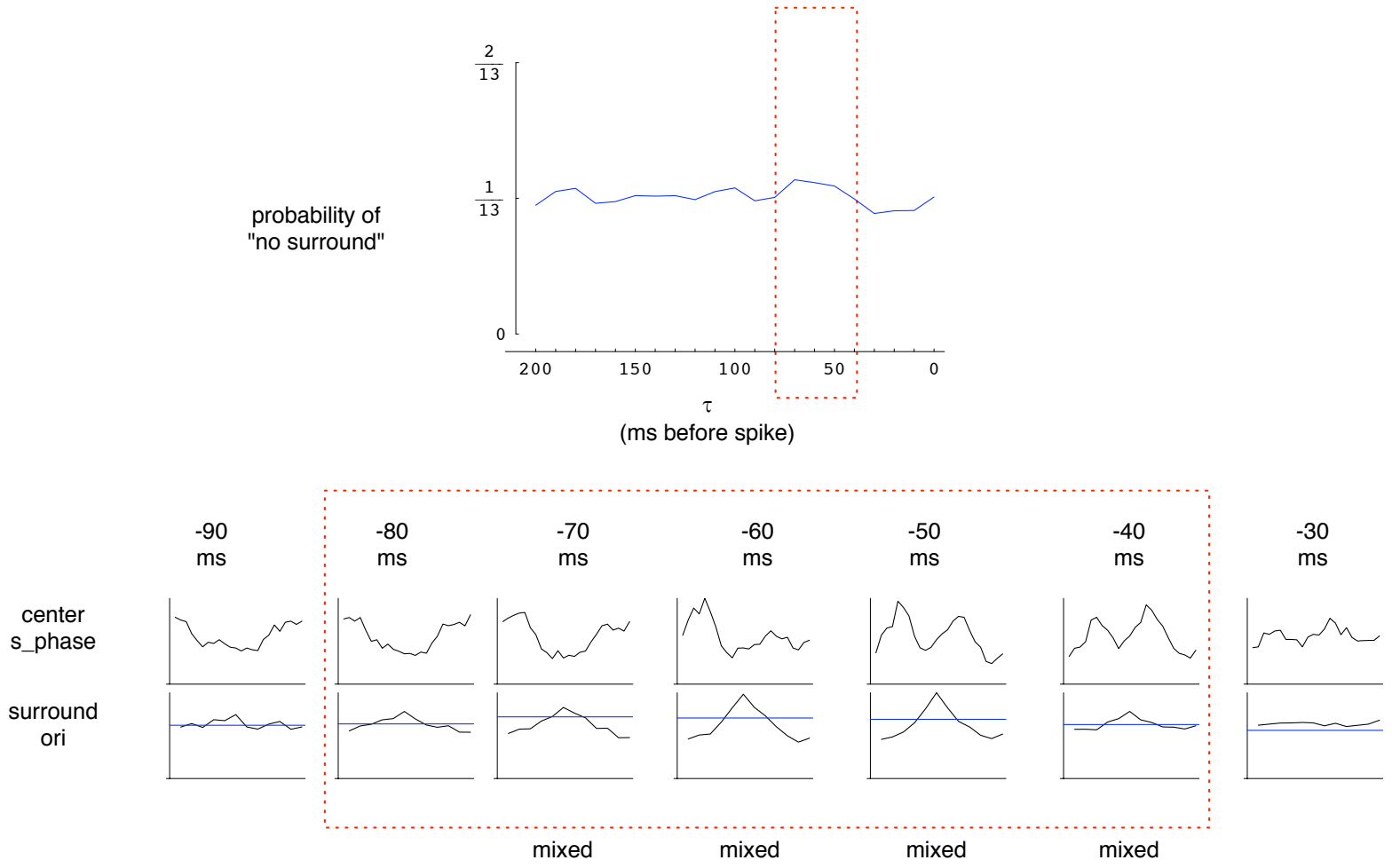

Figure 5.9: A example of surround orientation dynamics which showed no difference in timing between facilitation and suppression, unlike those shown in 5.6 and 5.7. Calculation based on 5893 spikes. Complex Type I_{fs} cell. $d = 21°$. $d' = 11.6°$. Diameter of center=$12°$. Diameter of surround=$30°$.

5.4 Discussions

5.4.1 Receptive field organization

The design of Stimulus 1 (as well as other stimuli) had two major features: i). it was bi-partitioned into a center component and a surround component; and ii). the two components were arranged concentrically. The former was motivated by the observation that the large GSF (grating summation field) described in Chapter III was too extensive to be considered the classical receptive field (CRF), given that the subfields (as revealed by reverse correlation) occupied only a fraction of the GSF. The latter was motivated by the assumption that the CRF (the region where the subfields occupied) was approximately circular and not elongated. The circular CRF assumption was justified by the observations than the MRFs were not elongated and that two-dimensional reverse correlation produced kernels that were also not elongated (Figure 13 in Chapter III).

When the GSF is divided into center and surround, it is expected that the two components represent distinct mechanisms, either as abstract computational units or as the results of different underlying neural circuits. Their differences should manifest themselves under appropriate experimental conditions. Indeed, many such differences have been reported - the most obvious one being that the surround is silent when stimulated by itself. DeAngelis et al. (1994) and Li and Li (1994), for example, further showed that surround suppression (for the cat) had broader orientation tuning and spatial frequency tuning than those of the center. From this perspective, results shown in Figure 5.3 to Figure 5.5 seemed unexpected. Two noteworthy observations: i.) Center kernels and surround kernels had very similar widths, demonstrating that facilitation originated from the end-position of the center, and that increasing the width of the stimulus contributed very little, if any, to stimulus summation. This is a confirmation of the grating experiments described in Section 4.4. of Chapter III. ii.) Surround kernel had well-defined

subfield structure which matched that of the center. Together with the grating results showing that surround by itself was also orientation selective (Figure 4 in Chapter III), it becomes clear that the surround RF had the same stimulus selectivity as the center, instead of being broadly tuned.

Based on these two observations, a model of the RF organization of Type I_{fs} cells is hereby proposed. The model is depicted schematically in Figure 5.10a. The stimulus integration behavior of Type I_{fs} cells in V1 of the California ground squirrel is best explained by a elongated integration field. The most sensitive (supra-threshold) region of the integration field (the black and white square in the middle of the figure) is not elongated. It is the region that is revealed by the two-dimensional reverse correlation experiments. It also responds to small spot of light or slits, although the hand-mapping technique tends to unveil one of the subfields and therefore underestimates its size. A significant part of the integration field (colored in light red in the figure) is sub-threshold and does not response to localized stimuli. However, if it is stimulated from both sides (as in annular stimulation experiments), spikes can be triggered and it contributes significantly to stimulus integration. The "tip-of-the-iceburg" model is supported by intracellular recording data, as discussed in Chapter III (Bringuier et al., 1999).

It is only a matter of semantics whether the term CRF should be used to refer to the whole elongated summation field, or only the non-elongated, supra-threshold region. The fact that reverse correlation revealed no obvious difference in subfield structure between the two seems to be a compelling reason to opt for the former. In such a case, Type I_{fs} would have a elongated CRF and no nCRF. However, grating experiments in Chapter III showed that direction selectivity of the center and the surround did not necessarily agree, which predicts that center kernels and surround kernels showing different spatialtemporal structures should be found. If it is indeed the case, the distinction of CRF and nCRF would be more compelling. Limited by the small number of cells whose center and surround had been examined by reverse correlation, the issue remains unsolved and requires

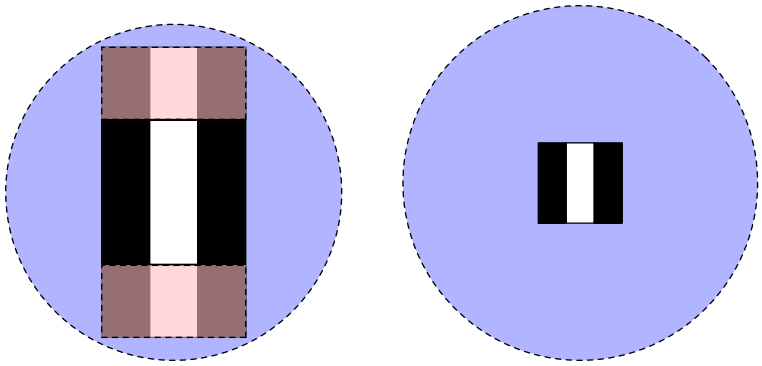

(a) (b)

Figure 5.10: Proposed RF organizations for Type I_{fs} cells (a) and Type II cells (b). The black-and-white squares represent the most sensitive (supra-threshold) part of the integration field, revealed by two-dimensional reverse correlation experiments. They are slightly larger than the MRF. The regions colored in light red represent sub-thrshold areas of the integration field. They are silent by themselves but can trigger spikes if stimulated concurrently. Both supra-threhold and sub-threshold regions are orientation and spatial frequency selective. The circle in light blue represents a suppressive mechanism that is not orientation selective and has a slightly different time course from that of the integration field. Suppression being non-localized in space is speculative.

further investigation. It would be very educational to test if facilitation can be elicited by stimulating the surround from the other eye (DeAngelis et al., 1994).

There are a few reports of spiking in V1 when the CRF was excluded from stimulation (Sillito et al., 1995; Knierim and Van Essen, 1992; Li et al., 2001; Rossi et al., 2001). The phenomena described by at least some of them (Li et al. (2001) and Rossi et al. (2001)) are clearly very different from the non-silent surround found in this study and are not simply subthreshold, because they have long time delays (about 100ms) and were not feature selective, while the S/S kernels had the same time course as the C/C kernels and were feature selective.

5.4.2 Time courses of facilitation and suppression

Grating experiments in Chapter III showed that center responses of Type I_{fs} cells were facilitated by the surround at iso-orientation and suppressed at ortho-orientation. Dynamic stimulus (Stimulus 2) allowed the surround orientation to be updated at a presentation rate much closer to physiological systems, and revealed finer details about the interaction between facilitation and suppression. In Figure 5.6, the surround was suppressive at all orientations at -70 ms, but 20 ms later (-50 ms), the surround was not suppressive at all. The facilitation/suppression pattern established by drifting gratings, in fact, did not occur at the same time. This subtle difference was hidden for grating experiments because the precise timing of spikes was ignored.

The results illustrated in Figure 5.6 can be interpreted as the interaction between two mechanisms: a orientation selective, facilitatory mechanism and a orientation non-selective, suppressive mechanism. The orientation selectivity of facilitation took about 30 ms to develop and peaked at the same time as the center (-50 ms). Suppression, on the other hand, was more transient and peaked earlier. The difference was about 10 to 30 ms. This model is more parsimonious than the alternative where both facilitation and suppression are orientation selective. Furthermore, it unites Type I_{fs} and Type II cells in one single architecture. Type II cells, under this model, are simply I_{fs} without the facilitation mechanism. However, this model might not explain every cells. Two cells recorded (Figure 5.9) did not seem to show a dissociation between facilitation and suppression.

Surround suppression being orientation non-selective predicts that a suppressive kernel should be found in center/surround reverse correlation. Such kernels have not been be found. It is possible that analytical methods more sophisticated that STC/STC are required. It is also possible that the design of Stimulus I made it difficult to trigger suppression. Although the spatial frequency selectivity of surround suppression was never tested directly in this study, it is possible that it

is non selective as well. If true, Stimulus 1 would tend to have too high a spatial frequency to generate suppression.

The time courses of surround effects have been studied by other researchers. Walker et al. (1999) reported that peak surround suppression was delayed with respect to peak center response by about 10 ms (cat). Knierim and Van Essen (1992) estimated that orientation-unspecific suppression took about 7 ms to develop and orientation-specific suppression took about 20 ms (alert monkey). Nothdurft et al. (1999) also found suppression to be delayed for 15 to 20 ms with respect to center (monkey). The first study used a reverse correlation stimulus while the latter two compared the PSTHs of repeated presentations of static textures. These estimates are comparable to the time course of suppression found in this study.

The suppressive mechanism is represented by circles in light blue in Figure 5.10. It is orientation non-selective. The circle representation implies that suppression is not focused on a localized region in space, although it is speculative. The spatial organization of suppression was not investigated directly in this study.

5.4.3 Cortical circuitry

As argued in Chapter III, surround facilitation is consistent with the intracellular recording results from Bringuier et al. (1999), who demonstrated large (facilitatory) depolarization fields outside the supra-threshold region. Based on estimation of propagation velocity, it was concluded that the depolarization field was mediated by horizontal connections in the cortex (reviewed in detail in Chapter II). It follows that horizontal connections are prime candidate for the substrate of facilitation in the ground squirrels. The slow propagation speed of horizontal axons (0.1 to 0.2 m/s. See Bringuier et al. (1999), Grinvald et al. (1994), and Hirsch and Gilbert (1991)) would predict a delay of 10 to 20 ms. However, such a delay is not seen in results from either Stimulus 1 or Stimulus 2. The expected delay time is barely matched by the refresh rate (50 hertz in most cases, 100 hertz

in rare circumstances), which may explain the absence of the evidence. It is likely that higher refresh rate and/or longer recording time is required to reveal the delay. Furthermore, propagation speed as well as cortical magnification factor (1mm cortical space corresponds to 1° visual space, see Tusa et al. (1978)) used in the calculation are based on estimates for cats. It is possible that the small size of the squirrel cortex would entail some differences in the relationship between cortical magnification factor and propagation speed, and thus reduces the expected delay.

Results from Stimulus 2 implies a suppressive mechanism that is orientation non-selective, and has a different time course than facilitation. It is unclear at this point where the suppressive signals come from. Horizontal axons make connections that are orientation selective, which casts doubts in their role as the substrate of surround suppression. However, it is certainly possible that some horizontal axons are non-selective. Other candidates for the source of suppressive signal include LGN, superior colliculus, pulvinar, claustrum, and extrastriate cortical areas (discussed in detail in Chapter II). Long-ranged (1mm) axons originated from GABAergic large basket cells, which make connects to neurons with a wide range of orientation selectivity (Kisvàrday, 1992; Kisvàrday et al., 1994), are possibly involved - although it is unclear at this point if they explain the time delay.

Note that physiological studies have previously reported small populations of V1 cells whose surround was orientation non-selective (Maffei and Fiorentini, 1976; Fries et al., 1977; Knierim and Van Essen, 1992; Sengpiel et al., 1997). The postulated suppression mechanism is therefore not a radical departure from existing data.

5.5 Acknowledgements

Parts of this chapter are being prepared for submission as “Spatialtemporal properties of classical/non-classical interaction in the orientation domain of V1 neurons of the California ground squirrel (*Spermophilus beecheyi*)” by Hsin-Hao

Yu, Virginia R. de Sa, and Martin I. Sereno.

Bibliography

Adelson, E. H., and Bergen, J. R., 1985: Spatialtemporal energy models for the perception of motion. *Journal of Optical Society of America A*, **2**, 284–299.

Albright, T. D., and Stoner, G. R., 2002: Contextual influences on visual processing. *Annual Review Neuroscience*, **25**, 339–379.

Albus, K., and Fries, W., 1980: Inhibitory sidebands of complex receptive fields in the cat's striate cortex. *Vision Research*, **20**, 369–372.

Allman, J., Meizin, F., and McGuinness, E., 1985: Stimulus specific responses from beyond the classical receptive field: neurophysiological mechanisms for local-global comparision in visual neurons. *Annual Reviews Neuroscience*, **8**, 407–30.

Alonso, J. M., Cudeiro, J., Perez, R., Gonzalez, F., and Acuna, C., 1993: Influence of layer 5 of area 18 of the cat visual cortex on responses of cells in layer 5 of area 17 to stimuli of high velocity. *Experimental Brain Research*, **93**, 363–366.

Anderson, J. C., and Martin, K. A. C., 2006: Synaptic connection from cortical area V4 to V2 in macaque monkey. *Journal of Comparative Neurology*, **495**, 709–721.

Anderson, J. S., Lampl, I., Gillespie, D. C., and Ferster, D., 2001: Membrane potential and conductance change underlying length tuning of cells in cat primary visual cortex. *Journal of Neuroscience*, **21**, 2104–2112.

Angelucci, A., and Bullier, J., 2003: Reaching beyond the classical receptive field of V1 neurons: horizontal or feedback axons? *Journal of Physiology, Paris*, **97**, 141–154.

Angelucci, A., Levitt, K. B., Walton, E. J. S., Hupe, J., Bullier, J., and Lund, J. S., 2002b: Circuits for local and global signal integration in primary visual cortex. *Journal of Neuroscience*, **22**, 8633–8646.

Barlow, H. B., Blakemore, C., and Pettigrew, J. D., 1967: The neural mechanism of binocular depth discrimination. *Journal of Physiology, Lond*, **193**, 327–342.

Bell, A. J., and Sejnowski, T. J., 1995: An information maximisation approach to blind separation and blind deconvolution. *Neural Computation*, **7**(6), 1129–1159.

Bishop, P. O., Coombs, J. S., and Henry, G. H., 1973: Receptive fields of simple cells in the cat striate cortex. *Journal of Physiology*, **231**, 31–60.

Blakemore, C., and Tobin, E. A., 1972: Lateral inhibition between orientation detectors in the cat's visual cortex. *Experimental Brain Research*, **15**, 439–440.

Bolz, J., and Gilbert, C. D., 1986: Generation of end-inhibition in the visual cortex via interlaminar connections. *Nature*, **320**(27), 362–365.

Bolz, J., and Gilbert, C. D., 1990: The role of horizontal connections in generating long receptive fields in the cat visual cortex. *European Journal of Neuroscience*, **1**, 263–268.

Bolz, J., Gilbert, C. D., and Wiesel, T. N., 1989b: Pharmacological analysis of cortical circuitry. *Trends in Neuroscience*, **12**, 292–296.

Bonds, A. B., 1989: Role of inhibition in the specification of orientation selectivity of cells in the cat striate cortex. *Visual Neuroscience*, **2**, 41–55.

Born, R. T., and Tootell, R. B. H., 1991: Single-unit and 2-deoxyglucose studies of side inhibition in macaque striate cortex. *Proceedings of National Academy of Science, USA*, **88**, 7071–7075.

Bosking, W. H., Zhang, Y., Schofield, B., and Fitzpatrick, D., 1997: Orientation selectivity and arrangement of horizontal connections in three shrew striate cortex. *Journal of Neuroscience*, **17**(6), 2112–2127.

Bringuier, V., Chavane, F., Glaeser, L., and Fregnac, Y., 1999: Horizontal propagation of visual activity in the synaptic integration field of area 17 neurons. *Science*, **283**, 695–699.

Cavanaugh, J. R., Bair, W., and Movshon, J. A., 2002a: Nature and interaction of signals from the receptive field center and surround in macaque V1 neurons. *Journal of Neurophysiology*, **88**, 2530–2546.

Cavanaugh, J. R., Bair, W., and Movshon, J. A., 2002b: Selectivity and spatial distribution of signals from the receptive fields surround in macaque V1 neurons. *Journal of Neurophysiology*, **202**, 2547–2556.

Chichilnisky, E. J., 2001: A simple white noise analysis of neuronal light responses. *Network*, **12**, 199–213.

Chisum, H. J., Mooser, F., and Fitzpatrick, D., 2003: Emergent properties of layer 2/3 neurons reflect the collinear arrangement of horizontal connections in tree shrew visual cortex. *Journal of Neuroscience*, **23**, 2947–2960.

Das, A., and Gilbert, C. D., 1995: Long-range horizontal connections and their role in cortical reorganization revealed by optical recording of cat primary visual cortex. *Nature*, **375**, 780–784.

Daugman, J. G., 1985: Uncertainty relatoin for resolution in space, spatial frequency and orientation optimized by two-dimensional visual cortical filters. *Journal of Optical Society of America A*, **2**, 1160–1169.

David, S. V., Vinje, W. E., and Gallant, J. L., 2004: Natural stimulus statistics alter the receptive field structure of V1 neurons. *The Journal of Neuroscience*, **24**(31), 6991–7006.

Dayan, P., and Abbott, L. F., 2001: Neural encoding I: Firing rates and spike statistics. In *Theoretical neuroscience: computational and mathematical modeling of neural systems*, chapter 1. The MIT Press, Cambridge, MA., USA.

de Ruyter van Steveninck, R., and Bialek, W., 1988: Real-time performance of a movenment-sensitive neuron in the blowfly visual system: coding and information transfer in short spike sequences. *Proceedings of the Royal Society of London B*, **234**, 379–414.

De Valois, R. L., Albrecht, D. G., and Thorell, L. G., 1982b: Spatial frequency selectivity of cells in macaque visual cortex. *Vision Research*, **22**, 545–559.

De Valois, R. L., Yund, E. W., and Hepler, N., 1982a: The orientation and direction selectivity of cells in macaque visual cortex. *Vision Research*, **22**, 531–544.

DeAngelis, G. C., Freeman, R. D., and Ohzawa, I., 1994: Length and width tuning of neurons in the cat's primary visual cortex. *Journal of Neurophysiology*, **68**, 144–163.

DeAngelis, G. C., Ohzawa, I., and Freeman, R. D., 1993a: Spatialtemporal organization of simple-cell receptive fields in the cat's striate cortex. I. general characteristics and postnatal development. *Journal of Neurophysiology*, **69**, 1091–1117.

DeAngelis, G. C., Robson, J. G., Ohzawa, I., and Freeman, R. D., 1992: Organization of suppression in receptive fields of neurons in cat visual cortex. *Journal of Neurophysiology*, **68**, 144–163.

Dobbins, A., Zucker, S. G., and Cynader, M. S., 1987: Endstopped neurons in the visual cortex as a substrate for calculating curvature. *Nature*, **329**, 438–441.

Dreher, B., 1972: Hypercomplex cells in the cat's striate cortex. *Investigative Ophthalmology and Visual Science*, **11**, 355–356.

Durack, J. C., and Katz, L. C., 1995: Development of horizontal projections in layer 2/3 of ferret visual cortex. *Cerebral Cortex*.

Ferster, D., and Jagadeesh, B., 1992: EPSP-IPSP interactions in cat visual cortex studied with *in vivo* whole-cell patch recording. *Journal of Neuroscience*, **12**, 1262–1274.

Ferster, D., and Koch, C., 1987: Neuronal connections underlying orientation selectivity in cat visual cortex. *Trends in Neuroscience*, **10**, 487–492.

Ferster, D., and Miller, K. D., 2000: Neural mechanisms of orientation selectivity in the visual cortex. *Annual Reviews Neuroscience*, **23**, 441–471.

Field, D. J., Hayes, A., and Hess, R. F., 1993: Contour integration by the human visual system: evidence for a local "association field". *Vision Research*, **33**, 173–193.

Fitzpatrick, D., 2000: Seeing beyond the receptive field in primary visual cortex. *Current Opinion in Neurobiology*, **10**, 438–443.

Fries, W., Albus, K., and Creutzfeldt, O. D., 1977: Effects of interacting visual patterns on simple cell responses in cat's striate cortex. *Vision Research*, **17**, 1001–1008.

Gallyas, F., 1979: Silver staining of myeline by means of physical development. *Neurological Research*, **1**, 293–209.

Gilbert, C. D., 1977: Laminar differences in receptive field properties of cells in cat primary visual cortex. *Journal of Physiology, Lond*, **268**, 391–421.

Gilbert, C. D., 1992: Horizontal integration and cortical dynamics. *Neuron*, **9**, 1–13.

Gilbert, C. D., and Wiesel, T. N., 1983: Clustered intrinsic connections in cat visual cortex. *Journal of Neuroscience*, **3**, 1116–1133.

Gilbert, C. D., and Wiesel, T. N., 1989: Columnar specificity of intrinsic horizontal and corticocortical connections in cat visual cortex. *Journal of Neuroscience*, **9**, 2432–2442.

Gilbert, C. D., and Wiesel, T. N., 1990: The influence of contextual stimuli on the orientation selectivity of cells in primary visual cortex of the cat. *Vision Research*, **30**, 1689–1701.

Girard, P., Hupé, J. M., and Bullier, J., 2001: Feedforward and feedback connections between area V1 and V2 of the monkey have similar rapid conduction velocity. *Journal of Neurophysiology*, **85**, 1328–1331.

Grieve, K. L., and Sillito, A. M., 1991: A re-appraisal of later VI of the visual cortex in the generation of cortical end inhibition. *Experimental Brain Research*, **87**, 521–529.

Grinvald, A., Lieke, E. E., Frostig, R. D., and Hildesheim, R., 1994: Cortical point-spread function and long-range lateral interactions revealed by real-time optical imaging of macaque monkey primary visual cortex. *Journal of Neuroscience*, **14**, 2545–2568.

Gulyás, B., Orban, G. A., Duysens, J., and Maes, H., 1987: The suppressive influence of moving textured backgrounds on responses of cat striate neurons to moving bars. *Journal of Neurophysiology*, **57**, 1767–1791.

Hall, W. C., Karten, H. J., Killackey, H., and Diamond, I. T., 1971: Cortical visual areas in the grey squirrel (Sciurus carolinensis): a correlaion between cortical evoked potential maps and architectonic subdivision. *Journal of Neurophysiology*, **34**, 437–452.

Hammond, P., and MacKay, D. M., 1981: Modulatory influences of moving texture backgrounds on responsiveness of simple cells in feline striate cortex. *Journal of Physiology*, **319**, 431–442.

Hartline, H. K., 1938: The response of single optic nerve fibers of the vertebrate eye to illumination of the retina. *Journal of Physiology*, **121**, 400–415.

Hartline, H. K., 1940: The receptive field of optic nerve fibers. *American Journal of Physiology*, **130**, 700–711.

Heeger, D. J., 1992: Normalization of cell responses in cat striate cortex. *Visual Neuroscience*, **9**, 181–197.

Heimel, J. A., Van Hooser, S. D., and Nelson, S. B., 2005: Laminar organization of response properties in primary visual cortex of the gray squirrel (Sciuris carolinensis). *Journal of Neurophysiology*, **94**, 3538–3554.

Hirsch, J. A., and Gilbert, C. D., 1991: Synaptic physiology of horizontal connections in the cat's visual cortex. *Journal of Neuroscience*, **11**, 1800–1809.

Hubel, D. H., and Wiesel, T. N., 1962: Receptive fields, binocular interaction and functional architecture in the cat's visual cortex. *Journal of Physiology, Lond*, **160**, 106.

Hubel, D. H., and Wiesel, T. N., 1965: Receptive fields and functional architecture in two non-striate visal areas (18 and 19) of the cat. *Journal of Neurophysiology*, **28**, 229–289.

Hubel, D. H., and Wiesel, T. N., 1968: Receptive field and functional architecture of monkey striate cortex. *Journal of Physiology, Lond*, **195**, 215–243.

Hubel, D. H., and Wiesel, T. N., 1974: Uniformity of monkey striate cortex: a parallel relationship between field size, scatter, and magnification factor. *Journal of Comparative Neurology*, **158**, 295–306.

Jacobs, G. H., Blakeslee, B., McCourt, M. E., and Tootell, R. B. H., 1980: Visual sensitivity of ground squirrels to spatial and temporal luminance variations. *Journal of Comparative Physiology*, **136**, 291–299.

Jones, B. H., 1970: Responses of single neurons in cat visual cortex to a simple and more complex stimulus. *American Journal of Physiology*, **218**, 1102–1107.

Jones, H. E., Grieve, K. L., Wang, W., and Sillito, A. M., 2001: Surround suppression in primate V1. *Journal of Neurophysiology*, **86**, 2011–2028.

Jones, H. E., Wang, W., and Sillito, A. M., 2002: Spatial organization and magnitude of orientation contrast interactions in primate V1. *Journal of Neurophysiology*, **88**, 2796–2808.

Jones, J., and Palmer, L., 1987a: The two-dimensional spatial structure of simple receptive fields in cat striate cortex. *Journal of Neurophysiology*, **58**, 1187–1211.

Jones, J., and Palmer, L., 1987c: An evaluation of the two-diemsional gabor filter model of simple receptive fields in cat striate cortex. *Journal of Neurophysiology*, **58**(6), 1233–1258.

Kapadia, M. J., Westgeimer, G., and Gilbert, C. D., 2000: Spatial distribution of contextual interactions in primary visual cortex and in visual perception. *Journal of Neurophysiology*, **84**, 2048–2062.

Kapadia, M. K., Ito, M., Gilbert, C. D., and Westheimer, G., 1995: Improvement in visual sensitivity by changes in local context: parallel studies in human observers and in V1 of alert monkey. *Neuron*, **15**, 843–856.

Kapadia, M. K., Westheimer, G., and Gilbert, C. D., 1999: Dynamics of spatial summation in primate visual cortex of alert monkey. *Proceedings of National Academy of Science, USA*, **96**, 12073–12078.

Kastner, S., Nothdurft, H. C., and Pigarev, I. N., 1997: Neuronal correlates of pop-out in cat striate cortex. *Vision Research*, **37**, 371–376.

Kato, H., Bishop, P. O., and Orban, G. A., 1978: Hypercomplex and the simple/complex cell classification in the cat striate cortex. *Journal of Neurophysiology*, **41**, 1071–1095.

Kisvàrday, Z. F., 1992: GABAergic networks of basket cells in the visual cortex. In *Progress in Brain Research*, editors R. R. Mize, R. Marc, and A. M. Sillito, volume 90. Mechanisms of GABA in the visual system, 385–405. Elsevier, Amsterdam.

Kisvàrday, Z. F., Kim, D. S., Eysel, U. T., and Bonhoeffer, T., 1994: Relationship between lateral inhibitory connection and the topology of the orientation map in cat visual cortex. *European Journal of Neuroscience*, **6**, 1619–1632.

Kisvàrday, Z. F., Martin, K. A. C., Freund, T. F., Maglóczky, Z., Whiteridge, D., and Somogyi, P., 1986: Synaptic targets of HRP-filled layer III pyramidal cells in the cat striate cortex. *Experimental Brain Research*, **64**, 541–552, cat.

Kisvàrday, Z. F., Toth, E., Rausch, M., and Eysel, U. T., 1997: Orientation-specicif relationship between populations of excitatory and inhibitory lateral connections in the visual cortex of the cat. *Cerebral Cortex*, **7**, 605–618.

Knierim, J. J., and Van Essen, D. C., 1992: Neuronal responses to static texture pattern in area V1 of the alert macaque monkey. *Journal of Neurophysiology*, **67**, 961–980.

Kuffler, S. W., 1953: Discharge patterns and functional organization of mammalian retina. *Journal of Neurophysiology*, **16**, 36–68.

Lamme, V. A. E., 2004: Beyond the classical receptive field: contextual modulation of V1 responses. In *The Visual Neurosciences*, editors L. M. Chalupa, and J. S. Werner, volume 1, chapter 45, 720–732. The MIT Press.

Lamme, V. A. F., 1995: The neurophysiology of figure-ground segregation in primary visual cortex. *Journal of Neuroscience*, **15**, 1605–1615.

Lamme, V. A. F., and Roelfsema, P. R., 2000: The distinct modes of vision offered by feedforward and recurrent processing. *Trends in Neuroscience*, **23**, 571–579.

Levitt, J. B., and Lund, J. S., 1997: Contrast dependence of contextual effects in primary visual cortex. *Nature*, **387**, 73–76.

Levitt, J. B., and Lund, J. S., 2002: The spatial extent over which neurons in macaque striate cortex pool visual signals. *Visual Neuroscience*, **19**, 439–452.

Li, C., and Li, W., 1994: Extensive integration field beyond the classical receptive field of cat striate cortical neurons - classification and tuning properties. *Vision Research*, **34**, 2337–2355.

Li, W., Thier, P., and Wehrhahn, C., 2001: Neuronal responses from beyond the classical receptive field in V1 of alert monkey. *Experimental Brain Research*, **139**, 359–371.

Livingstone, M. S., and Hubel, D. H., 1984: Specificity of intrinsic connections in primate primary visual cortex. *Journal of Neuroscience*, **4**, 2830–2835.

Long, K. O., and Fisher, S. K., 1983: The distribution of photoreceptors and ganglion cells in California ground squirrel, *Spermophilus beecheyi*. *The Journal of Comparative Neurology*, **221**, 329–340.

Lund, J. S., Lund, R. D., Hendrickson, A. E., Bunt, A. H., and Fuchs, A. F., 1975: The origin of efferent pathways from the primary visual cortex, area 17, of the macaque monkey as shown by retrograde transport of horseradish peroxidase. *Journal of Comparative Neurology*, **164**, 287–304.

Maffei, L., and Fiorentini, A., 1976: The unresponsive region of visual cortical receptive fields. *Vision Research*, **16**, 1131–1139.

Malach, R., Amir, Y., Harel, M., and Grinvald, A., 1993: Relationship between intrinsic connections and functional architecture revealed by optical imaging and *in vivo* targeted bioctin injection. *Proceedings of National Academy of Science, USA*, **90**, 10469–10473.

Marmarelis, P. Z., and Marmarelis, V. Z., 1978: *Analysis of physiological systems: the white noise approach*. Plenum Press.

Marrocco, R. T., McClurkin, J. W., and Young, R. A., 1982: Modulation of geniculate nucleus cell responsiveness by visual activation of the cortico-geniculate pathway. *Journal of Neuroscience*, **2**, 256–263.

Matsubara, J., Cynader, M., and Swindale, N. V., 1987: Anatomical properties and physiological correlates of the intrinsic connections in cat area 18. *Journal of Neuroscience*, **7**, 1428–1446.

Matsubara, J., Cynader, M., Swindale, N. V., and Stryker, M. P., 1985: Intrinsic projections within visual cortex: evidence for orientation-specfic local connections. *Proceedings of National Academy of Science, USA*, **82**, 935–939.

McCourt, M. E., and Jacobs, G. H., 1984a: Refractive state, depth of focus and accomodation of the eye of the California ground squirrel *Spermophilus beecheyi*. *Vision Research*, **24**, 1261–1266.

McGuire, B. A., Gilbert, C. D., Rivlin, P. K., and Wiesel, T. N., 1991: Targets of horizontal connections in macaque primary visual cortex. *Journal of Comparative Neurology*, **305**, 370–392.

Mignard, M., and Malpeli, J. G., 1991: Paths of information flow through visual cortex. *Science*, **251**, 1249–1251.

Mizobe, K., Polat, U., Pettet, M. W., and Kasamatzu, T., 2001: Facilitation and suppression of single striate-cell activity by spatially discrete pattern stimuli presented by beyond the receptive field. *Visual Neuroscience*, **18**, 377–391.

Morrone, M. C., Burr, D. C., and Maffei, L., 1982: Functional implications of cross-orientation inhibition of cortical visual cells. I. neurophysiological evidence. *Proceedings of the Royal Society, London, B.*, **216**, 335–354.

Murphy, P. C., and Sillito, A. M., 1987: Corticofugal feedback influences the generation of length tuning in the visual cortex. *Nature*, **329**, 727–729.

Murphy, W. J., Eizirik, E., O'Brien, S. J., Madsen, O., Scally, M., Douady, C. J., Teeling, E., Ryder, O. A., Stanhope, M. J., de Jong, W. W., and Springer, M. S., 2001: Resolution of the early placental mammal radiation using bayesian phylogenetics. *Science*, **294**, 2348–2351.

Nelson, J. I., and Frost, B., 1985: Intracortical facilitation among co-orientated, co-axially aligned simple cells in cat striate cortex. *Experimental Brain Research*, **61**, 54–61.

Nelson, J. I., and Frost, B. J., 1978: Orientation selective inhibition from beyond the classic visual receptive field. *Brain Research*, **139**, 359–365.

Nothdurft, H. C., 1991: Texture segmentation and pop-out from orientation contrast. *Vision Research*, **31**, 1073–1078.

Nothdurft, H. C., 1993: The role of features in preattentive vision: comparison of orientation, motion, and colour cues. *Vision Research*, **33**, 1937–1958.

Nothdurft, H. C., Gallant, J. L., and Van Essen, D. C., 1999: Response modulation by texture surround in primate area V1: correlates of "popout' under anesthesia. *Visual Neuroscience*, **16**, 15–34.

Nowak, L. G., and Bullier, J., 1997: The timing of information transfer in the visual system. In *Extrastriate visual cortex in primates*, editors K. S. Rockland, J. H. Kaas, and A. Peters, volume 12, 205–241. Plenum, New York.

Ohzawa, I., DeAngelis, G. C., and Freeman, R. D., 1996: Encoding of binocular disparity of complex cells in the cat's visual cortex. *Journal of Neurophysiology*, **75**, 1779–1805.

Olavarria, J., and Van Sluyters, R. C., 1985: Unfolding and flattening the cortex of gyrencephalic brains. *Journal of Neuroscience*, **15**, 191–202.

Orban, G. A., Gulyás, B., and Vogels, R., 1987: Influence of a moving textural background on direction selectivity of cat striate neuron. *Journal of Neurophysiology*, **57**, 1767–1791.

Orban, G. A., Kato, H., and Bishop, P. O., 1979b: End-zone region in receptive fields of hypercomplex and other striate neurons in the cat. *Journal of Neurophysiology*, **42**, 818–832.

Orban, G. A., Kato, H., and Bishop, P. O., 1979c: Dimensions and properties of end-zone inhibitory areas in receptive fields of hypercomplex cells in cat striate cortex. *Journal of Neurophysiology*, **42**, 833–849.

Paolini, M., and Sereno, M. I., 1998: Direction selectivity in the middle lateral and lateral (ML and L) visual areas in the California ground squirrel. *Cerebral Cortex*, **8**, 362–371.

Peterhans, E., and von der Heydt, R., 1989: Mechanisms of contour perception in monkey visual cortex. II. contours bridging gaps. *Journal of Neuroscience*, **9**, 1749–1763.

Polat, U., 1999: Functional architecture of long-range perceptual interactions. *Spatial Vision*, **12**, 143–162.

Polat, U., Mizobe, K., Pettet, M. W., Kasamatsu, T., and Norcia, A. M., 1998: Colinear stimuli regulate visual responses depending on cell's contrast threshold. *Nature*, **391**, 580–584.

Polat, U., and Sagi, D., 1993: Lateral interactions between spatial channels, suppression and facilitation revealed by lateral masking experiments. *Vision Research*, **33**, 993–999.

Polat, U., and Sagi, D., 1994: The architecture of perceptual spatial interaction. *Vision Research*, **34**, 73–78.

Rieke, F., Warland, D., de Ruyter van Steveninck, R., and Bialek, W., 1999: *Spikes: Exploring the neural code*. The MIT Press, Cambridge, MA., USA.

Ringach, D., Hawken, M., and Shapley, R., 1997: Dynamics of orientation tuning in the macaque primary visual cortex. *Nature*, **387**, 281–284.

Ringach, D. L., 2004: Mapping receptive fields in primary visual cortex. *Journal of Physiology*, **558**, 717–28.

Ringach, D. L., Hawken, M. J., and Shapley, R., 2002: Receptive field structure of neurons in monkey primary visual cortex revealed by stimulation with natutal image sequences. *Journal of Vision*, **2**, 12–24.

Rockland, K. S., 1997: Elements of cortical hierarchy revisited. In *Cerebral Cortex*, editors K. S. Rockland, and A. Peters, volume 12. Extrastriate Cortex in primates, 243–293. Plenum, New York.

Rockland, K. S., and Lund, J. S., 1982: Widespread periodic intrinsic connections in the three shrew visual cortex. *Science*, **215**, 1532–1534.

Rockland, K. S., and Lund, J. S., 1983: Intrinsic laminar lattice connections in primate visual cortex. *Journal of Comparative Neurology*, **216**, 303–318.

Rockland, K. S., Lund, J. S., and Humphrey, A. L., 1982: Anatomical banding of intrinsic connections in striate cortex of three shrews (Tupaia glis). *Journal of Comparative Neurology*, **209**, 41–58.

Rockland, K. S., and Virga, A., 1989: Terminal arbors of individual "feedback" axons projecting from area V2 to V1 in the macaque monkey: a study using immunohistochemstry of anterogradely transported *Phaseolus vulgaris-leucoagglutinin*. *Journal of Comparative Neurology*, **285**, 54–72.

Rossi, A. F., Desimone, R., and Ungerleider, L. G., 2001: Contextual modulation in primary visual cortex of macaques. *Journal of Neuroscience*, **21**, 698–1709.

Rust, N. C., Schwartz, O., Movshon, J. A., and Simoncelli, E. P., 2005: Spatial-temporal elements of macaque V1 receptive fields. *Neuron*, **46**, 945–956.

Ruthazer, E. S., and Stryker, M. P., 1996: The role of activity in the development of long-range horizontal connections in area 17 of the ferret. *Journal of Neuroscience*, **16**, 7253–7269.

Sandell, J. H., and Schiller, P. H., 1982: Effect of cooling area 18 on striate cortex cells in the squirrel monkey. *Journal of Neurophysiology*, **48**, 38–48.

Sceniak, M. P., Ringach, D. L., Hawken, M. J., and Shapley, R., 1999: Contrast's effect on spatial summation by macaque V1 neurons. *Nature Neuroscience*, **2**, 733–739.

Schwartz, O., Chichilinsky, E. J., and Simoncelli, E. P., 2002: Characterizing neural gain control using spike-triggered covariance. In *Advances in Neural Information Processing Systems 14*, editors T. Dietterich, S. Becker, and Z. Ghahramani. MIT Press.

Sengpiel, F., Sen, A., and Blakemore, C., 1997: Characteristics of surround inhibition in cat area 17. *Experimental Brain Research*, **116**, 216–228.

Sereno, M. I., Rodman, H. R., and Karten, H. J., 1991: Organization of visual cortex in the California ground squirrel. In *Society for Neuroscience Abstracts*, volume 17, 844. .

Sharpee, T., Rust, N. C., and Bialek, W., 2004: Analyzing neural responses to natural signals: maximally informative dimensions. *Neural Computation*, **16**, 223–250.

Sherk, H., and LeVay, S., 1983: Contribution of cortico-claustral loop to receptive field properties in area 17 of the cat. *Journal of Neuroscience*, **3**, 2121–2127.

Sillito, A. M., Cudeiro, J., and Murphy, P. C., 1993: Orientation sensitivity elements in the corticofugal influence on center-surround interactions in the dorsal lateral geniculate nucleus. *Experimental Brain Research*, **93**, 6–16.

Sillito, A. M., Grieve, K. L., Jones, H. E., Cudeiro, J., and David, J., 1995: Visual cortical mechanisms detecting focal orientation discontinuities. *Nature*, **378**, 492–496.

Sillito, A. M., and Jones, H. E., 2004: Feedback systems in visual processing. In *The Visual Neurosciences*, editors L. M. Chalupa, and J. S. Werner, volume 1, chapter 37, 609–624. The MIT Press.

Sillito, A. M., and Versiani, V., 1977: The contribution of excitatory and inhibitory inputs to the length preference of hypercomplex cells in layer II and III of the cat's striate cortex. *Journal of Physiology, Lond*, **273**, 775–790.

Sincich, L. C., and Blasdel, G. G., 2001: Oriented axon projections in primary visual cortex of the monkey. *Journal of Neuroscience*, **21**, 4416–4426.

Smyth, D., Willmore, B., Baker, G. E., Thompson, I. D., and Tolhurst, D. J., 2003: The receptive-field organization of simple cells in primary visual cortex of ferrets under natural scene stimulation. *Journal of Neuroscience*, **23**, 4746–4759.

Stettler, D. D., Das, A., Bennett, J., and Gilbert, C. D., 2002: Lateral connectivity and contextual interactions in macaque primary visual cortex. *Neuron*, **36**, 739–750.

Szulborski, R. G., and Palmer, L. A., 1990: The two-dimensional spatial structure of nonlinear subunits in the receptive fields of complex cells. *Vision Research*, **30**(2), 249–254.

Tootell, R. B. H., and Silverman, M. S., 1985: Two methods for flat-mounting cortical tissue. *Journal of Neuroscience Methods*, **15**, 177–190.

Toth, L. J., Rao, S. C., Kim, D., Somers, D., and Sur, M., 1996: Subthreshold facilitation and suppression in primary visual cortex revealed by intrinsic signal imaging. *Proceedings of National Academy of Science, USA*, **93**, 9869–9874.

Touryan, J., Felsen, G., and Dan, Y., 2005: Spatial structure of complex cell receptive fields measured with natural images. *Neuron*, **45**, 781–791.

Touryan, J., Lau, B., and Dan, Y., 2002: Isolation of relevant visual features from random stimuli for cortical complex cells. *The Journal of Neuroscience*, **24**, 10811–10818.

Ts'o, D. Y., and Gilbert, C. D., 1988: The organization of chromatic and spatial interaction in the primate striate cortex. *Journal of Neuroscience*, **8**, 1712–1727.

Tucker, T. R., and Fitzpatrick, D., 2004: Contributions of vertical and horizontal circuits to the response properties of neurons in primary visual cortex. In *The Visual Neurosciences*, editors L. M. Chalupa, and J. S. Werner, volume 1, chapter 46, 733–746. The MIT Press.

Tusa, R. J., Palmer, L. A., and Rosenquist, A. C., 1978: The retinotopic organization of area 17 (striate cortex) in the cat. *Journal of Comparative Neurology*, **177**, 213–236.

Van Hooser, S. D., Heimel, J. A., and Nelson, S. B., 2006: Lack of patchy horizontal connectivty in primary visual cortex o a mammal without orientation maps. *The Journal of Neuroscience*, **19**, 7680–7692.

von der Heydt, R., 2003: Image parsing mechanisms of the visual cortex. In *The Visual Neurosciences*, editors L. M. Chalupa, and J. S. Werner, chapter 76, 1139–1150. The MIT Press.

von der Heydt, R., Peterhans, E., and Baumgartner, G., 1984: Illusory contours and cortical neuron responses. *Science*, **224**, 1260–1262.

Walker, G. A., Ohzawa, I., and Freeman, R. D., 1999: Asymmetric suppression outside the classical receptive field of the visual cortex. *The Journal of Neuroscience*, **19**, 10536–10553.

Walker, G. A., Ohzawa, I., and Freeman, R. D., 2000: Suppression outside the classical cortical receptive field. *Visual Neuroscience*, **17**, 369–379.

Weliky, M., Kandler, K., Fitzpatrick, D., and Katz, L. C., 1995: Patterns of excitation and inhibition evoked by horizontal connections in visual cortex share a common relationship to orientation columns. *Neuron*, **15**, 541–552.

Yabuta, N. H., and Callaway, E. M., 1998: Cytochrome-oxidase blobs and intrinsic horizontal connections of layer 2/3 pyramidal neurons in primate V1. *Visual Neuroscience*, **15**, 1007–1027.

Yoshioka, T., Blasdel, G. G., Levitt, J. B., and Lund, J. S., 1996: Relation between patterns of intrinsic lateral connectivity, ocular dominance, and cytochrome oxidase-reactive regions in macaque monkey striate cortex. *Cerebral Cortex*, **6**, 297–310.

Zipser, K., Lamme, V. A. F., and Schiller, P. H., 1996: Contextual modulation in primary visual cortex. *Journal of Neuroscience*, **16**, 7376–7389.